THE UNIVERSITY OF CALGARY

Air Fuel Ratio Control of Spark-ignition Engines Using Sliding Modes

by

Rahul Mehrotra

A THESIS

SUBMITTED TO THE FACULTY OF GRADUATE STUDIES

IN PARTIAL FULFILMENT OF THE REQUIREMENTS FOR THE

DEGREE OF MASTER OF SCIENCE

DEPARTMENT OF MECHANICAL ENGINEERING

CALGARY, ALBERTA

MAY, 1998

Abstract

Demands for high output performance, stringent fuel consumption and emission regulations have become some of the major challenges for engineers in the automotive field, especially control engineers. Precise control of air-fuel ratio during both steady and transient engine operation is the key for better engine performance and reduced exhaust emissions.

In this thesis, a nonlinear, fuel injected spark-ignition engine numerical model is developed. This physically motivated model includes intake manifold air dynamics, fuel wall-wetting dynamics, load speed effects, crank shaft dynamics and process delays inherent in a four-stroke engines. The developed model is unique in that it incorporates all of the above noted phenomenon. A sliding mode controller is then designed based on a linearized version of the mathematical engine model. The linear model is compared favorably with a non linear model in open loop simulated throttling tests. The speed of the system response is limited due to the delay time from the air-fuel ratio (AFR) metering location to the sensor using a conventional feedback control design. Modern control and estimation theory was used to design a high bandwidth closed-loop AFR controller. The sliding mode controller is robust to rapidly changing throttle maneuvers and disturbances. In order to implement the inherent state feedback control scheme, an optimal state estimator is developed.

The sliding mode control method offers a strong potential for future engine control problems, since: it results in a relatively simple control structure; it is robust to model errors; and it can be easily adapted to a wide family of engines.

Acknowledgements

This thesis is dedicated to my parents Kailash Narain Mehrotra and Sita Mehrotra and also to my Uncle Rana Mehrotra and aunt Anchal Mehrotra. Their support and inspiration made this work possible.

I would like to express my appreciation to my supervisor Dr. Jeff Pieper for his guidance and motivation throughout this research. I also thank Dr J. A.C Kentfield and Dr. W. Y. Svrcek for their constructive evaluation and criticism of this research.

Finally, I wish to give thanks to my friends Rupal, Dr. Sivaram, Dr. Rao, Sanja and my other family members for their encouragement during the course of this research.

Table of Contents

List of Figures

List of Tables

List of Symbols

A_{th}	Throttle open area
C_d	Discharge coefficient
d	Throttle shaft diameter
D	Throttle bore diameter
I_{eff}	Moment of inertia
K_f	Fuel injector parameter (Eq. 3.24)
L	Estimator gain matrix
m	mass
m_{at}	Mass of air entering into the intake manifold
m_{ap}	Mass of air entering into the cylinder
m_f	Mass of fuel entering the cylinder
m_{fi}	Mass of fuel injected
m_{ff}	Mass of liquid fuel film
m_{fv}	Mass of fuel vapor
n	Number of moles
n_{cyl}	Number of cylinders
N	Engine speed
p	Pressure
p_o	Atmospheric pressure
p_m	Intake manifold pressure
q	Approximation of Control Derivative.
R	Gas Constant
t	Time
t_o	Fuel injector parameter (Eq. 3.24)
t_d	Exhaust transport delay
t_{inj}	Fuel injection pulse width

T	Sampling period in time
T_o	Atmospheric temperature
T_m	Intake manifold temperature
T_{ind}	Indicated torque
T_{fric}	Engine friction torque
T_{aero}	Aerodynamic drag
T_{roll}	Rolling friction torque
u	Control signal
v	Feedback Signal
V_d	Displacement volume
V_m	Manifold volume
X	Fraction of injected fuel entering the puddle

Greek Letters

α	Throttle plate angle
α_o	Throttle plate closed angle
γ	Specific heat ratio
η_v	Volumetric efficiency
θ	Crank angle
θ_{EVO}	Crank angle of exhaust valve opening
ρ	Density
τ	Time constant
τ_e	UEGO sensor time constant
τ_f	Evaporation time constant
ϕ	Air/Fuel equivalence ratio
ϕ_c	In-cylinder equivalence ratio
ϕ_m	Measured equivalence ratio
ω_e	Engine speed in revolutions per second.

Abbreviations

AFR, A/F	Air-fuel ratio (mass basis)
$(A/F)_s$	Stoichiometric air-fuel ratio
BDC	Bottom dead center
DBW	Drive-by wire
ECU	Electronic control unit
EGO	Exhaust gas oxygen
EGR	Exhaust gas recirculation
EVC, EVO	Exhaust valve closing, opening
HC	Unburned hydrocarbon
IC	Internal combustion
imep	Indicated mean effective pressure
isfc	Indicated specific fuel consumption
IVC,IVO	Intake valve closing, opening
NO_x	Oxides of nitrogen
PFI	Port fuel injection
RPM	Revolutions per minute
SA	Spark advance
SI	Spark-ignition
TBI	Throttle body injection
TDC	Top dead center
TWC	Three way catalytic converter

CHAPTER 1

Introduction

1.1 Problem Statement

A vehicle internal combustion engine needs to operate smoothly, from an idle speed of several hundred revolutions per minute (rpm) to a maximum speed of thousands of rpm, under varying inertial loads and disturbance forces as well as constantly varying throttle commands by the driver. In addition to the wide operating range, the automotive industry is faced with the formidable task of meeting increasingly stringent fuel consumption and emissions regulations within driveability constraints. Parallel to these challenges is a significant advancement of control theory and the availability of powerful low-cost microprocessors to solve nonlinear control problems. These, together with the demands for best output performance and better driveability has become one of the major tasks for

engineers in the automotive field, especially control engineers. This work is devoted to the air/fuel ratio control problem of spark ignition engines with the objective of obtaining improved performance, reduced exhaust emissions and better fuel economy.

Application of control theory to the motor car has been somewhat late compared to the other industries and has focused primarily on electronic engine controls. Starting in the late 60's and carrying on into the 70's and 80's, emission standards have been established in many parts of the world. Prior to these regulations, the basic focus was on improved engine designs and detailed engine calibrations for the successful operation of the internal combustion (IC) engine as the primary power plant for automobiles. During the past two decades, because of the projected increases in the stringent emissions requirements, the use of engine control became increasingly crucial.

The state-of-the art advancement of engine control from mechanical to electronic and from open-loop look up tables to closed-loop computer based diagnostic reflects the ongoing research effort and improvement in both hardware and software. Probably the most significant advance which has allowed the implementation of engine control systems is the availability of low-cost electronics, primarily the microcomputer. By 1982, the use of microcomputers had grown to such an extent that many motor car manufacturers were using them in their entire car line for engine control as well as other functions. Because of the elevated increases in microcomputer capability with little or no additional cost, many of the types of sophisticated control algorithms that were originally developed for the aerospace industry, that is, those that require a great deal of computational capability became practical for use on motor cars.

In addition to the microcomputer significant advances in electronics have provided us with low cost, high performance and reliable actuators and sensors which enhanced the sensing accuracy, actuation capability, and flexibility of algorithm design. All of these contribute to a better coordination of engine control variables. This refined coordination led to the systematic solution of specific problems that require a slightly out-of-the ordinary solution resulting in better efficiency, engine performance and emissions reductions under both steady state and transient conditions.

This work focuses on the specific problem of air/fuel (A/F) ratio control of spark-ignition (SI) internal combustion (IC) engines. First of all a physically motivated dynamic engine model is developed that represents the dominant engine dynamics in close proximity to the actual engine behavior. Based on the model, state space design methodology is developed in order to apply modern control and estimation theory. The sliding mode control theory in conjunction with an estimator is then applied to achieve the required accuracy in air/fuel ratio control.

1.2 Motivation of Air-Fuel Ratio Control

1.2.1 Engine Performance

Engine performance, efficiency, and emissions depends widely on precise control of air-fuel ratio (AFR) during both steady and transient engine operation. Steady operation includes operation at given speed and load over several engine cycles with a warmed up engine. Transient operation includes engine starting, engine warm-up to steady state

temperatures and changing rapidly from one engine load and speed to another. Mixture composition effects are usually discussed in terms of the air/fuel ratio. However, the relative proportions of air and fuel can be stated more generally in terms of the equivalence air/fuel ratio λ (the actual air/fuel ratio normalized by dividing by the stoichiometric air fuel ratio, thus: $\lambda = \phi_m / \phi_s$). Where appropriate, therefore, the equivalence ratio will be used as the defining parameter. Fig. 1.1 shows the effect of fuel /air equivalence ratio on indicated mean effective pressure, specific fuel consumption and fuel conversion efficiency in a typical engine. The mean effective pressure or maximum torque stage is reached when the engine operates slightly richer than stoichiometric. Following combustion of a stoichiometric mixture, due to dissociation at the high temperatures, molecular oxygen is present in the burned gases and some additional fuel can be added and partially burned. This increases the temperature and the number of moles of the burned gases in the cylinder resulting in increased power and mean effective pressure (Heywood 1988). For mixtures leaner than stoichiometric, fuel economy keeps improving but only up to a certain point when the combustion quality starts to decline. .Combustion of mixtures leaner than stoichiometric produces products at lower temperature, and with less dissociation of the triatomic molecules CO_2 and H_2O . Thus the fraction of chemical energy of the fuel which is released as sensible energy is greater; hence a greater fraction of the fuel's energy is transferred as work to the piston during expansion and, the fraction of the fuel's available energy rejected to the exhaust system decreases.

1.2.2 Engine Exhaust Emissions

The spark-ignition engine exhaust gases contain oxides of nitrogen (nitric oxide, NO,

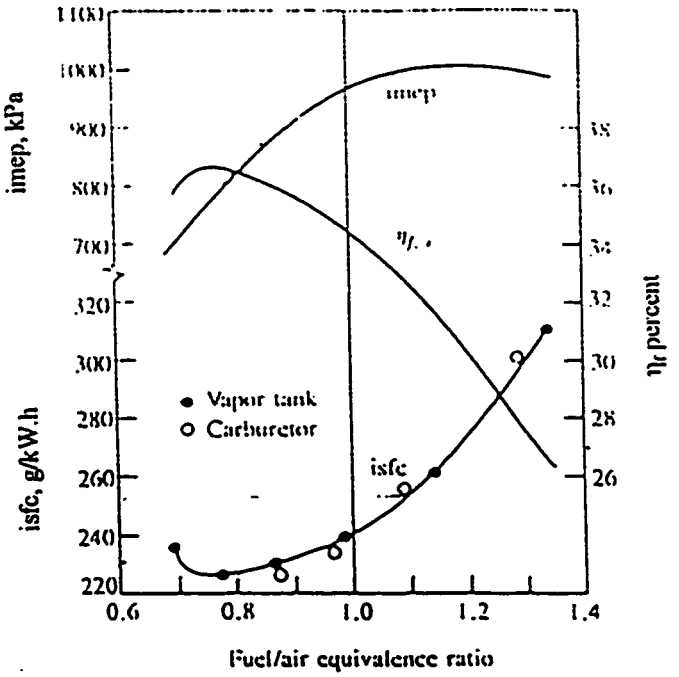

Figure 1.1: Effect of Fuel/Air Equivalence Ratio on Indicated Mean Effective Pressure, Indicated Specific Fuel Consumption and Fuel Conversion Efficiency.(Heywood 1988)

and small amounts of nitrogen dioxide, NO_2 - collectively known as NO_x), carbon monoxide(CO),and organic compounds which are unburned or partially burned hydrocarbons (HC). The relative amounts are of order: NO_x, 500 to 1000 ppm or 20 g/kg fuel; CO 1 to 2 percent or 200 g/kg fuel; and HC, 3000 ppm (as C_1) or 25 g/kg fuel. The processes by which pollutants form within the cylinder are complicated (Heywood 1988). NO_x is formed during combustion because of the high temperature burned gases and CO also forms during the combustion process with rich air-fuel mixtures, as there is insufficient oxygen to burn fully all the carbon in the fuel to CO_2. Primarily, HC is incompletely burned fuel. During compression and combustion, the increasing cylinder pressure forces some of the gas in the cylinder into the volumes between the piston, rings, and cylinder wall which escapes the primary combustion process. This gas, which leaves these crevices later in the expansion and exhaust

processes, is one basic source of unburned hydrocarbon.

One of the most important variables in determining spark-ignition engine emissions is the relative air/fuel ratio λ. Fig. 1.2 shows qualitatively how NO, CO and HC exhaust emission vary with this parameter. Emissions are lower for leaner mixtures until the combustion quality starts to degrade (and eventually misfire occurs), when HC emissions rise sharply and engine operation becomes erratic. The shapes of these curves indicate the complexities of emission control. Nevertheless the spark-ignition engine has normally been operated close to stoichiometric, or slightly fuel rich to ensure smooth and reliable operation as far as emission control is the key issue.

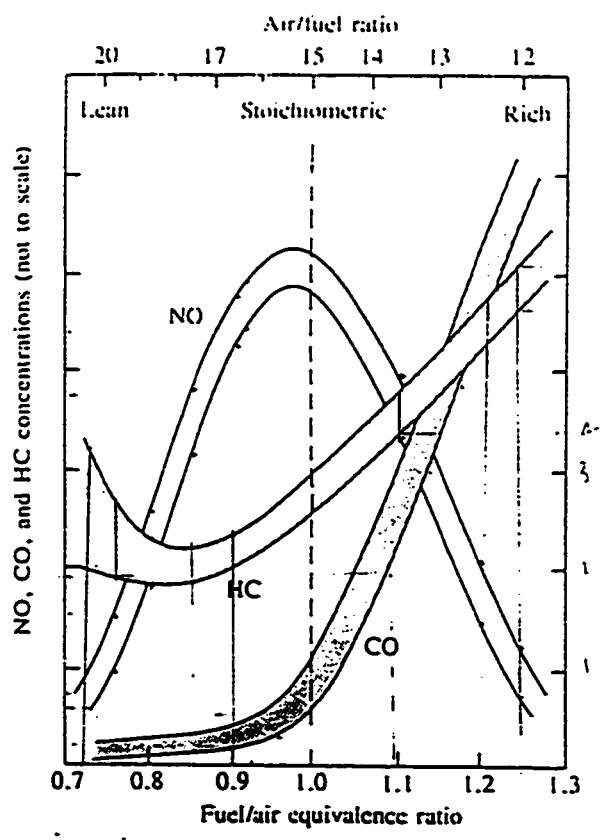

Figure 1.2: Effect of Fuel/Air Equivalence Ratio on Exhaust Emissions (Heywood 1988)

As depicted by Figs. 1.1 and 1.2 it is evident that there is no single value of AFR that satisfy all aspects over the entire load and speed range. Therefore scheduling the AFR ideally is a requirement in order to attain the optimal goal of satisfying both the engine operating conditions and driver's desire.

1.2.3 Emission Controls

Automotive emissions has become a major source of air pollution resulting in stricter regulations on allowable limits of exhaust pollutants. The harmful effects of these pollutants are many. CO itself is a poisonous gas, which affects cardiac and pulmonary functions due to high affinity with hemoglobin. While HC irritates the eyes and throat (and some are carcinogenic) and form smog along with NO_x, the latter causes respiratory disorders and adverse changes in the cell structure and lung walls. Tackling automobile emissions is a very complex task. For one thing, emissions are not constant and depend on the driving mode. Acceleration will cause an increase in CO_2, NO_x and HC. No_x will be high during cruising and HC will increase during deceleration.

Controlling the mass-flow of pollutants emitted into the atmosphere and also meeting government regulations has resulted in many techniques being found useful in the automotive industry. Some of these are fuel system optimization, control of ignition timing, exhaust gas recirculation, engine design modifications, exhaust- gas after treatment using catalysts and fuel modifications. The emission reductions of the 1970's came about because of fundamental improvements in engine design. Exhaust gas recirculation is one such option where a portion of the inert gases is recirculated to the intake side, controlled by a pneumatic or electric valve,

causing a reduction in combustion temperature and peak pressure, and hence NO_x. As for engine design modifications, devices such as turbulence generating ports, clean air jets and air induction systems can be incorporated to ensure stable combustion even when lean mixtures are employed. Unfortunately, many of these reductions were achieved at a cost of engine performance and fuel economy.

The advent of "first generation" catalytic converters in 1975 significantly reduced carbon monoxide emissions. The catalytic converter is a device installed between the exhaust manifold and muffler in an exhaust system that converts pollutants to harmless by-products through a catalytic chemical reaction. Noble metals such as platinum, palladium and rhodium are used as catalysts. 1975 saw the widespread introduction of unleaded gasoline which alleviated environmental concerns associated with lead pollution.

The next major milestone in vehicle emission control technology came in 1980-81 with the incorporation of three-way catalytic converter (TWC), which destroys all the three pollutants (CO_x , NO_x and HC) simultaneously. It advances the oxidation of CO and HC to CO_2 and water, and also helps reduce NO_x to nitrogen and oxygen thereby lowering their concentrations significantly. As is commonly known, cars with catalytic converters have to use unleaded fuel.

Fig. 1.3 shows the conversion efficiency for a three-way catalytic converter as a function of air/fuel ratio. The conversion efficiency for NO_x decreases rapidly for lean mixtures and the conversion efficiencies for CO and HC decrease rapidly for rich mixtures. As oxidation and reduction have to take place simultaneously, the air/fuel ratio window .

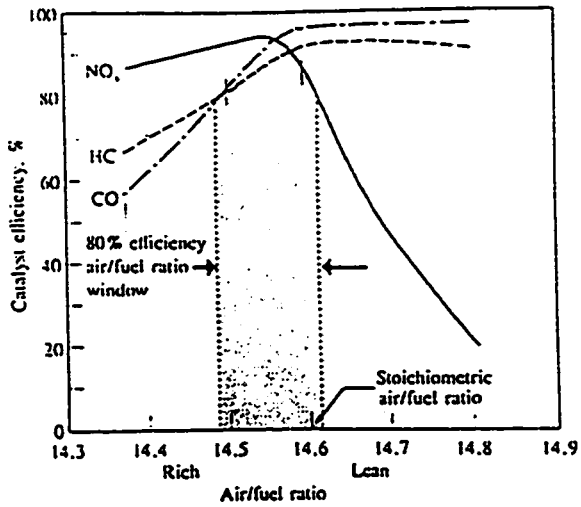

Figure 1.3: Variation of Three Way Catalytic Converter Efficiency with Air/Fuel Ratio (Kummer 1980)

should be as narrow as possible, near stoichiometric, ensuring neither lean or rich condition. It is evident that this extremely narrow conversion window can not be achieved by employing open-loop control only in the face of changing operating conditions and degradation with time. Thus, a closed loop AFR management system which provides on-line out-of-ordinary solution is necessary.

1.3 Physical Effects Causing Transient AFR Excursions

AFR control would not be overly difficult to untangle if engines operated at steady state at all the time. During a practical driving cycle, engine come across many transients such as engine starting, engine warm-up to steady-state temperatures and rapidly changing speed and load requirements. Engines seldom operate at one steady state for prolonged periods. During, engine transients, when the throttle position is changed, the fact that processes which govern the air and the fuel flow to the cylinder are substantially different leading to

govern the air and the fuel flow to the cylinder are substantially different leading to momentary undesirable excursions. This section identifies the various possible causes and physical effects of AFR excursions, to quantify their relative importance, and to lay the groundwork for the design of a control system to compensate for these effects. Following are the six main causes for transient AFR excursions.

(1) Wall-wetting

When the fuel is injected into the intake system, a portion of the fuel droplets strike the walls of the manifold and throttle body and are deposited in liquid form along the walls of intake system components. Only a modest fraction of fuel vaporizes upstream of the throttle. The liquid puddle formed at the walls is re-entrained as the air flows at high velocity past the throttle plate causing a delay or lag in the quantity of fuel entering the cylinders during the current intake stroke, thus resulting in AFR excursion. Droplet deposition on the manifold walls may occur due to gravitational settling and inertial effects as the flow going round bends in the manifold and is more pronounced when the distance between the intake valve and injector is large as in the case of throttle body injection, but still exists in the port injection system. The effect of wall-wetting to the throttle tip in (fast throttle opening) and throttle tip out (fast throttle closing) is as follows:

tip in ⇨ lean excursion

tip out ⇨ rich excursion

(2) Manifold air charging:

When the throttle is opened, the air flow at the throttle is momentarily greater than that at the inlet port to the engine. The essence of this dynamic is that, the fuel flow should be metered based on the air mass flow where the fuel injector is located; otherwise, an AFR excursion results. In throttle body injection cases the throttle air flow should be used and in the port fuel injection port air mass flow should be used to meter fuel flow.

For instance, for a system in which fuel is injected at the intake valve and air entering is measured by an air flow meter located upstream of the throttle plate, then

tip in ⇨ rich excursion

tip out ⇨ lean excursion

(3) Throttle movement after air flow measurement:

Generally the measurement of air flow is conducted in two ways, using air flow meter or calculated using manifold density. The key point is, regardless of which method is employed, that it must be computed way before the intake valve closes to compensate for sensor response delays, computation time required by controller and, above all, fuel transport time.

If there is any movement of the throttle after the air flow signal is

taken and before the closure of the intake valve, it will give an erroneous value of the exact amount of air inducted (Patrick et al. 1991). For instance, acceleration transient demands slightly further opening of the throttle after the air flow sample is taken, causing more air being inducted into the cylinder than indicated by the sample. This behavior is expressed as:

tip in ⇨ lean excursion

tip out ⇨ rich excursion

(4) Sensor and computation delays

Sensor, actuator and computation delays are the leading cause of AFR excursions. Clearly, if there is any delay in sensed engine variables, e.g., air flow rate, manifold pressure, engine speed, etc. the change in fuel flow corresponding to these variables will be delayed, thus leading to AFR excursions. The sensors have certain response times and computation also requires some finite time.

(5) Backflow

During the entire intake stroke, fuel is injected only for a small portion of the induction stroke and typically the injector pulse width ends with a sudden discharge of fuel released in to the air flowing into the cylinder. The air-fuel ratio of the charge entering the cylinder is thus not homogenous throughout its volume.

The charge entering in to the cylinder exerts inertia thereby increasing the volumetric efficiency and this is the reason why the intake valve closes after bottom dead center (BDC).

The phenomenon of backflow is generally observed at low engine speeds, when the inertia exerted is less and some of the entering charge is pushed back early in the compression stroke. This pushed back charge may not have the same AFR as compared to the one that is still in the combustion chamber leading to an AFR excursion.

This excursion is highly predominant when using gaseous fuels (e.g., CH_4) and provides strong support to this argument (Eaton and Patrick, 1992). It is worth noting that when using gaseous fuels no excursion is present because of a wall-wetting phenomenon. The excursion depends on the fuel injection timing with respect to the intake event. When the injection timing is too close to the intake valve closing,

tip in ⇨ lean excursion

tip out ⇨ rich excursion

(6) Shear effect

If the fuel injector is placed just downstream of the throttle plate it may happen that a sudden inflow of air due to a fast throttle opening extracts fuel out of the liquid film in the intake system components and takes into the

cylinder. Thus a rich excursion occurrs for throttle tip-in's in this case. However, for systems in which fuel is injected at the intake port, an AFR excursion is not significant due to a shear effect.

tip in ⇨ rich excursion

tip out ⇨ no significant effect

1.4 Thesis Organization

This chapter introduces the various concerns and the importance of precise air/fuel ratio (AFR) control for better fuel economy, reduced exhaust emissions and engine performance during steady and transient operating conditions. Also the physical reasons for AFR excursions during transient engine operation are analyzed and their modeling importance is discussed.

Following this chapter, Chapter 2 establishes the previous work done in this field and a brief history of the development cycle of dynamic engine models with specific focus on AFR control. Also discussed are the various approaches adopted by the researchers to model the engine dynamics as close by as possible to actual engine operation. This literature review discusses the various conventional AFR control methodologies briefly in order to emphasize the contrast to a sliding mode estimator-based approach, adopted in this research.

In order to apply control methodology it is very important to have a good dynamic engine model for applying the control design. This is the focus of the Chapter 3 which develops a physically motivated, nonlinear dynamic engine model. The dynamic reasons

inherent in the engine operation and are crucial in determining the air-fuel ratio of the mixture in the combustion chamber are identified and modeled separately as subsystems. The main subsystems are intake manifold dynamics, fuel wall wetting dynamics, crank shaft dynamics, process delays and exhaust gas sensor dynamics. The physics of each engine subsystem are described and the equations used to model these processes are collected for a spark-ignition internal combustion engine. The nonlinear model is linearized to design a sliding mode controller.

In Chapter 4, the sliding mode control methodology is discussed, which is the approach taken in this work to design a closed loop feedback control structure based on the mathematical engine model formulated in Chapter 3. The importance of sliding mode control and the concept of sliding surfaces is described which is a relatively new control methodology allowing the models to be imprecise. Two approaches used for designing the sliding surfaces, single loop filtering and optimal hyperplane design (Pieper, 1992, 1994) are discussed in detail.

In Chapter 5, the control law based on sliding mode control is developed and also the estimation technique to be implemented in the feedback loop is discussed. Further the concept of combined observer-controller compensator to be used in this work is discussed. After that the implementation of control design on the model developed in Chapter 3 is presented . For that, a non linear and linear SIMULINK models are designed and simulations are carried out for various throttle maneuvers. The simulation results are analyzed for state feedback alone and also for the combined estimator-controller in the feedback loop. Simulations are used to study the robustness and effectiveness of the control structure

described in Chapter 4.

Chapter 6 summarizes this research, draws conclusion, and recommends further study.

1.5 Contributions

The major contributions of this research work are as follows:

- Development of physically motivated, dynamic, control oriented nonlinear and linear mathematical engine model. The model is based on a contribution of previous models found in the literature. This new combined model represents a significant contribution in terms of capability of prediction of engine dynamic behavior.
- Design of control structure using sliding mode control methodology via sliding modes. While sliding mode control has been previously developed , application of the technique to A/F problems is not well studied.
- Implementation of a control scheme with observer in the feedback loop. A fully implementable scheme is derived using sliding mode control and Kalman filter state estimation
- Demonstration of AFR control in single cylinder spark ignition engine undergoing rapid throttle maneuvers. Simulation results shows excellent behavior with very good AFR tracking despite large throttling commands and other load disturbances over a large operating range.

CHAPTER2

Literature Review

2.1 Introduction

This chapter is devoted to the brief history of the evolution of engine control with specific attention to engine modeling and air/fuel ratio control strategies. The modeling of engine processes and systems continues to provide engineers with effective tools for both understanding and controlling engine systems. It is of the utmost importance to consider the various aspects addressed by researchers in the past before developing a comprehensive model for the spark ignition engine. This chapter reflects the state of activity in field of electronic engine control by bringing together a collection of summary of papers in this field. The use of modern mathematical control techniques in engine engineering has advanced in

the recent years and some of the control oriented models are identified and addressed here with specific focus on air/fuel ratio control for port fuel-injection spark ignition engines. This review demonstrates the academic and commercial importance of AFR control and the varied dimensions of engine management.

2.2 Why Electronic Control

Spark-ignition internal combustion (SI - IC) engines which are hydrocarbon fueled engines are simple. A controlled amount of air and fuel is ignited in a confined space and as the gases expand they create a pressure which pushes a piston, moving it, which is translated into rotary motion through a connecting rod and crank-shaft mechanism. Like all simple things, there is more than meets the eye. In the 1970's, engines relied on mechanically generated signals to ignite the fuel-air mixture (Heywood, 1988). Electrical energy from a battery was stepped up from 12 volts to many thousand volts by a coil. A mechanical distributor selected the appropriate spark plug and sent a signal along a wire. That selection window was wide, the ignition signal (spark) could be initiated any time within many degrees of rotation as a rotor contacted mechanical switch points inside the distributor.

Science knew that the outcome of combustion - both power and pollutants - was significantly affected by how precisely the fuel/air mixture approached theoretical perfection and when the ignition event took place. To get a clean exhaust, fuel had to be precisely mixed in a stoichiometric 14.7:1 ratio. The mixture also had to be ignited at a precise instant that varied with load, speed and other factors. Mechanical devices could not achieve the required precision and automakers soon realized the necessity of electronic control. Electronic engine

control came to light in 1978 and was certainly a response to skyrocketing fuel prices due to energy crisis. But early engine controls were far from the sophisticated devices we use today.

2.3 Development of Dynamic Engine Models

In the 1980's, with a growing concern for emission controls and meeting fuel economy standards, special engine control components were employed using on-board engine testing as the major development step. Although this turned out to be promising, it was not efficient in terms of hardware and manpower, and it ignored the wealth of control system methodology that had evolved during the period. With a better understanding of the physical phenomena affecting engine operation, it was soon realized that the ability to model engine control components would help in system analysis and these design techniques could then be applied to engine control problems. However, the absence of dynamic engine models inhibited the application of these control techniques.

It was not the case that engine models had not been developed and utilized. Literature of the late 1970's had models of combustion process and intake manifold gas flow but intake manifold dynamics were not addressed completely (Dobner 1983). An interesting fact during this period was the development of engine models employing compression-ignition which take into account manifold dynamics especially when superchargers and turbo chargers are included. The appearance of dynamic linear perturbation models of spark-ignition engines was attributed to Cassidy, Athans and Lee (1980) and Morris, Hopkins and Borcherts (1981).These models had the drawback that they were only valid in a proximity of the operating point where input-output measurements were taken to define the model

parameters.

There is abundant knowledge in the literature about the operation and performance of spark-ignition engines from the engine process point of view. This knowledge can be employed to develop dynamic engine models that are useful for the implementation of control algorithms. The relevance of this approach was recognized by the continuous, time based models developed by Powell (1978, 1979) and Dobner (1980, 1983). The work of Dobner was devoted to both non-linear and linear dynamic engine models of spark ignition engines and emphasis was placed on the relationships between the input and output variables with a limited amount of testing to determine the crucial engine model characteristics and parameter values. These models took into account the dynamics of intake air, torque production and the process delays of four stroke engines. Dobner also developed a hybrid engine model by combining the basic linear model with the non-linear effect of air/fuel on torque

Coats and Fruechte (1983) added a new dimension by deriving the transfer functions for the linear model formulated by Dobner (1980) which provided both an insight into engine operation and a basis for describing significant dynamic characteristics. Their approach relied on test and data evaluation methodology for identifying the model parameters via a series of simple on-vehicle tests. The paper shows comparison between simulation results for a 2.5 litre four-cylinder engine operating at idle and measured engine data to confirm the engine model and methods for obtaining the model parameters. It was also realized that the models depicting the dominant dynamics while retaining the interrelationships between measured variables consistent with the physical processes is key for control system design.

2.3.1 Transportation of Liquid Fuel Droplets

Entrainment of fuel droplets in a steady air flow within the spark ignition engine intake manifold received significant attention because it was considered to cause adverse effects on engine transient performance. In view of the highly pulsative nature of air flow into the intake system, researchers were confronted with the limitations of any steady flow model in its application to a real engine system. However, the transportation of fuel in the engine intake system was critical in understanding the behaviour of the fuel-air mixture induced into an engine cylinder.

The prime purpose of the induction system of a spark-ignition engine is to supply the finely atomized fuel and air to the cylinders evenly. Fuel distribution studies done by Yu (1963) brought forth the fact that there is maldistribution in the strength of fuel-air mixture reaching the cylinders and varied from cylinder to cylinder and from time to time. These phenomena are respectively known as geometrical and time varying maldistribution. Yu and Traser (1969) later found that in the case of fully evaporated fuel, maldistribution was significantly reduced. Lo (1976) brought the fuel film on the manifold into the scenario and suggested that intrinsic discontinuities in the flow of the liquid fuel film in the manifold was responsible for the time varying maldistribution.

Goulbourn and Hughes (1977) investigated the mixing of air and fuel in the inlet tract of spark ignition engines. Tanaka and Durbin (1977) analysed the transient response of carburetted engines and came out with a model of fuel film flow along the manifold wall. Their model was fundamental to understanding the fuel flow lag causing the lag in the engine

torque. Kay (1978) took a very close look into the problem and observed visually the liquid fuel film in the induction system. Based on observations, Kay formulated quantitatively the effects of the fuel film on maldistribution of the AFR among the cylinders of a multi-cylinder engine. Finlay and Welsh (1978) also did a photographic study of fuel atomization in intake system of spark ignition engine.

With the advent of microprocessor-controlled electronic fuel metering it was soon realized that if the model describing the fuel film lag was developed, more complicated schemes to compensate for engine transient AFR excursions can be utilized. If the interrelationship between AFR excursion and variables such as throttle angle and manifold pressure were known, programs involving logical calculations could be computed in the microprocessor to furnish an adequate quantity of fuel as a function of the appropriate variables. The very first efforts in this direction are attributed to Stivender (1978) who illustrated the fuel dynamics with simple transfer functions. Stivender then formulated the time constant of the fuel lag as a function of engine coolant temperature. Wu (1980) worked on the same lines and developed a model in compliance with the physical description of fuel impaction on manifold walls and subsequent vaporization into the air stream. This model yielded a first order transfer function similar to that of Stivender.

It was during this period when transient AFR behaviour received a extended interest with the development of a fast response A/F ratio monitor by Ricardo of England. Probably, a high degree of precision in following the AFR excursions with rise times on the order of one-second made this device very popular. With ongoing research efforts, came forth the dynamic model of Aquino (1981) incorporating the fuel film lag. This model is now referred

to most researchers working on the topic. Aquino examined various possible causes of transient AFR excursions, quantified their relative importance and provided a basis for transient compensation scheme which was almost non-existent in the available literature at that time. His work was basically obtaining experimental evidence in support of a source suggested by Stivender and Wu and indicates that a fair proportion of transient air-fuel excursions can be described by a primary first order transfer functions as suggested by Wu. Hires and Overington (1981) augmented the scope of the work done by Aquino over a wider range of engine operating conditions. They developed a vehicle calibration method for implementing a dynamic model similar to those of Aquino, Stivender and Wu.

2.3.2 Air Control vs. Fuel Control

AFR control by fuel flow variation is the only system used in production today but for the sake of discussion fuel-air management control strategies can be classified under three categories—fuel control, air control and combined air/fuel control. Fuel control is a natural progression from a carburetor system, in which the fuel amount is regulated to match the air flow requested by the driver through the throttle. In contrast, engine air control system regulates the air flow to match the demands of fuel flow commanded by the driver. Stivender (1978) and Woods (1979) considered this issue and provided a comparison between these two schemes. Stivender realized that in fuel control systems because of response lags in the air sensing elements and transport lags in the fuel flow circuit there is an effective time lag between air input and torque whereas in air-flow control system the response and transport lags of the slower fuel circuit occur simultaneously with those of air flow circuit. Hence air

control systems seems to be self compensating in this regard The engine air control philosophy grew out of the unique requirements of the intake valve throttled (IVT) engine. Due to the absence of an intake manifold vacuum in this engine, fuel carburetion was extremely difficult. Also, due to the mechanical forces required by the IVT valve lift mechanism, an air controller servo system was required (Stivender, 1978). The engines in production today are mostly intake manifold throttled port fuel injected engines and a fuel control strategy is mostly used.

2.3.3 Time-Based vs. Crank-Angle Based

Chin and Coats (1986) explored the significance of reference bases for formulating the compensation of engine dynamics and compared the validity of either time-based or crank-angle based dynamics to eliminate the trial-and-error approach used by the engine control designers of that period. They deduced the transformation formulae between time-based and crank-angle based dynamics to compare the two as engine operating conditions changed. They concluded that engine dynamics seemed to be less varying in the crank-angle domain than in the time domain with the exception of fuel dynamics. Crank-angle based characteristics have also been addressed by Hopkins and Borcherts (1980), Morris and Warlick (1982). For crank angle based dynamics a sampling period which corresponds to the rate of occurrence of intake events is selected for cycle-to-cycle monitoring and control of an engine. In our case, time constant associated with the control dynamics are of the order of 0.2 seconds. This corresponds to about (3000/60) x 0.2 = 10 revolutions. Therefore controlling individual engine cycles is not practical.

2.3.4 Control Oriented Engine Modeling

From time to time, dynamic engine modeling has allured researchers and it is still an active research area today especially with the point view of ongoing advances in the field of nonlinear control theory. Powell (1987) and Powell and Cook (1987) have compiled reviews of many control-oriented engine models and their various aspects of implementation. A large number of dynamic simulation models developed in references noted earlier in this chapter fail to represent accurately the entire engine and give acceptable levels of completeness for engineering purposes. In order to design control algorithms, an automotive engine model should be able to run in real time, as opposed to a large off-line simulation. A real time simulation model must be able to integrate the states of the model and calculate the modeled parameters online.

The characteristic feature of real time control models is that the control algorithm may have embedded in it part or all of the engine model to be used as an observer if the engine states are not directly measurable. These reconstructed states would then be used by the rest of the model to estimate parameters. As mentioned by Moskwa and Hedrick (1987) in their paper, the typical approach to engine control using a real time embedded model would be to:

i. define the engine model structure which in turn would define the states of the nonlinear system,

ii. develop a control algorithm, and

iii. estimate parameters in real time which are required by the control law

iv. if the engine states are not directly measurable then the model can be used as a real

time observer for state estimation.

Moskwa and Hedrick (1987,1988,1989) did extensive work in this field. Apart from developing a real time control model they also devised the nonlinear algorithms for automotive engine control.They conducted a series of experiments at the General Motors Research Laboratories to boost confidence in the real time model. Though their model includes intake manifold dynamics, fuel dynamics, process delays inherent in the four stroke engine cycle and EGR dynamics, but they used it for different engine control problems, not AFR control. They looked into the modulation of engine torque during transmission shift to provide smooth shift transient and discussed the sliding-mode approach to solve the problem.

Into the 1990s, mean value engine modeling of spark ignition engines took shape in the hands of Hendricks, Sorensen and Vesterholm (1990,1991,1992). This model is named "mean value" because it describes the dynamic time development of the mean or average values of important observable engine variables (such as crank-shaft speed, manifold pressure, etc.) as well as key internal engine variables which can not be measured directly (the thermal and volumetric efficiencies, etc.) This nonlinear model claimed to have the same steady state accuracy as a typical dynamometer measurement of the engine over its entire speed/load operating range. This thesis follows very closely the "mean value" engine model because it is so mathematically compact, has relatively few adjustable parameters and can be used on a given engine either on the basis of measurements or steady state results of larger cycle simulation packages. The authors (Hendricks, Vesterholm et al.) being impressed by the excellent steady state and dynamic accuracy of the model, developed a nonlinear, closed loop, control observer for the transient air/fuel ratio control accuracy. Their work evolved a

nonlinear fuel film compensator and closed loop observer. The former furnished a justification for cancelling the need to study fuel-film dynamics; the latter improved robustness with respect to modeling error and measurement noise. The closed loop observer was based on a constant gain extended Kalman filter. The new observer setup is competent to carry out condition monitoring while at the same time controlling the primary air/fuel ratio task.

The latest generation of micro controllers exemplified the transition from sensor based electronic engine control systems (EECS) to chip based engine computer/controller. One of the main reason for this shift was EECS cannot keep track of production line A/F ratio control accuracy over an engine's life time. They were not robust with respect to modelling errors resulting from engine wear, aging or lack of maintenance. Electronic engine control strategies were based on static engine maps and semi-static models of engine dynamics leading to control strategies based on rudimentary classical frequency domain methods and were applicable in principle only to linear, SISO (single input, single output) systems. The instantaneous control accuracy possible with such strategies were limited. The fact that engines are a set of coupled nonlinear systems with multiple inputs and outputs (with widely differing response times) posed heavy challenges to the EECS strategies. The present generation control systems are a much more novel innovation motivated at augmenting the A/F ratio control accuracy over the entire engine operation cycle. It has lead to the implementation of multivariable state variable feedback loops and optimal control techniques to engine control. Cassidy, Athens and Lee (1980), Morris and Powell (1983), Hendricks and Poulsen (1986, 1991) are some researchers who looked into A/F ratio control problem emerging from the limitations of first generation control strategies. Hendricks and Sorenson

(1991,1993) emphasized that state variable feedback is inherently robust from a stability point of view but it cannot increase the accuracy of air/fuel ratio control because the major problem is not one of stability but has been shown to be mainly a measurement and/or estimation problem (1991). The solution proposed by them is to use an observer to obtain information about the engine which can- not be measured directly.

The observer based approach to the air-fuel ratio control problem generated a new interest among the researchers. Chang (1993) explores the application of state-space design methodology in high band-width AFR control and came out with event-based observer. He emphasized the fact that the operation of a reciprocating IC engine corresponds to four events (intake, compression, power and exhaust) and hence the dynamics can be best described by their rate of change with respect to crank angle since the crank angle is the natural "clock" instead of time. He developed a microprocessor controlled cycle-to-cycle fuel metering scheme which differs from off-line simulation model or a simple phenomenological transfer function model and was verified by experiments on an SI engine implemented with state-of-the-art electronics. The potential of using state-space control methods as a means of achieving accurate A/F ratio control was researched thereafter by Fekete, Amstutz and Powell (1995) and Jones, Ault and Franklin (1995). All these authors stressed heavily the method for estimating the parameters such as time constants and delay times which need to be determined experimentally. Jones, Ault and Franklin used a nonlinear least squares identification technique to determine accurately the model parameters using normal engine operating data.

Recently drive-by-wire throttle systems are getting popular because of their potential

for improving both drivability and fuel economy (Danno et al.,1989; Ganoung, 1990). They are analogous to the fly-by-wire concept in aircraft applications. In drive-by-wire throttle systems, the accelerator pedal is connected to an electronic controller rather than directly to the throttle valve and hence facilitates the ability to control the air flow.

2.4 Conclusion

Based on this literature review this thesis looks at mean value engine models with time domain fuel metering and sliding mode control with kalman filtering as a state estimator. The spread of papers reviewed here are also an indication of the widening use of control techniques in the automotive industry. They provide an insight into the current status of electronic engine controls along with the understanding of the main principles involved and their applications.

CHAPTER 3

Engine Modeling

3.1 Introduction

This chapter is dedicated to the development of control-oriented nonlinear and linear dynamic engine models for spark ignition engines. The first half deals with the derivation of a compact mathematical nonlinear engine model which emphasizes the relationships between input and output variables and has a modular structure. Unlike models developed earlier in the literature, this model (to be developed) has applicability over the entire operating range of the engine and with very few changes for simultaneous multi point injection or electronic fuel injection (EFI) and sequential fuel injection (SEFI) engines. During the entire construction of the model, the supposition is that if the relevant engine subsystems have been

described correctly then when they are assembled into an engine unit they will describe the overall engine accurately. Since both the overall system and its subsystems are nonlinear the focus is placed on the subsystem equations to be transparent enough to physical reality with a view towards expediting control system design. The second section deals with a linear engine model using the functional relationships described in nonlinear engine models.

3.2 Why Modeling ?

A model is the dynamic picture of a physical plant and is the mathematical description of the dynamics of the plant. One can then predict the response of the physical plant to a prescribed input, from the outputs of the model when the same input is applied to the mathematical model.

3.2.1 Simulation

A model is a tool which can be utilized in various ways to carry out engineering analysis and design. Simulations reflect the actual engine behaviour and provide directions for overall improvement in system performance. There are various ways for improvement and simulations are open for each one of them such as through embellished design or implementing a better control scheme. Simulations can handle effectively various subsystems such as on-board computers, electronics, actuators and sensors of an electronic engine control system providing useful information about their performance specifications. Apart from using the simulation alone to predict the actual engine behaviour, a combination of actual hardware components with a real-time model can be used as a reliable experimental tool facilitating

online calibration and validation.

3.2.2 Formulation of Control Scheme

The model is the key for the implementation of modern model-based control algrothims for efficient system control. The control schemes are getting more and more sophisticated with advances in microprocessors and can be realized only with an accurate and efficient model of the physical plant in hand. The engine model embedded in a control algorithm should be simple enough to run in real time while still incorporating the critical dynamics.

This work develops such a model of a spark ignition engine and the utility of the engine model for the development of an efficient and effective control system is illustrated by simulation. Emphasis is placed on capturing the main transient effects during engine operation for use in AFR control system design.

3.2.3 Characteristics

A model is not judged by its complexity or simplicity. It relies heavily on how well it can characterize the interrelationships among the internal engine process or components and how efficiently they can be computed. Especially for control system design purposes, the model need only portray the dominant dynamics that are relevant to the proposed usage without losing track of other characteristics to be discussed below which calls for reasonable engineering judgement.

There are certain judging parameters which certify the overall effectiveness of the model in describing the engine dynamics and predicting the effects of control inputs on engine outputs. These characteristics are as follows:

3.2.3.1 Physical Process Based

Engine models based on steady state mapping between input and output variables require extensive engine testing which is both time consuming and often inconsistent. It also demands the building of a prototype engine in order to be capable of predicting behaviour. On the other hand, a model may be formulated based on physical laws governing the engine processes that require very few tests to predict the physically significant engine parameters.

3.2.3.2 Reduced Computation Time

A model, which incorporates very complex and detailed features of fluid dynamics, chemistry and thermodynamics, will require relatively great amount of computation time. This may not be consistent with its applicability for embedded controller design. Hence great emphasis should be placed on reducing the total time cost by developing a computationally efficient model.

3.2.3.3 Averaged Behaviour Approximation

There are certain lumped parameters such as volumetric efficiency

for the induction process and fuel conversion efficiency for the combustion process, which are calibrated from engine data. They are given a functional form having strong physical significance and are used to characterize engine processes. The model predicts an averaged value of the variable over one cycle instead of an accurate instantaneous value.

3.2.3.4 Global and Dynamic

The model should be both globally applicable and dynamic. When driving a vehicle, the engine encounters various transients with rapidly changing speed and load and occasionally operates in a steady state condition for a prolonged period. The dynamic nature of the model lies in the fact that it should be able to capture the transients and predict the slightly-out-of -the-ordinary solutions for tracking transients effectively. Since the engine operates in conditions with widely fluctuating loads and speeds, the model should be globally applicable to the entire operating range of the engine. This is important for characterizing the engine behaviour over the entire operating range taking into account system nonlinearity and time varying characteristics.

3.2..3.5 Modularity

Modularity is one of the basic features of any real-time model used for simulating a physical plant. It is not only good practise but highly recommended in view of technology advancement, which calls for

incorporation of new features or installation of improved components. The entire physical plant is divided into separate entities or components which are modeled and verified separately. The complete model reflects the actual input and output integration of all subsystems. This has the effect of accelerating the application of the same model to a variety of engines with same or different engine components. Modularity permits the model to evolve, and to be tailored to suit current interests and it is relatively easy to tune to a particular application.

In a nutshell, the model of an engine developed with the above attributes is efficient in terms of manpower, hardware and test cell utilization.

3.3 Engine model development

In the case of a four-stroke SI engines the whole process of power generation is divided into four processes. These processes are intake, compression, power and exhaust. The air-fuel mixture goes into the cylinder during the intake stroke which is then subjected to a compression stroke. The mixture is ignited before the end of compression stroke by a spark plug leading to the combustion of the compressed mixture which expands during the power stroke thereby converting the chemical energy of the mixture into mechanical work at the crank-shaft. Finally, the exhaust stroke drives the burned mixture out of the combustion chamber. A diagram of an SI engine with a port fuel injection system and intake and exhaust systems is shown in Fig. 3.1. In the following sections a nonlinear engine model will be developed which will portray the response of the engine to various inputs.

3.3.1 Nonlinear Model Formulation

The model to be developed will consist of following dynamic elements modeled separately:

a. Intake Manifold Dynamics

(1) air flow dynamics

(2) fuel flow dynamics

b. Engine crankshaft rotational kinetics and load

c. Cycle Delay and Exhaust Transport Delay

d. Exhaust and Exhaust Gas Oxygen (EGO) sensor dynamics

Inputs / Outputs

The key inputs are:

a. Throttle Angle (α)

b. Load (T_L)

c. Fuel flow rate (via pulse width modulated injection) $\left(\dot{m}_f\right)$

The first two inputs are considered disturbances while the third is the manipulated variable of the control system to achieve a desired air-fuel ratio. The throttle angle is commanded by the driver of the vehicle while the load is a function of external driving environmental factors.

The outputs of concern are:

a. Intake manifold pressure (p_m)

b. In-Cylinder AFR (ϕ_c)

c. Engine Speed (N)

d. EGO Sensor Output (ϕ_m)

Of these, the second is the desired variable to be controlled while the fourth is the actual variable measured.

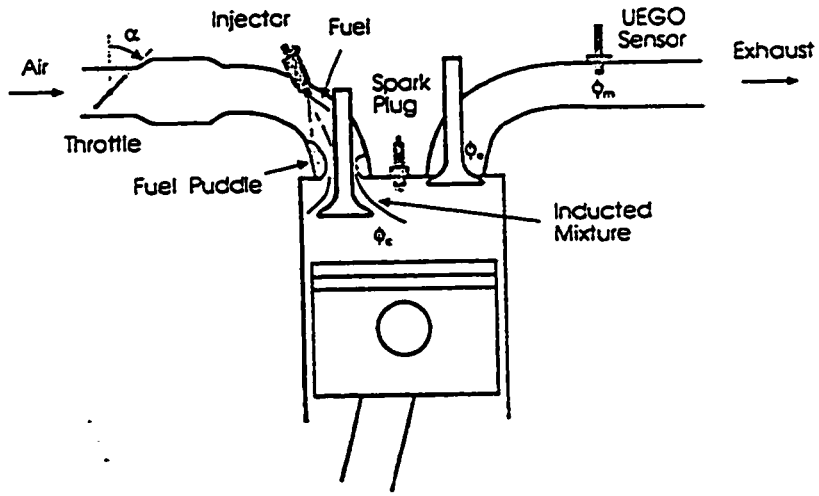

Figure 3.1: Port Fuel-Injected Engine

3.3.2 Intake Manifold Dynamics

Intake manifold is comprised of a throttle valve followed by conduit and runners leading to individual cylinders. The following sub sections will focus on the dynamics of air flow and fuel flow in the manifold. Emphasis is placed on keeping the dynamics consistent to the real physical process that occur during normal driving mode.

3.3.2.1 Air Flow

As the throttle valve opens gradually, air flows into the manifold plenum and then into the cylinder. The first device it encounters is the throttle valve, which is commanded by the driver through the accelerator pedal and can vary significantly based on load and speed requirements. This allows a wide range of air flow rates through the throttle valve as the throttle open area changes. For this work, a simple throttle with round bore and elliptical throttle plate is considered. The throttle open area A_{th} as a function of throttle plate angle α was derived by Harrington and Bolt (1970).

$$A_{th}(\alpha) = \frac{\pi D^2}{4}\left(1 - \frac{\cos\alpha}{\cos\alpha_0}\right) + \frac{D^2}{2}\left[\frac{a}{\cos\alpha}\left(\cos^2\alpha - a^2\cos^2\alpha_0\right)^{1/2} + \frac{\cos\alpha}{\cos\alpha_0}\sin^{-1}\left(\frac{a\cos\alpha_0}{\cos\alpha}\right) - a\left(1-a^2\right)^{1/2} - \sin^{-1}\alpha\right] \tag{3.1}$$

$$\text{for } \alpha_0 \le \alpha \le \cos^{-1}(a\cos\alpha_0)$$

where $a = d/D$

d is the throttle shaft diameter, D is the throttle bore diameter, where d = 0.79 cm and D = 3.16 cm as given in Fig. 3.2 , and α_0 is the angle at the closed throttle . The throttle open area increases as the throttle angle increases and reaches its maximum value when $\alpha = \cos^{-1}(a\cos\alpha_0)$

The maximum value of throttle open area A_{th} is reached when $\alpha = \cos^{-1}(a\cos\alpha_0)$:

$$A_{th}(\alpha) = \frac{\pi D^2}{4} - \frac{D^2}{2}\left[a\left(1-a^2\right)^{1/2} + \sin^{-1}\alpha\right] \cong \frac{\pi D^2}{4} - dD$$

If the throttle angle is further increased the effective throttle open area remains unaffected as it is restricted by the throttle bore and shaft. An approximation based on Harrington and Bolt's formula is given by Hendricks (1990) in his Mean Value SI Engine Model

$$A_{th}(\alpha) = \frac{\pi D^2}{4}\beta(\alpha) \tag{3.2}$$

where

$$\beta(\alpha) = \begin{cases} 0, & 0 \le \alpha \le \alpha_0 \\ 1 - \cos(\alpha) - b_0, & \alpha_0 \le \alpha \le \alpha_2 \\ A_N & \alpha_2 \le \alpha \le 90^0 \end{cases} \tag{3.3}$$

where a = D/d

$b_0 = \alpha_0^2 / 2$, $\alpha_2 = \cos^{-1}(a \cos(\alpha_0))$

$A_N = 1 - 4a/\pi$

Fig. 3.2 depicts the throttle open area as a function of throttle plate angle calculated using Eqs. (3.1) and (3.2). As it is evident from Fig. 3.1 that the approximation suggested by Hendricks matches very well with the formula suggested by Eq. (3.1) except for large throttle plate angles where the effects of throttle plate shaft become significant.

The flow rate of air past the throttle is given by the one-dimensional orifice equation for compressible fluid flow is as follows (Heywood,1988):

$$\dot{m}_{at} = \frac{C_d A_{th} p_o}{\sqrt{RT_o}} \left(\frac{2\gamma}{\gamma - 1}\right)^{1/2} \left[\left(\frac{p_m}{p_o}\right)^{2/\gamma} - \left(\frac{p_m}{p_o}\right)^{(\gamma+1)/\gamma} \right]^{1/2} \tag{3.4a}$$

or for choked flow with $\frac{p_m}{p_o} < \left(\frac{2}{\gamma+1}\right)^{\gamma/\gamma-1}$

$$\dot{m}_{at} = \frac{C_d A_{th} p_o}{\sqrt{RT_o}} \gamma^{1/2} \left(\frac{2}{\gamma+1}\right)^{(\gamma+1)/2(\gamma-1)} \tag{3.4b}$$

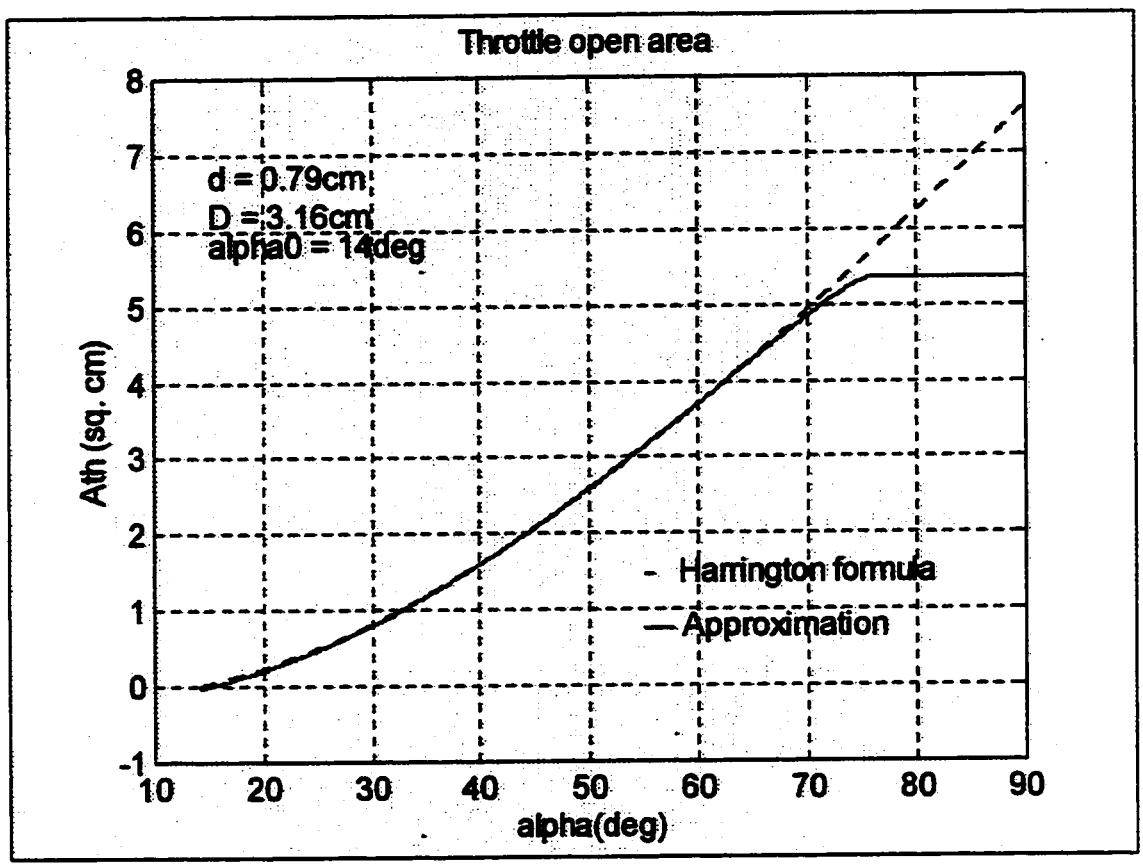

Figure 3.2: Throttle open area Vs. throttle plate angle.

where p_o and T_o are the upstream stagnation pressure and temperature , which are assumed to be at atmospheric conditions. p_m is the manifold pressure downstream of the throttle

plate, $C_d = 0.5$ is the discharge coefficient. which is assumed constant, $\gamma = 1.4$ is the ratio of specific heats for air and $R = 8.314$ J/K-mol is the universal gas constant.

3.3.2.2 Volumetric Efficiency

As the air flow proceeds the next major restriction is the inlet valve to the combustion chamber. The air flow rate through an inlet valve can be modeled in a similar fashion to that used in calculating the air flow through the throttle. The orifice flow equation can be utilized to calculate the air flow into the cylinder using the pressure difference between upstream intake manifold pressure and downstream cylinder pressure. From a design point of view the valve open area depends on the valve geometry and should be kept large in order to minimize inlet-pressure loss, exhaust blowdown loss and pumping losses. It also depends on the valve lift which is not constant during the engine cycle. Inclusion of all these features will give a good physical description of the process but increases complexity and computation time which is not preferable for a control oriented model. Hence the air flow rate into the cylinder is given as:

$$\dot{m}_{ap} = \frac{\eta_v V_d (N/60)\rho_{ai}}{2}, \tag{3.5}$$

where η_v is the volumetric efficiency, N is the crank shaft speed, V_d is the engine displacement volume and ρ_{ai} is the inlet air density. Volumetric efficiency is an internal engine variable which can not be measured directly. It is defined as the mass of fresh mixture which passes into the cylinder in one suction stroke, divided by the mass of this mixture which would fill the piston displacement at inlet density. In order to evaluate this

quantity, it is necessary to define the inlet density as the density of fresh mixture in or near the inlet port. It may not be always be convenient, or even possible, to measure ρ_{ai} at the inlet port, however it can always be measured in the atmosphere near the air intake to the engine. When ρ_{ai} is measured at this point the resulting volumetric efficiency measures the flow performance of all the equipment in the system between air intake and cylinder, as well as the pumping performance of the cylinder itself. The volumetric efficiency based on this method of measurement is called the over-all volumetric efficiency.

In constructing the instantaneous functional expression for the volumetric efficiency, air flow measurements were conducted on a Ford 1.1 L engine and the volumetric efficiency, η_v, calculated for each measurement by Hendricks and Sorenson for their Mean value engine model (1990) . At any given crankshaft speed the volumetric efficiency, η_v, was found to be linearly dependent on the manifold pressure, p_m, and the speed N dependence was found to be quadratic. The functional dependence of the volumetric efficiency for the engine model is

$$\eta_v(N, p_n) = \eta_{vn0} + \eta_{vn1} N + \eta_{vn2} N^2 + \eta_{vp1} p_m \tag{3.6}$$

where η_{vn0}=0.63, η_{vn1} = 6.3e-5, η_{vn2} = -1e-8 and η_{vp1} = 0.13 are constants.

Fig. 3.3 shows the Volumetric efficiency based on the ambient pressure plotted against the crankshaft speed with the manifold pressure as a parameter. These points were obtained using the relation between η_{vol} and η_{vamb} ;

$$\eta_{vamb}\rho_{amb} = \eta_{vol}\rho_{man}$$

assuming that $T_{amb} \cong T_{man}$ and ρ_{amb} and ρ_{man} are the ambient and manifold air densities respectively.

For the intake manifold air density ,the ideal gas law gives

$$\rho_{ai} = \frac{p_m}{RT_m}, \tag{3.7}$$

where p_m and T_m are the manifold pressure and temperature, respectively. Therefore the flow rate for a four stroke engine is

$$\dot{m}_{ap} = \frac{\eta_v V_d (N/60) p_m}{2RT_m} \tag{3.8}$$

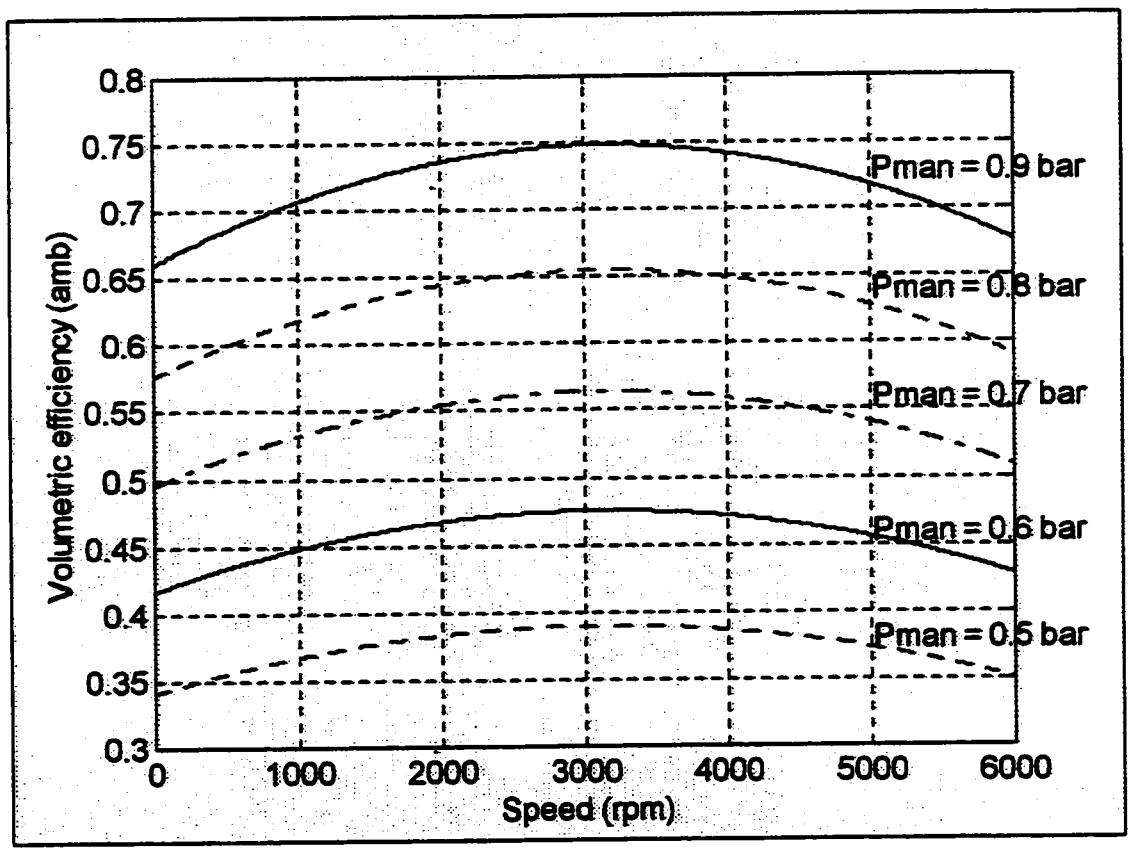

Figure 3.3: Volumetric efficiency based on the ambient pressure plotted against the crank-shaft speed with the manifold pressure as a parameter.

3.3.2.3 Air Flow Model for Manifold

The air flow through the manifold is modeled as per the filling and emptying model suggested by Heywood(1988). $\dot{m}_{at}$ is the air flow that enters the manifold through the throttle and $\dot{m}_{ap}$ is the air flow pumped out of the manifold into the cylinder.

The continuity equation for air flow into and out of the intake manifold is

$$\frac{dm_{ai}}{dt} = \dot{m}_{at} - \dot{m}_{ap} \tag{3.9}$$

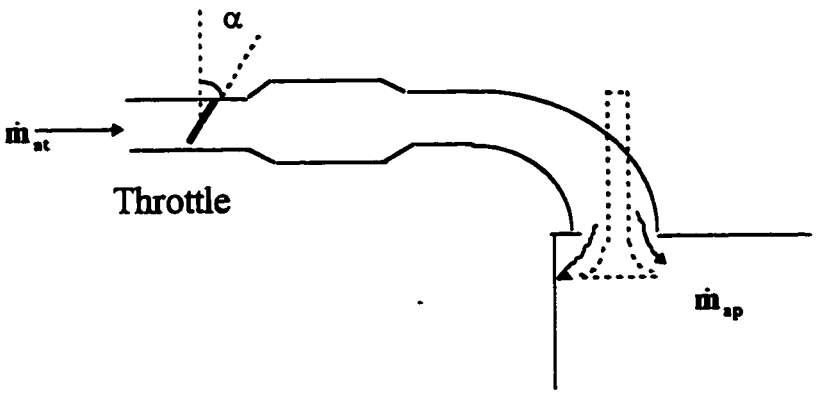

Figure 3.4: Air flow in manifold

Assuming that at any given time the manifold pressure is uniform throughout the intake manifold (Chang and Powell,1993), the intake manifold temperature is constant, and the ideal gas law is valid($p_m V_m = m_{ai} R T_m$). Using Eqs. (3.8) and (3.9)

$$\frac{V_m}{RT_m}\dot{p}_m = -\frac{\eta_v V_d (N/60) p_m}{2RT_m} + \dot{m}_{at} \tag{3.10}$$

Rearranged, we have

$$\dot{p}_m = \frac{-\eta_v N V_d}{120 V_m} p_m + \frac{R T_m}{V_m} \dot{m}_{at} \tag{3.11}$$

since $\dot{m}_{at}(\alpha, p_m)$ is not linear in p_m and $\eta_v(N, p_m)$ is dependent on p_m, therefore Eq. (3.10) is not a linear differential equation.

3.3..2.4 Fuel Flow

The model to be presented here divides fuel flow into two parts: a fuel vapor flow and a liquid fuel film flow. When the fuel comes out of the injector, a part of it strikes the wall of manifold and becomes fuel film while the remaining fuel vapor reaches the engine port together with the air flow within an engine cycle. The intake manifold is assumed to be heated by the engine coolant. The portion of the fuel flow which becomes the fuel film in the manifold is evaporated off the heated intake manifold with a time constant, τ_f. The evaporated fuel then combines with the fuel vapor flow and becomes the total fuel flow into the intake valves of the engine.

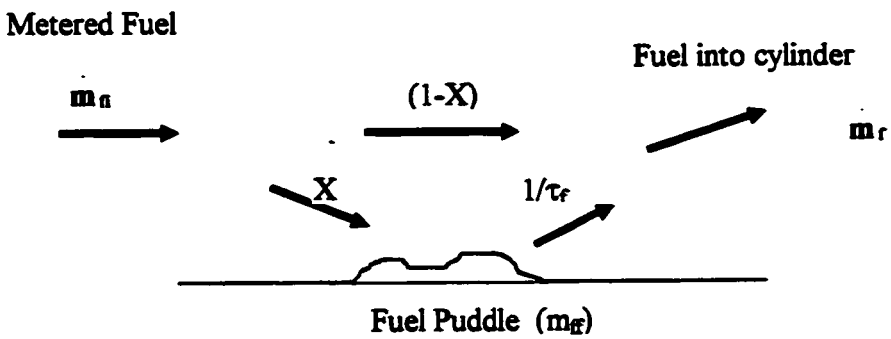

Figure 3.5: Fuel Film Model on Manifold Wall

The fraction of the fuel flow which strikes the manifold and becomes fuel film is defined as X while that which becomes fuel vapor is 1-X. At a given manifold temperature, X is either a function of throttle angle α or is a constant depending on the type of engine.

The model can be expressed in equation form as (Hendricks, 1990):

$$\begin{aligned} \dot{m}_{fv} &= (1-X)\dot{m}_{fi} \\ \dot{m}_{ff} &= \left(\frac{1}{\tau_f}\right)(-\dot{m}_{ff} + X\dot{m}_{fi}) \\ \dot{m}_f &= \dot{m}_{fv} + \dot{m}_{ff} \end{aligned} \tag{3.12}$$

where

m_{ff} : liquid fuel film mass

m_{fi} : injected fuel

m_{fv} : mass of fuel vapor

m_f : fuel entering the cylinder

X : fraction of fuel flow which strikes the manifold and becomes fuel film

τ_f : time constant of the fuel evaporation process

The function $X(\alpha)$ can be fitted closely by the expression (Hendricks 1991)

$$X(\alpha) = \begin{cases} 0, & 0 \le \alpha \le \alpha_0 \\ a_0(1-\cos(\alpha)-b_0), & \alpha_0 \le \alpha \le \alpha_2 \\ X_1 & \alpha_2 \le \alpha \le 90^0 \end{cases} \tag{3.13}$$

where closed throttle angle, α_0, is small, $a_0 \approx 1$, α_o is the closed throttle angle (in radians), $b_o \approx \alpha_o^2 /2!$ and $\alpha_1 \approx 60^0$ and $X_1 \approx 0.5$ - 0.8 are constants. Fig. 3.6 shows the block diagram of the fueling dynamics of an injection engine. Both the fuel vapor path and fuel film path are illustrated separately. The sum of these contributions is the cylinder intake valve fuel flow.

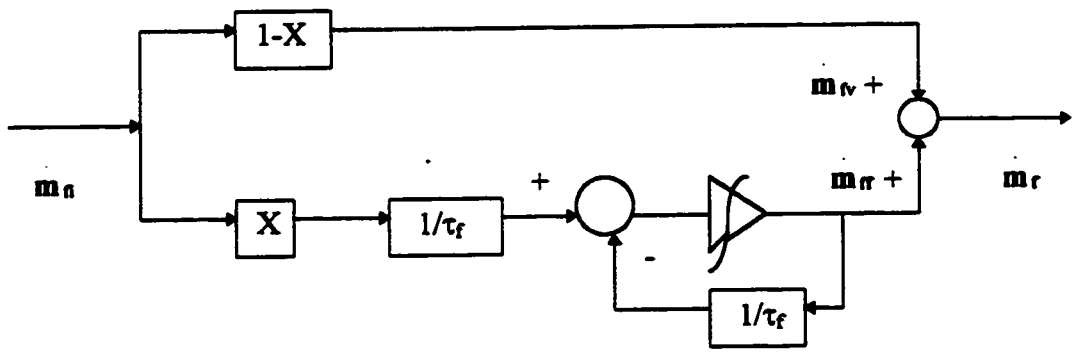

Figure 3.6: Block diagram of the fueling dynamics of an injection engine

3.3.3 Engine Inertia and Load

This section describes the rotational dynamics and derives the crank shaft speed state equation. It is based on physical submodels of the frictional and aerodynamic losses as given by Hedrick and Cho (1988). In equation form it is expressed as

$$I_{eff}\,\dot{\omega}_e(t) = T_{ind}(t) - T_{fric}(t) - T_{aero}(t) - T_{roll}(t) \qquad (3.14)$$

where

T_{ind} = indicated torque

T_{fric} = engine friction torque

T_{aero} = aerodynamci drag

T_{roll} = rolling friction torque

I_{eff} is the effective rotational inertia, listed in table 3.1, which includes vehicle mass reflected through the tires and transmission. The engine speed N in RPM is obtained as:

$$\mathbf{N} = \left(\frac{60}{2\pi}\right).\omega_e \tag{3.15}$$

where the indicted torque, $T_{ind}(t)$, is

$$\mathbf{T_{ind}(t) = k_1.\frac{\dot{m}_{at}(t-\Delta t_{it})}{\omega_e(t-\Delta t_{it})}.AFI(t-\Delta t_{it}).SI} \tag{3.16}$$

where k_1 is a constant, listed in table 3.1, $\dot{m}_{at}$ is the air flow rate into the intake manifold, $\Delta t_{it} \approx 5.5/\omega_e$ (Hedrick and Cho,1988) is the intake to torque production time delay, AFI(t) is a normalized air fuel influence function through which the air-to-fuel ratio at the intake runners affects the torque production, and SI(t) is a normalized spark influence function through which spark retard (or advance) at the time of combustion affect the torque production. Table 3.1 lists the parameters used in this study, which are typical to midsize vehicle in first gear. Fig. 3.7 shows a typical air fuel influence function as a function of air-to-fuel ratio, and Fig. 3.8 shows a typical spark influence function as a function of the deviation in spark angle from MBT (that is., minimum spark advance for best torque) in degrees.

The engine friction torque, $T_{fric}(t)$, is

$$\mathbf{T_{fric}(t) = k_2 + k_3.\omega_e(t)} \tag{3.17}$$

Table 3.1 Parameters for Speed Model

Symbol	Numerical Value
k_1	$1.0451*10^6$ N.m./kg
k_2	15.0 N.m
k_3	0.107 N.m.s
k_4	$6.339*10^{-4}$N.m.s^2
k_5	6.129 N.m
I_{eff}	2.675 kg.m^2

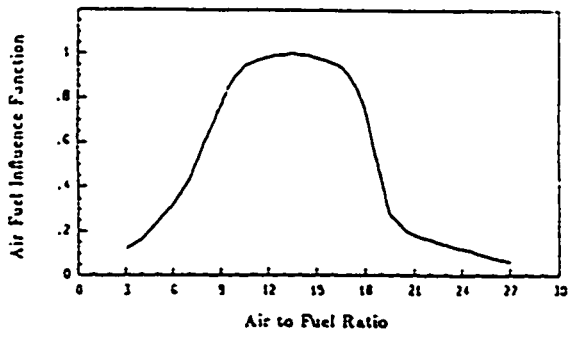

Figure 3.7: Air-Fuel Influence Function (adapted from Hedrick and Cho, 1988)

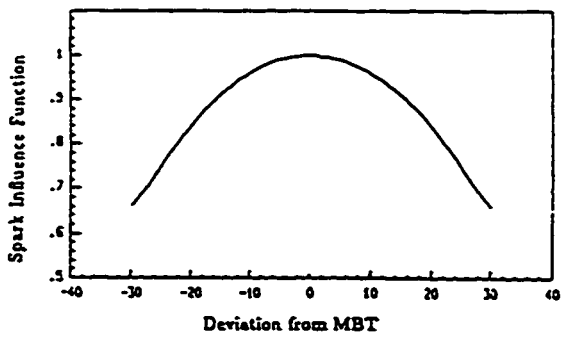

Figure 3.8: Spark Influence Function (adapted from Hedrick and Cho)

The aerodynamic drag term lumped to the rotational dynamics , $T_{aero}(t)$, is

$$T_{aero}(t) = k_4 . \omega_e^2(t) \tag{3.18}$$

The rolling friction term, $T_{roll}(t)$, is,

$$T_{roll}(t) = k_5 \tag{3.19}$$

The average time delay Δt_{it} from the intake stroke to the power stroke is approximately 360 degrees in crank angle. In the time domain this corresponds to Δt_{it} = 60/N. The constants k_1 through k_5 and I_{eff} in equations (3.13) through (3.18) need to be determined empirically for different engines. They are listed for a typical mid size vehicle in table 3.1.

3.3.4 Process Delays

The output, air-to-fuel ratio, is measured at the exhaust using a universal exhaust gas oxygen (EGO) sensor. Thus, the output measurement is delayed by two factors: the cycle delay due to engine events and the exhaust gas transport delay.

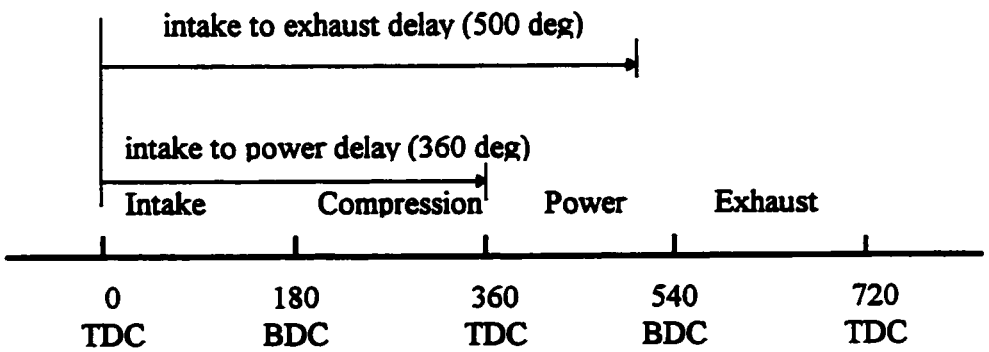

Figure 3.9 Engine Cycle Delay

3.3.4.1 Cycle Delay

The mixture in the cylinder after the intake valve closes is subject to a compression stroke and then a power stroke. Before the end of the power stroke, the exhaust valve opens and the burned gases start to leave the cylinder. This occurs approximately 500 crank angle ($\theta_{EVO} = 500^0$) after the beginning of the intake stroke, when the metered mixture was first inducted.

3.3.4.2 Exhaust Transport Delay

The sensor measures the AFR at a location downstream from the exhaust valve. There is a transport delay for the exhaust gases to flow from the exhaust valve to the oxygen sensor. This causes an extra phase lag in the system. In this work, it is assumed that the sensor is located very close to the exhaust valve (22 cm downstream)and hence the exhaust transport delay is treated as a constant (in the time domain) for all the speed ranges (Chang and Powell, 1993) as $t_d = 0.0042$ sec. The inherent cycle delay of 4-stroke engines along with the transport delay present a challenge when designing the control system.

3.3.5 Exhaust and EGO Sensor Dynamics

3.3.5.1 EGO Sensor

The sensors provide a signal dependent on the oxygen concentration in the exhaust gas which is an indication of the air-fuel ratio. The wide range type UEGO(Universal Air-Fuel Ratio Heated Exhaust Gas Oxygen) sensor is used in this work to provide a high resolution AFR feedback signal to the engine controller.

Regarding the dynamic behavior, the combined exhaust gas transport + UEGO sensor response was modeled as a transport delay followed by a first order lag (Chang and Powell, 1993):

$$\tau_e \dot{\phi}_m(t) + \phi_m(t) = \phi_e(t - t_d) \tag{3.20}$$

where ϕ_m is the equivalence ratio measured by the UEGO sensor, ϕ_e is the equivalence ratio at the exhaust valve, τ_e is the lag time constant and t_d is the transport delay. This can also be written as :

$$\tau_e \dot{\phi}_m(t) + \phi_m(t) = \phi_e(t - \delta) \tag{3.21}$$

where ϕ_c is the equivalence ratio of the induced mixture also termed as In-Cylinder Equivalence Ratio:

$$\phi_c = \left(\frac{1}{(A/F)_s}\right).\frac{\dot{m}_{ap}}{\dot{m}_f} \tag{3.22}$$

(A/F)s is the stoichiometric air-fuel ratio and δ is

$$\delta = \left(\frac{\theta_{EVO}}{720}\right)T + t_d \tag{3.23}$$

T is the sampling period. $T = \frac{120}{n_{cyl}N}$ sec, where n_{cyl} is the number of cylinders and N is the engine speed in RPM. The total delay δ includes the engine cycle delay and the exhaust transport delay.

3.3.6 Fuel Injector

The amount of fuel injected per injection is more or less linearly proportional to the duration of the current pulse that excites the solenoid coil. The amount of fuel injected is approximated by

$$\mathbf{m_{fi} = K_f\left(t_{inj} - t_0\right)} \tag{3.24}$$

where t_{inj} is the fuel pulse width and $t_o = 0.41$ ms is the injector no-flow period and $K_f = 4.52 \times 10^{-3}$ (gm/ms) is the injector parameter..

3.3.7 Summary of Non-linear Model

3.3.7.1 Air Flow

The throttle open area as a function of throttle plate angle is,

$$\mathbf{A_{th}}(\alpha) = \frac{\pi \mathbf{D}^2}{4}\beta(\alpha)$$

The air flow rate past the throttle into the intake manifold is,

$$\dot{\mathbf{m}}_{at} = \frac{\mathbf{C_d A_{th} p_o}}{\sqrt{\mathbf{RT_o}}}\left(\frac{2\gamma}{\gamma - 1}\right)^{1/2}\left[\left(\frac{\mathbf{p_m}}{\mathbf{p_o}}\right)^{2/\gamma} - \left(\frac{\mathbf{p_m}}{\mathbf{p_o}}\right)^{(\gamma+1)/\gamma}\right]^{1/2}$$

or for choked flow with $\frac{p_m}{p_o} < \left(\frac{2}{\gamma + 1}\right)^{\gamma/\gamma - 1}$

$$\dot{\mathbf{m}}_{at} = \frac{\mathbf{C_d A_{th} p_o}}{\sqrt{\mathbf{RT_o}}}\gamma^{1/2}\left(\frac{2}{\gamma + 1}\right)^{(\gamma+1)/2(\gamma-1)}$$

The air flow rate from the intake manifold into the cylinder is given as,

$$\dot{m}_{ap} = \frac{\eta_v V_d (N/60) p_m}{2RT_m}$$

The intake manifold pressure dynamics is given by:

$$\dot{p}_m = \frac{-\eta_v N V_d}{120 V_m} p_m + \frac{RT_m}{V_m} \dot{m}_{at}$$

3.3.7.2 Fuel Flow

The fuel flow $\dot{m}_f$, entering the cylinder is given by the following model equations.

$$\dot{m}_{fv} = (1 - X)\dot{m}_{fi}$$

$$\dot{m}_{ff} = \left(\frac{1}{\tau_f}\right)(-\dot{m}_{ff} + X\dot{m}_{fi})$$

$$\dot{m}_f = \dot{m}_{fv} + \dot{m}_{ff}$$

3.3.7.3 Engine Inertia and Load

The rotational dynamics and the crank shaft speed state equation is given as

$$I_{eff}\, \omega_e(t) = T_{ind}(t) - T_{fric}(t) - T_{aero}(t) - T_{roll}(t)$$

3.3.7.4 EGO Sensor Dynamics

The equivalence ratio ϕ_m measured by the UEGO sensor is given as

$$\tau_e \dot{\phi}_m(t) + \phi_m(t) = \phi_c(t - \delta)$$

3.3.7.5 Fuel Injector

The amount of fuel injected is given by

$$m_{fi} = K_f(t_{inj} - t_0)$$

The set of equations in sec. 3.3.7 comprise the non linear engine model.

3.4 Linear Engine Model

The use of linear engine models is attractive for two reasons (Franklin et al 1996). First, it facilitates a convenient technique to analyze the dynamics of a nonlinear system in such a way that it can be generalized to a wide variety of physical systems. Second, frequency response techniques can be utilized to validate the linear system models. Once a linear system model is obtained, it can be modified and extended to consider the effects of known non-linearities via robustness analysis techniques. This section deals with the formulation of a linear engine model based on the functional relationships expressed by the non-linear engine model in sections 3.1 and 3.2.

3.4.1 Linearization and Deviation Variables

3.4.1.1 Deviation Variables

In order for an equation to be linear each of its terms must contain no more than one variable or derivative, and it must appear to the first power. The basic assumption is that the response of the linear approximation represents the response of the process in the region near the operating point around which the linearization has been performed. The manipulation of linearized equations is greatly facilitated by the use of deviation variables. A deviation variable is defined as the difference between the value of a variable and its value at the operating point:

$$\hat{x}(t) = x(t) - \bar{x} \tag{3.25}$$

where

$\hat{x}(t)$ is the deviation variable

x(t) is the corresponding absolute variable

$\bar{x}$ is the value of x at the operating point (base value)

In other words, the deviation variable is the difference of a variable from its operating or base value. As the base or operating value of the variable is a constant, the derivatives of the deviation variables are always equal to the corresponding derivatives of the variables:

$$\frac{d^n\tilde{x}(t)}{dt^n} = \frac{d^n x(t)}{dt^n} \qquad \text{for n = 1,2, etc.} \tag{3.26}$$

The operating point is usually at steady state which means that the initial conditions of the deviation variables and their derivatives are all zero:

$$x(0) = \bar{x} \qquad \tilde{x}(0) = 0$$

Also

$$\frac{d^n\tilde{x}}{dt^n}(0) = 0 \qquad \text{for n = 1, 2, etc.}$$

3.4.1.2 Linearization of Functions of Two or More Variables

Consider a nonlinear function of two variables f [x(t), y(t)]. The Taylor series expansion around a point $(\bar{x},\bar{y})$ is given by (Smith and Corripio, 1985)

$$\begin{aligned} f[x(t),y(t)] = f(\bar{x},\bar{y}) &+ \frac{\partial f}{\partial x}(\bar{x},\bar{y})[x(t)-\bar{x}] \\ &+ \frac{\partial f}{\partial y}(\bar{x},\bar{y})[y(t)-\bar{y}] + \frac{1}{2!}\frac{\partial^2 f}{\partial x^2}(\bar{x},\bar{y})[x(t)-\bar{x}]^2 \\ &+ \frac{1}{2!}\frac{\partial^2 f}{\partial y^2}(\bar{x},\bar{y})[y(t)-\bar{y}]^2 \\ &+ \frac{\partial^2 f}{\partial x \partial y}(\bar{x},\bar{y})[x(t)-\bar{x}][y(t)-\bar{y}] + \cdots\cdots \end{aligned} \tag{3.27}$$

The linear approximation consists of dropping the second and higher-order terms to obtain

$$\mathbf{f}\left[\mathbf{x}(t),\mathbf{y}(t)\right]=\mathbf{f}(\bar{\mathbf{x}},\bar{\mathbf{y}})+\frac{\partial \mathbf{f}}{\partial \mathbf{x}}(\bar{\mathbf{x}},\bar{\mathbf{y}})\left[\mathbf{x}(t)-\bar{\mathbf{x}}\right]+\frac{\partial \mathbf{f}}{\partial \mathbf{y}}(\bar{\mathbf{x}},\bar{\mathbf{y}})\left[\mathbf{y}(t)-\bar{\mathbf{y}}\right]$$

or, substituting the definition of deviation variables $\hat{\mathbf{x}}(t)$ and $\hat{\mathbf{y}}(t$

$$\mathbf{f}\left[\mathbf{x}(t),\mathbf{y}(t)\right]=\mathbf{f}(\bar{\mathbf{x}},\bar{\mathbf{y}})+\frac{\partial \mathbf{f}}{\partial \mathbf{x}}(\bar{\mathbf{x}},\bar{\mathbf{y}})\hat{\mathbf{x}}(t)+\frac{\partial \mathbf{f}}{\partial \mathbf{y}}(\bar{\mathbf{x}},\bar{\mathbf{y}})\hat{\mathbf{y}}(t)$$

or

$$\mathbf{F}=\frac{\partial \mathbf{f}}{\partial \mathbf{x}}(\bar{\mathbf{x}},\bar{\mathbf{y}})\hat{\mathbf{x}}(t)+\frac{\partial \mathbf{f}}{\partial \mathbf{y}}(\bar{\mathbf{x}},\bar{\mathbf{y}})\hat{\mathbf{y}}(t) \tag{3.28}$$

where F is a linear deviation function about the operating point $(\bar{\mathbf{x}},\bar{\mathbf{y}})$ The difference between the linear approximation and the actual function is small near the operating point $(\bar{\mathbf{x}},\bar{\mathbf{y}})$ and large away from it. The more nonlinear a function is, the smaller the region over which the linear approximation is accurate.

Thus if a dynamic system were to follow $\dot{\mathbf{x}}=\mathbf{f}(\mathbf{x},\mathbf{y})$ The linearized model would be

$$\dot{\hat{x}}=F=\frac{\partial f}{\partial x}\hat{x}+\frac{\partial f}{\partial y}\hat{y} \tag{3.29}$$

3.4.2 Linearization of Engine Model

From Eq. 3.4 the flow rate of air past the throttle is dependent on throttle angle α and manifold pressure p_m and form Eq. 3.10 the manifold pressure is dependent on speed N, manifold pressure p_m and $\dot{m}_{at}$. That is,

$$\dot{\mathbf{m}}_{at}=\mathbf{f}(\alpha,\mathbf{p}_m)$$

$$\dot{p}_m = F_1(p_m, N, \alpha) \tag{3.30}$$

Upon linearization, functionally,

$$\dot{\hat{p}}_m = K_1 \hat{p}_m + K_2 \hat{N} + K_3 \hat{\alpha} \tag{3.31}$$

where,

$$\dot{\hat{p}}_m = \dot{p}_m - \dot{\bar{p}}_m(\bar{p}_m, \bar{N}, \bar{\alpha})$$
$$\hat{p}_m = p_m - \bar{p}_m$$
$$\hat{N} = N - \bar{N}$$
$$\hat{\alpha} = \alpha - \bar{\alpha}$$

are deviation variables and $\bar{p}_m, \bar{N}, \bar{\alpha}$ are steady state values or operating values for intake manifold pressure, speed and throttle angle respectively. By comparing Eqs. 3.29 and 3.31 it can be shown that

$$K_1 = \frac{\partial F_1}{\partial p_m},$$
$$K_2 = \frac{\partial F_1}{\partial N}$$
$$\text{and} \quad K_3 = \frac{\partial F_1}{\partial \alpha}$$

From Eq. 3.5 the air flow rate into the cylinder is directly related to the intake manifold pressure p_m and crank shaft speed N as

$$\dot{m}_{ap} = F_2(p_m, N) \tag{3.32}$$

Upon linearization

$$\dot{\hat{m}}_{ap} = K_4 \hat{p}_m + K_5 \hat{N} \tag{3.33}$$

where $\dot{\hat{m}}_{ap} = \dot{m}_{ap} - \dot{\bar{m}}_{ap}(\bar{p}_m, \bar{N})$

By comparing Eqs. 3.27 and 3.33 it is found that

$$\mathbf{K}_4 = \frac{\partial \mathbf{F}_2}{\partial \mathbf{p}_m}$$

$$\mathbf{K}_5 = \frac{\partial \mathbf{F}_2}{\partial \mathbf{N}}$$

From Eq. 3.12 the liquid fuel film mass deposited on the wall of the manifold is dependent on the fuel film mass, fuel film injected and the throttle angle as given by

$$\dot{\mathbf{m}}_{ff} = \mathbf{F}_3\left(\dot{\mathbf{m}}_{ff}, \dot{\mathbf{m}}_{fi}, \alpha\right) \tag{3.34}$$

Upon linearization

$$\dot{\hat{\mathbf{m}}}_{ff} = \mathbf{K}_6\hat{\mathbf{m}}_{ff} + \mathbf{K}_7\hat{\mathbf{m}}_{fi} + \mathbf{K}_8\hat{\alpha} \tag{3.35}$$

where

$$\dot{\hat{\mathbf{m}}}_{ff} = \dot{\mathbf{m}}_{ff} - \dot{\mathbf{m}}_{ff}\left(\bar{\mathbf{m}}_{ff}, \bar{\mathbf{m}}_{fi}, \bar{\alpha}\right)$$

$$\hat{\mathbf{m}}_{ff} = \mathbf{m}_{ff} - \bar{\mathbf{m}}_{ff}$$

$$\hat{\mathbf{m}}_{fi} = \mathbf{m}_{fi} - \bar{\mathbf{m}}_{fi}$$

are deviation variables and $\bar{\mathbf{m}}_{ff}, \bar{\mathbf{m}}_{fi}$ are the steady state or operating values for the fuel film mass and mass of fuel injected respectively. Again using Eq. 3.29 in comparison with Eq. 3.35 gives

$$\mathbf{K}_6 = \frac{\partial \mathbf{F}_3}{\partial \dot{\mathbf{m}}_{ff}}$$

$$\mathbf{K}_7 = \frac{\partial \mathbf{F}_3}{\partial \dot{\mathbf{m}}_{fi}}$$

$$\mathbf{K}_8 = \frac{\partial \mathbf{F}_3}{\partial \alpha}$$

Again from Eq. 3.12 the fuel mass flow entering the cylinder is dependent upon fuel film mass, mass of fuel injected and throttle angle.

$$\dot{m}_f = F_4(\dot{m}_{ar}, \dot{m}_a, \alpha) \tag{3.36}$$

Upon linearization

$$\hat{\dot{m}}_f = K_9\hat{\dot{m}}_{ar} + K_{10}\hat{\dot{m}}_a + K_{11}\hat{\alpha} \tag{3.37}$$

where $\hat{\dot{m}}_f = \dot{m}_f - \bar{\dot{m}}_f(\bar{\dot{m}}_{ar}, \bar{\dot{m}}_a, \bar{\alpha})$

Again using Eq. 3.29 in comparison with Eq. 3.37 gives

$$K_9 = \frac{\partial F_4}{\partial \dot{m}_{ar}}$$

$$K_{10} = \frac{\partial F_4}{\partial \dot{m}_a}$$

and $$K_{11} = \frac{\partial F_4}{\partial \alpha}$$

As per the Eq. 3.13 the rate of change of crankshaft speed is dependent upon manifold pressure and crankshaft speed:

$$\dot{N} = F_5(p_m, N) \tag{3.38}$$

Upon linearization

$$\hat{\dot{N}} = K_{12}\hat{p}_m + K_{13}\hat{N} \tag{3.39}$$

where $\hat{\dot{N}} = \dot{N} - \bar{\dot{N}}(\bar{p}_m, \bar{N})$

Using Eqs. 3.29 at 3.39 gives

$$K_{12} = \frac{\partial F_5}{\partial p_m}$$

$$K_{13} = \frac{\partial F_5}{\partial N}$$

The dependence of the rate of change of equivalence ratio on various engine parameters is shown in Eq. 3.38.

$$\dot{\phi}_m = F_6\left(\phi_m, p_m, N, \dot{m}_{ff}, \dot{m}_{fl}, \alpha\right) \tag{3.40}$$

Upon linearization

$$\dot{\hat{\phi}}_m = K_{14}\hat{\phi}_m + K_{15}\hat{p}_m + K_{16}\hat{N} + K_{17}\dot{\hat{m}}_{ff} + K_{18}\dot{\hat{m}}_{fl} + K_{19}\hat{\alpha} \tag{3.41}$$

where $\dot{\hat{\phi}}_m = \dot{\phi}_m - \dot{\bar{\phi}}_m\left(\bar{\phi}_m, \bar{p}_m, \bar{N}, \dot{\bar{m}}_{ff}, \dot{\bar{m}}_{fl}, \bar{\alpha}\right)$

Using Eq. 3.29 in comparison with Eq. 3.41 gives

$$K_{14} = \frac{\partial F_6}{\partial \phi_m}$$

$$K_{15} = \frac{\partial F_6}{\partial p_m}$$

$$K_{16} = \frac{\partial F_6}{\partial N}$$

$$K_{17} = \frac{\partial F_6}{\partial \dot{m}_{ff}}$$

$$K_{18} = \frac{\partial F_6}{\partial \dot{m}_{fl}}$$

$$K_{19} = \frac{\partial F_6}{\partial \alpha}$$

Table 3.2: Engine variables and their steady state values

Variables	Operating Values
Manifold Pressure (p_m)	$8.1*10^4$ (N/m^2)
Crankshaft Speed (N)	3700(rpm)
Fuel-FilmMass Rate($\dot{m}_{ff}$)	$2.5*10^{-4}$(Kg/s)
Equivalence Ratio (ϕ_m)	1

Table 3.3 Linear Model Parameters

Symbol	Numerical
K_1	-84.6593
K_2	$-1.4749*10^{-3}$
K_3	$2.02*10^{6}$
K_4	$6.96*10^{-6}$
K_5	$1.28*10^{-4}$
K_6	-1.0526
K_7	0.0596
K_8	$3.14*10^{-5}$
K_9	1
K_{10}	0.9434
K_{11}	$-3.14*10^{-5}$
K_{12}	0.0646
K_{13}	-1.636
K_{14}	-6.67
K_{15}	$7.25*10^{-6}$
K_{16}	0.0132
K_{17}	$-9.13*10^{-6}$
K_{18}	$-8.614*10^{-6}$
K_{19}	$2.868*10^{-10}$

Eqs. 3.31, 3.33, 3.35, 3.37, 3.39 and 3.41 can be combined into a linearized model of the engine. The engine dynamics can be better observed by putting the linear equations in to a state space system.

$$\dot{\mathbf{x}} = \mathbf{A}\mathbf{x} + \mathbf{B}\mathbf{u} + \mathbf{B}_{\alpha} * \alpha \tag{3.42}$$

where the state vector x is

$$\mathbf{x} = \begin{bmatrix} \mathbf{p}_m \\ \mathbf{m}_{ap} \\ \mathbf{m}_{rr} \\ \dot{\mathbf{m}}_{rr} \\ \mathbf{m}_f \\ \phi_m \\ \mathbf{N} \end{bmatrix}$$

and $$\mathbf{B} = \begin{bmatrix} 0 \\ 0 \\ 0 \\ \mathbf{K}_7 \\ \mathbf{K}_{10} \\ \mathbf{K}_{18} \\ 0 \end{bmatrix}, \qquad \mathbf{B}_\alpha = \begin{bmatrix} \mathbf{K}_3 \\ 0 \\ 0 \\ \mathbf{K}_8 \\ \mathbf{K}_{11} \\ \mathbf{K}_{19} \\ 0 \end{bmatrix}$$

$$\mathbf{A} = \begin{bmatrix} \mathbf{K}_1 & 0 & 0 & 0 & 0 & 0 & \mathbf{K}_2 \\ \mathbf{K}_4 & 0 & 0 & 0 & 0 & 0 & \mathbf{K}_5 \\ 0 & 0 & 0 & 1 & 0 & 0 & 0 \\ 0 & 0 & 0 & \mathbf{K}_6 & 0 & 0 & 0 \\ 0 & 0 & 0 & \mathbf{K}_9 & 0 & 0 & 0 \\ \mathbf{K}_{15} & 0 & 0 & \mathbf{K}_{17} & 0 & \mathbf{K}_{14} & \mathbf{K}_{16} \\ \mathbf{K}_{12} & 0 & 0 & 0 & 0 & 0 & \mathbf{K}_{13} \end{bmatrix}$$

Based on the linear and nonlinear models developed in this chapter a control algorithm and compensator will be devised and discussed in Chapter 5. The linear model facilitates the modern state space design methodology and embedded control algorithm.

CHAPTER 4

Sliding Mode Control

4.1 Introduction

In this chapter, sliding mode control will be reviewed. Sliding mode control is a nonlinear control design technique to achieve guaranteed performance robustness, despite bounded plant uncertainty and disturbances. In Sec. 4.1 the basics of nonlinear control and feedback are highlighted. Then in Sec. 4.2 the sliding mode control law is developed. In Sec. 4.3 two methods for sliding surface design are considered: first order filtering and the linear quadratic optimal method. Sliding control has been applied successfully to robot manipulators, underwater vehicles, automotive transmissions, high performance electric motors, and power systems.

4.2 Nonlinear Control Systems Design

The objective of control design can be stated as: given a physical system to be controlled and the specification of its desired behaviour, construct a feedback law to make the closed loop system display the desired behaviour. If the tasks of a control system involve large range and/or high speed motions, nonlinear effects will be significant in the dynamics and nonlinear control may be necessary to achieve the desired performance.

In linear control, the desired behaviour of a control system can be specified systematically, either in the time domain or in the frequency domain but the systematic specification for nonlinear systems is much less obvious because the response of a nonlinear system to one command does not reflect its response to another command. The following attributes can be considered regarding the desired behaviour of nonlinear control systems:

4.2.1 Stability

The model used for design of a control law must be stable either in a local sense or in a global sense. The region of stability and convergence are also of interest The stability of a nonlinear system often does not imply the ability to withstand persistent disturbances of even small magnitudes (Slotine and Li, 1991).

4.2.2 Accuracy and Speed of Response

It should be considered for some qualitative specifications of the desired behaviour in the operating region of interest for instance some "typical" motion trajectories in the region

of operation. For some classes of systems, appropriate controller design can actually guarantee consistent tracking accuracy independent of the desired trajectory.

4.2.3 Robustness

The effects of persistent disturbance on nonlinear system behaviour are addressed by the concept of robustness which is defined as the sensitivity to effects which are not considered in the design such as disturbance and unmodeled dynamics. The system should be able to withstand these neglected effects when performing the tasks of interest.

4.2.4 Cost

Cost of a control system is determined mainly by the number and type of actuators, sensors, and computers necessary to implement it. Simply put, the cost and controller complexity should be consistent with the customer needs and the particular application.

It is hard to achieve or satisfy all the above attributes because they are usually conflicting in nature and a good control system can be obtained only based on effective trade-offs in terms of for example stability/robustness, stability/performance and cost/performance for examples.

4.3 Sliding Mode Control

The so-called sliding mode control (Utkin, 1977) will be the design methodology used for this work which will allow the models to be imprecise. It is a robust control strategy

aimed at dealing with model uncertainty. Model imprecision are basically of two types:

- **Parametric imprecision** which is uncertainty about plant parameters.
- **Unmodeled dynamics** which is an underestimation or simplified representation of the system dynamics and in certain cases it is a purposeful choice.

Sliding control methodology is based on the remark that it is much easier to control 1^{st}-order systems (i.e., systems described by 1^{st}-order differential equations), be they nonlinear or uncertain, than it is to control general n^{th}-order systems (i.e., systems described by the n^{th}-order differential equations). So n^{th}-order problems are replaced by equivalent 1^{st}-order problems using a notational simplification and it is then relatively easy to achieve "perfect" performance in principle in the presence of a certain class of parametric uncertainties. Modeling inaccuracies can have strong detrimental effects on nonlinear control systems. For the class of systems to which sliding mode control methodology is applicable , it furnishes a systematic approach to the problem of maintaining stability and consistent performance in the face of modeling imprecisions.

In the following sections a notational simplification for transforming the n^{th}-order systems to 1^{st}-order systems will be discussed followed by sliding surface design using single loop filtering and optimal hyperplane design. The canonical form that is employed throughout the design of the hyperplane matrix is also discussed.

In a nutshell the aim of a sliding controller is to

i. Design a control law to account effectively for
    - parameter uncertainty

- the presence of unmodeled dynamics

ii. Quantify the resulting modeling/performance trade-offs, and in particular, the effect on tracking performance of discarding any particular term in the dynamic model.

Sliding controller design provides a systematic approach to the problem of maintaining stability in the face of modeling imprecisions. Finally, it offers the potential of simplifying higher level programming, by accepting reduced information about both task and system.

Practical applications of sliding control are described, for example Yoerger, et al., (1986) underwater vehicles , Hedrick et al., (1988) automotive applications, Harshima, et al.,(1988) robot manipulators. The literature in the field has been active in the past few years.

4.3.1 Sliding Modes

Consider the n^{th} order linear time invariant dynamic system with, in general, m control inputs, modelled by

$$\dot{x}(t) = Ax(t) + Bu(t) + Bd(t) \tag{4.1}$$

where $x \in R^m, u \in R^m, d \in R^m$ The system is assumed to be controllable (that is, any finite state can be reached within finite time by the application of an appropriate finite

control). Initially, it will be assumed that $u \in R^1$ or that a single scalar control only is available. By construction, the disturbance of d(t) are considered matched in that they enter the plant in the same channels as u (t). The disturbance d contains external signals e, as well as plant modeling errors due to linearization and unmodelled dynamics, ΔAx. That is $d = \Delta Ax + e$.

Constraining a linear combination of the states to be zero, that is setting

$$Cx = 0 \tag{4.2}$$

for some row vector C, is equivalent to constraining the n^{th} order dynamics of Eq. 4.1 to an $(n-1)^{th}$ order differential equation given by Eq .4.2. To see this more clearly, transform Eq. 4.1 into a controllable canonical form with

$$\begin{aligned} \dot{x}_1 &= x_2 \\ &\vdots \\ \dot{x}_{n-1} &= x_n \\ \dot{x}_n &= \sum_{i=1}^{n} a_i x_i + bu. \end{aligned}$$

Then Eq. 4.2 can be written

$$\dot{x}_n = \sum_{i=1}^{n-1} c_i x_i. \tag{4.3}$$

where $C_n = 1$ is assumed without loss of generality.

Define a time-varying surface s(t) in the state space $\mathbf{R}^n$ by the scalar equation s=0,

where

$$s = Cx \tag{4.4}$$

is the sliding function so that when the state is not in the sliding mode (on the hyperplane), then s^2 is a measure of the distance from the state to the hyperplane. If the vector C can be chosen so that the dynamics of Eq. 4.4 are in some sense good, then a control which encourages the system state to move onto the sliding mode and thereafter stay on the hyperplane would be desirable.

Assuming a good choice for C is available, then a control which satisfies

$$\frac{d}{dt}s^2 < 0 \tag{4.5}$$

would achieve this goal of inducing the sliding mode in the original system. Eq. 4.5 is sufficiently satisfied if

$$\frac{1}{2}\frac{d}{dt}s^2 = -\eta|s| \tag{4.6}$$

for some $\eta > 0$. Essentially, Eq. 4.6 states that the "squared" distance to the surface, as measured by s^2, decreases along all system trajectories. Thus, it constrains trajectories to point towards the surface s(t). In particular, once on the surface, the system trajectories

remain on the surface . In other words, satisfying the condition of Eq. 4.6 and s=0, or the sliding condition , makes the surface an invariant set. S(t) verifying Eq. 4.6 is referred to as a sliding surface, and the system's behaviour once on the surface is called a sliding regime or sliding mode. Expanding and evaluating Eq. 4.6 gives

$$s\dot{s} = -\eta|s|$$

or

$$\dot{s} = -\eta\, sign(s) \tag{4.7}$$

where

$$sign(s) = \begin{cases} 1 & s>0 \\ 0 & s=0 \\ -1 & s<0 \end{cases}.$$

But, using the nominal plant of Eq. 4.1 with assumed zero disturbances.

$$\dot{s} = C\dot{x} = CAx + CBu \tag{4.8}$$

Therefore,

$$CAx + CBu = -\eta\, sign(s)$$

$$u = -(CB)^{-1}(CAx + \eta\, sign(s)) \tag{4.9}$$

where it is assumed that $(CB)^{-1}$ exists. These same arguments apply if $u \in R^m$ and

$$sign(s) = \begin{vmatrix} sign(s_1) \\ sign(s_2) \\ \vdots \\ sign(s\ ) \end{vmatrix}$$

and the sliding function definer becomes a matrix as. $C \in R^{mxn}$

Substituting the control of Eq. 4.9 into the plant of Eq. 4.1 gives the closed loop system

$$\dot{x} = Ax + B(-CB)^{-1}\left(CAx + \eta\, sign(s)\right) + Bd \tag{4.10}$$

$$\dot{s} = C\dot{x} = CAx + CB(-CB)^{-1}(CAx + \eta\, sign(s)) + CBd \tag{4.11}$$

$$\dot{s} = -\eta\, sign(s) + CBd \tag{4.12}$$

Therefore,in order to have s^2 decrease, the design parameter η must be chosen thus

$$\eta \succ |CB||d(t)| \tag{4.13}$$

If this condition holds, Eq. 4.5 will be guaranteed to be satisfied

4.3.2 Hyperplane Design by Single Loop Filtering

One method for the design of sliding surfaces is to decompose the system into subsystems controlled by a single input. Then design a sliding hyperplane suitable for each input in turn. Then finally recombine the overall system to get a sliding surface matrix definer which is the concatenation of the individually designed sliding surface row vectors

as

$$C = \begin{pmatrix} c_1 \\ \vdots \\ c_m \end{pmatrix}.$$

Thus, in sliding, the system will reside on the intersection of the individual surfaces. The criterion that each component of the sliding function vector, s, get smaller in magnitude will ensure movement towards this intersection. It is noteworthy that for the control of an n^{th} order system with m controls available, the intersection of sliding surfaces will be a subspace of $(n\text{-}m)^{th}$ order and thus m degrees of system freedom have been constrained. The use of filtering concepts was first introduced in Slotine and Sastry (1983) and Pieper (1992, 1994).

For the system of Eq. 4.1, take B_j as the j^{th} column of B and transform the corresponding subsystem given by (A,B_j) into controllable canonical form via the transformation matrix T_j. That is

$$\Phi_j = T_j A T_j^{-1} = \begin{pmatrix} 0 & & I_{n-1} & \\ a_1 & a_2 & \cdots & a_n \end{pmatrix}$$

$$\Gamma_j = T_j B_j = (0 \quad \cdots \quad 0 \quad 1)^T.$$

Then it is reasonable to set the sliding surface for this input as a (n-1)th order low pass filter with time constant λ_j. That is, a filter with laplace domain characteristic equation

$$(s + \lambda_j)^{n-1} = 0$$

or in terms of the output state, x_1,

$$(\frac{d}{dt} + \lambda_j)^{n-1} x_1 = 0. \tag{4.10}$$

Since, by construction, the system state is in controllable canonical form, Eq. 4.10 can be written

$$\left(\lambda_j^{n-1} \quad \cdots \quad \frac{(n-1)!}{i!\,(n-1-i)!} \lambda_j^{n-1-i} \quad \cdots \quad 1 \right) x = 0.$$

Thus

$$C^j = \left(\lambda_j^{n-1} \quad \cdots \quad \frac{(n-1)!}{i!\,(n-1-i)!} \lambda_j^{n-1-i} \quad \cdots \quad 1 \right). \tag{4.11}$$

This procedure can be repeated for each input and in terms of the original systems coordinates, the sliding surface matrix can be written

$$C = \begin{pmatrix} C^1 T_1^{-1} \\ C^2 T_2^{-1} \\ \vdots \\ C^m T_m^{-1} \end{pmatrix}.$$

4.3.3 Optimal Sliding Hyperplane

In finding an appropriate matrix C to specify the sliding dynamics, it is often convenient to transform Eq. 4.1 into the form

$$\begin{pmatrix} \dot{z}_1 \\ \dot{z}_2 \end{pmatrix} = \begin{pmatrix} A_{11} & A_{12} \\ A_{21} & A_{22} \end{pmatrix} \begin{pmatrix} z_1 \\ z_2 \end{pmatrix} + \begin{pmatrix} 0 \\ B_2 \end{pmatrix} u \tag{4.12}$$

and

$$s = \begin{pmatrix} C_1 & C_2 \end{pmatrix} \begin{pmatrix} z_1 \\ z_2 \end{pmatrix} \tag{4.13}$$

where $z_2 \in R^m$ and $B_2 \in \Re^{m \times m}$ and is full rank. Then setting $C_2 = B_2^{-1}$ guarantees that $CB = C_2 B_2 = I_m$. A suitable method for finding the transformation matrix, T, used according to $z = Tx$ is the so-called LU factorization (Dorling and Zinober, 1986) where the square matrix

$$\begin{pmatrix} B & 0_{n\times(n-m)} \end{pmatrix} = L_{n\times n} \begin{pmatrix} U_{m\times m} \\ 0_{(n-m)\times n} \end{pmatrix}.$$

with $L \in R^{n\times n}$ and with orthogonal rows and columns and $U \in R^{m\times n}$, and where U is non-singular and upper triangular.Then

$$B_2 = \begin{pmatrix} \Lambda_{m\times m} & 0_{m\times(n-m)} \end{pmatrix} U \tag{4.14}$$

and $T = \Lambda_{n\times n} L^{-1}$ where $\Lambda_{2\times 2} = \begin{pmatrix} 0 & 1 \\ 1 & 0 \end{pmatrix}$ (That is, .a reverse diagonal identity matrix). A reasonable goal of the system in sliding motion is to minimize some energy cost function as

$$J = \int_0^{\infty} x^T Q x \, dt \tag{4.15}$$

for some admissible postive semi definite weighting matrix, Q. This type of design is contained in Dorling and Zinober (1986). In the transformed coordinates,

$$J = \int_0^{\infty} z^T T^{-T} Q T^{-1} z \, dt$$

Partitioning

$$T^{-T}QT^{-1} = \begin{pmatrix} Q_{11} & Q_{12} \\ Q_{21} & Q_{22} \end{pmatrix}$$

conformably (that is, setting $Q_{11} \in \Re^{(n-m)\times(n-m)}$ and $Q_{22} \in \Re^{m\times m}$) then setting

$$Q^* = Q_{11} - Q_{12}Q_{22}Q_{21}$$
$$A^* = A_{11} - A_{12}Q_{22}^{-1}Q_{21}$$

and

$$\nu = z_2 + Q_{22}^{-1}Q_{21}z_1$$

Then an optimization problem equivalent to minimizing the cost function of Eq. 4.15 subject to the system of Eq. 4.12 can be written as

$$\min_{\nu} J = \int_0^{\infty} z_1^T Q^* z_1 + \nu^T Q_{22}\nu \, dt \tag{4.16}$$

subject to constraint dynamics

$$\dot{z}_1 = A^* z_1 + A_{12}\nu. \tag{4.17}$$

Eqs. 4.16 and 4.17 make up a standard optimal control problem in the pseudo-control ν.

The solution is

$$v = -Q_{22}^{-1} A_{12}^{T} P z_1 \tag{4.18}$$

where P solves the Ricatti equation

$$PA^{*} + A^{*T}P - PA_{12}Q_{22}^{-1}A_{12}^{T}P + Q^{*} = 0. \tag{4.19}$$

Expanding Eq. 4.18 gives

$$z_2 = -Q_{22}^{-1}\,(Q_{21} + A_{12}^{T}P)\,z_1. \tag{4.20}$$

Recall that in sliding, from Eqs. 4.2 and 4.13,

$$\begin{pmatrix} C_1 & C_2 \end{pmatrix} \begin{pmatrix} z_1 \\ z_2 \end{pmatrix} = 0$$

or

$$z_2 = -C_2^{-1} C_1 z_1 \tag{4.21}$$

Now comparing Eqs. 4.20 and 4.21 and using $C_2 = B_2^{-1}$ as previously specified, gives

$$C_1 = B_2^{-1} Q_{22}^{-1} (Q_{21} + A_{12}^{T}P) \tag{4.22}$$

and $$C = (C_1\ C_2)T^{-1} \tag{4.23}$$

where $T = \Lambda T_{max}\ L^{-1}$.

4.4 Conclusions

The sliding mode control methodology using the controller of Eq. 4.9 and the surface design methods of sec. 4.3.2 and 4.3.3 will be used in Chapter 5. The engine model in this work incorporates slow variations in fuel flow dynamics and intake manifold parameters and also considers pure time delay due to combustion process and transport phenomenon. In view of the above differentiating functions, model errors and disturbances, sliding mode control method offers a viable option for robust and systematic approach to design a stable control structure in the face of modeling imprecisions.

CHAPTER 5

Implementation on SI Engine

5.1 Introduction

During the last two decades, optimal control and estimation techniques have been employed in dynamic system applications to aid in development of strategies for control and system identification problems. The model developed in Chapter 3 forms the basis for the application of sliding mode control theory together with estimation theory to design an AFR controller. The controller calculates, for the commanded AFR, the amount of fuel to be injected to match the amount of air induced. Previous work on sliding mode controllers for the exhaust air/fuel ratio is extended and a sliding mode controller with improved performance is developed. Just as multivariable control problems arise in automotive systems, so do problems of multivariable estimation. A state estimator is thus developed to

utilize the potential of state-space control methods and to implement the sliding mode control methods of Chapter 4 which rely on various forms of state feedback. The estimator is used to find the states of the system for use in control function.

5.2 Control Law and Estimator Design

Normally the design for a physical system using state-space methodology comprises two steps.

- Design a control law assuming all the states are available.
- In the real world, however, all the states are not available for measurement so design an observer or estimator.

In most cases not all the state variables are measured. The cost of the required sensors may be prohibitive, or it may be physically impossible to measure all the state variables. The role of estimator is to estimate the entire state vector given measurements of only some of the states. When the control law design is combined with the estimator design and control law is implemented using the estimated state variables rather than actual state variables, we get what is known as compensator or regulator. The estimator can be used for purposes of either implementing a state variable feedback controller or displaying the status of the system variables to the driver as performance or diagnostic information.

5.2.1 Design of Control Law

The fuel pulse width is calculated to provide the appropriate amount of fuel for the air flow at each speed and load. As per the linear model presented in chapter 3

$$\dot{\mathbf{x}} = \mathbf{A}\mathbf{x} + \mathbf{B}\dot{m}_{fi} + \mathbf{B}_{\alpha}\alpha \tag{5.1}$$

where α is a measurable disturbance and

$$\begin{aligned}(\dot{m}_{fi})_s &= \mathbf{K}_{30}\mathbf{p}_m + \mathbf{K}_{31}\mathbf{N} + \mathbf{K}_{32}\alpha + \mathbf{K}_{33}\dot{m}_{fr} \\ &= \mathbf{A}_m\mathbf{x} + \mathbf{B}_m\alpha\end{aligned} \tag{5.2}$$

is the stochiometric input, $(\dot{m}_{fi})_s$, which is the amount of fuel flow per second required theoretically for perfect and complete combustion calculated as

$$(\dot{m}_{fi})_s = \frac{\dot{m}_{ap}}{\left(A/F\right)_s} \tag{5.3}$$

where, $\dot{m}_{ap}$ is the air mass flow rate into the cylinder as found from Eq. 3.5 and $\left(A/F\right)_s$ is the stochiometric air to fuel ratio and the value used for this work is 14.7 (Heywood 1988).

Assuming that the true fuel flow input to the intake manifold is

$$\dot{m}_{fi} = (\dot{m}_{fi})_s + (\dot{m}_{fi})_c \tag{5.4}$$

where $(\dot{m}_{fi})_c$ is the control input, the task of the controller is to adjust the actual fuel flow away from stochiometric in order to dynamically respond to system changes due to load disturbances and throttle commands. Combining Eq. 5.4 with 5.1 gives the new system with the new control input $(\dot{m}_{fi})_c$:

$$\begin{aligned}\dot{\mathbf{x}} &= \mathbf{A}\mathbf{x} + \mathbf{B}\left(\mathbf{A}_m\mathbf{x} + \mathbf{B}_m\alpha + (\dot{m}_{fi})_c\right) + \mathbf{B}_{\alpha}\alpha \\ \dot{\mathbf{x}} &= (\mathbf{A} + \mathbf{B}\mathbf{A}_m)\mathbf{x} + \mathbf{B}(\dot{m}_{fi})_c + (\mathbf{B}_{\alpha} + \mathbf{B}\mathbf{B}_m)\alpha \\ \dot{\mathbf{x}} &= \mathbf{A}_1\mathbf{x} + \mathbf{B}(\dot{m}_{fi})_c + \mathbf{B}_1\alpha\end{aligned} \tag{5.5}$$

We have available as control input, an amount of injected fuel given as a pulse width modulated injection.

$$(\mathbf{m}_f)_t = \mathbf{K}(\mathbf{t}_{inj} - \mathbf{t}_0) \tag{5.6}$$

That is to say we need $\dot{\mathbf{m}}_f$ but we have $\mathbf{m}_f$. Therefore we need a method to derive $\dot{\mathbf{m}}_f$ based on the pulse injection $(\mathbf{m}_f)_t$.

The basic idea is as follows (Pieper, 1992)

If we set

$$\mathbf{d} = \tau(\mathbf{u} - \mathbf{v}) \tag{5.7}$$

and use $$\mathbf{v} = \frac{1}{\mathbf{s}}\mathbf{d} \tag{5.8}$$

as in Fig. 5.1 $$\begin{aligned} \mathbf{sv} &= \mathbf{d} \\ \dot{\mathbf{v}} &= \mathbf{d} \end{aligned} \tag{5.9}$$

and $$\mathbf{d} = \tau\mathbf{u} - \frac{\tau}{\mathbf{s}}\mathbf{d} \tag{5.10}$$

$$\left(1 + \frac{\tau}{\mathbf{s}}\right)\mathbf{d} = \tau\mathbf{u} \tag{5.11}$$

so that we get the transfer function

$$\frac{\mathbf{d}}{\mathbf{u}} = \frac{\tau\mathbf{s}}{\mathbf{s} + \tau} \tag{5.12}$$

Now as $\tau \to \infty$,

$$\frac{\mathbf{d}}{\mathbf{u}} \approx \mathbf{s} \tag{5.13}$$

or $$\begin{aligned} \mathbf{d} &= \mathbf{su} \\ \mathbf{d} &= \dot{\mathbf{u}} \end{aligned} \tag{5.14}$$

Using the above methodology (Pieper, 1992), introduce q as

$$\dot{\mathbf{q}} = \tau \left((\mathbf{m}_n)_t - \mathbf{q} \right) \tag{5.15}$$

In this way as τ gets large

$$\lim_{t \to \infty} \frac{1}{\tau} \dot{\mathbf{q}} = \left((\mathbf{m}_n)_t - \mathbf{q} \right) \quad \rightarrow \quad 0 \tag{5.16}$$

that is $\mathbf{q} \approx (\mathbf{m}_n)_t$ (5.17)

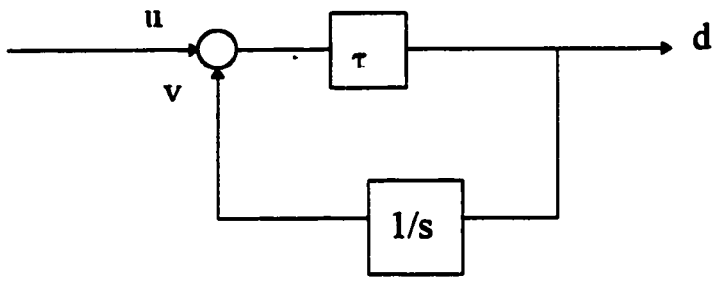

Figure 5.1: Control loop representing the introduction of q.

and note that, by construction

$$(\dot{\mathbf{m}}_n)_c = (\dot{\mathbf{m}}_n)_t \approx \dot{\mathbf{q}} = \tau \left((\dot{\mathbf{m}}_n)_t - \mathbf{q} \right) \tag{5.18}$$

and thus we have found a method for expressing $(\dot{\mathbf{m}}_n)_c$ as a dynamic function of $(\mathbf{m}_n)_t$ and the dynamic variable q. For practical purposes, we normally choose $\tau \in \{10, 1000\}$. Incorporating this technique into the revised system state gives

$$\mathbf{z} = \begin{bmatrix} \mathbf{x} \\ \mathbf{q} \end{bmatrix} \tag{5.19}$$

$$\dot{\mathbf{z}} = \begin{bmatrix} \mathbf{A}_1 & -\tau\mathbf{B} \\ 0 & -\tau \end{bmatrix} \mathbf{z} + \begin{bmatrix} \tau\mathbf{B} \\ \tau \end{bmatrix} (\mathbf{m}_{fi})_t + \begin{bmatrix} \mathbf{B}_1 \\ 0 \end{bmatrix} \alpha \tag{5.20}$$

$$\dot{\mathbf{z}} = \mathbf{A}_N \mathbf{z} + \mathbf{B}_N \mathbf{u} + (\mathbf{B}_\alpha)_N \alpha \tag{5.21}$$

where

$$\mathbf{A}_1 = \mathbf{A} + \mathbf{B}\mathbf{A}_m$$
$$\mathbf{B}_1 = \mathbf{B}_\alpha + \mathbf{B}\mathbf{B}_m$$
$$\mathbf{A}_N = \begin{bmatrix} \mathbf{A}_1 & -\tau\mathbf{B} \\ 0 & -\tau \end{bmatrix}, \qquad \mathbf{B}_N = \begin{bmatrix} \tau\mathbf{B} \\ \tau \end{bmatrix}, \quad (\mathbf{B}_\alpha)_N = \begin{bmatrix} \mathbf{B}_1 \\ 0 \end{bmatrix}$$

Based on this revised system, the sliding mode controller calculates the amount of fuel to be injected so that the amount of fuel entering the cylinder will match the amount of air inducted into the cylinder, taking into account the lag dynamics and associated delays.

5.2.2 Design of Estimator

The only state which is measured is the air fuel equivalence ratio ϕ_m, coming out of Universal Exhaust Gas Oxygen sensor (UEGO). All other states associated with the state vector z, are not measured but are required for the control law computation. This is achieved by designing an estimator which reconstructs the variables of a system from a few measurements. The estimated states $\hat{\mathbf{z}}$ are then used for the control law in place of actual states $\mathbf{z}$.

The basic idea behind estimator design is to use the classical way of overcoming the potential difficulties of open-loop systems, that is use feedback to try to zero the error by driving the system with a term proportional to the error in the estimate. This term is often called an innovations signal. The system output y which is not used in the open loop solution, comes in now because it is related to the quantity z we are interested in:

$$\mathbf{y} = \mathbf{cz} \tag{5.22}$$

and y is available via measurement as the system output , that is $y = \phi_m$ in our application.Therefore an error signal can be generated using the measurement and an estimate of the system output $\hat{\mathbf{y}} = \mathbf{c}\hat{\mathbf{z}}$ where $\hat{\mathbf{z}}$ is the current best estimate of the system states. The innovations signal can be written as

$$\mathbf{y}(t) - \hat{\mathbf{y}}(t) = \mathbf{y}(t) - \mathbf{c}\hat{\mathbf{z}}(t) = \mathbf{c}\left[\mathbf{x}(t) - \hat{\mathbf{x}}(t)\right] = \mathbf{c}\tilde{\mathbf{x}}(t) \tag{5.23}$$

and it can be used to drive the estimator equation for z. Hence the estimator for z can be designed in the form

$$\dot{\hat{\mathbf{z}}}(t) = \mathbf{A}_N\hat{\mathbf{z}}(t) + \mathbf{B}_N\mathbf{u}(t) + \mathbf{L}\left[\mathbf{y}(t) - \mathbf{c}\hat{\mathbf{z}}(t)\right] \tag{5.24}$$

where $\hat{\mathbf{z}}(t)$ = estimated state vector

and L = a feedback gain vector to be suitably chosen.

The system yielding $\hat{\mathbf{z}}$ is called an observer or estimator.

By making the estimated state vector available we have eliminated the cost involved in measuring the actual states that is the cost of the sensors required to measure the states and the transducers needed to convert these measurements to useful quantities for control. In a nutshell, if we know the state of the system at some instant, we can construct a dummy system (realization) with this given initial state and drive it with the

same input as the original system from that time on. An observer is basically a weighted average of the measured quantity and that obtained from an embedded model of the process.

5.3 Combined Observer-Controller Compensator

The control law design and the estimator design are combined and the control law is implemented using the estimated state variables, to give a combined observer-controller compensator. The two well proven facts (Kailath, 1980) regarding the incorporation of the observer dynamical system into the feedback loop are as follows

- Incorporation of a stable asymptotic observer does not impair stability.
- The observer and the controller can be designed independently of each other.

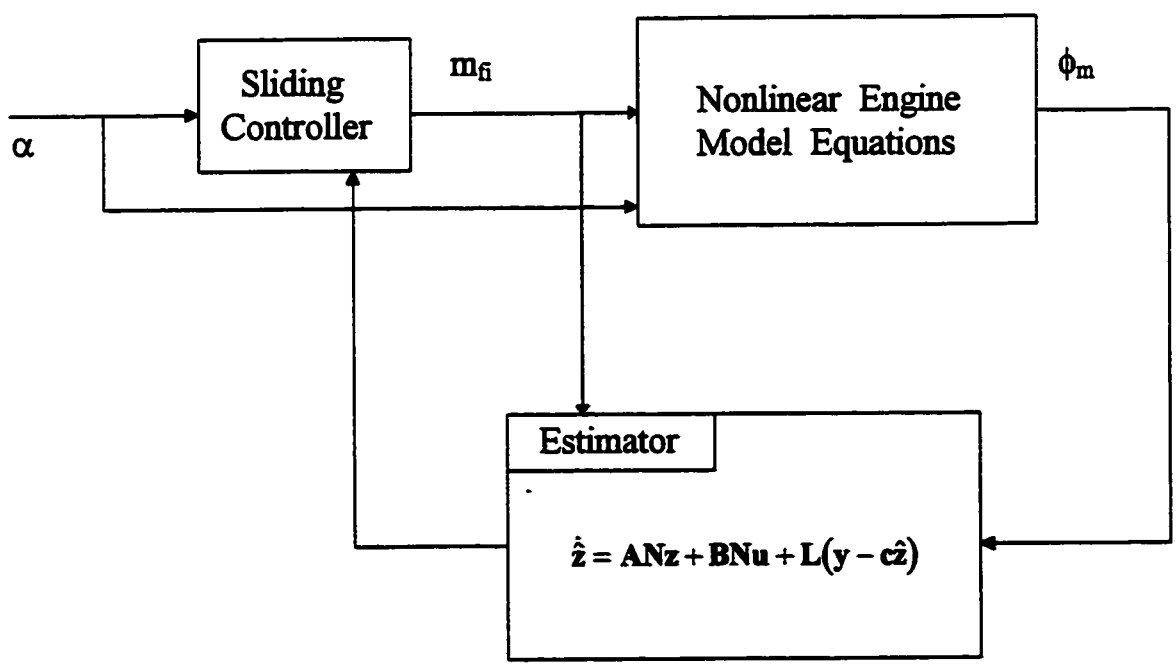

Figure 5.2: Compensator: Control Law + Observer

The overall fuel control scheme consisting of a combination of control law and observer is shown in Fig 5.2

For our system

$$\dot{\mathbf{z}} = \mathbf{A}_N\mathbf{z} + \mathbf{B}_N\mathbf{u} + (\mathbf{B}_\alpha)_N\alpha$$
$$\mathbf{y} = \mathbf{cz} \tag{5.25}$$

The input u to the system is given by the sliding mode controller based on estimated states

$$\mathbf{u} = \mathbf{K}_{SL}\hat{\mathbf{z}} - (\mathbf{CB})^{-1}\eta\,\mathbf{sign}(\mathbf{C}\hat{\mathbf{z}}) \tag{5.26}$$

where $K_{SL} = -(CB)^{-1}CA$ and C is the sliding surface matrix as explained in chapter 4. The estimator equation developed in Eq. 5.25 for the system in sliding mode with $\mathbf{s} = \mathbf{C}\hat{\mathbf{z}} = 0$ is

$$\dot{\hat{\mathbf{z}}} = \mathbf{A}_N\hat{\mathbf{z}} + \mathbf{B}_N\mathbf{u} + \mathbf{L}(\mathbf{y} - \mathbf{c}\hat{\mathbf{z}})$$
$$\dot{\hat{\mathbf{z}}} = \mathbf{A}_N\hat{\mathbf{z}} - \mathbf{B}_N * \mathbf{K}_{SL}\hat{\mathbf{z}} + \mathbf{Lcz} - \mathbf{Lc}\hat{\mathbf{z}} \tag{5.27}$$
$$\dot{\hat{\mathbf{z}}} = (\mathbf{A}_N - \mathbf{B}_N * \mathbf{K}_{SL} - \mathbf{L} * \mathbf{c})\hat{\mathbf{z}} + \mathbf{Lcz}$$

or
$$\begin{bmatrix}\dot{\mathbf{z}}\\ \dot{\hat{\mathbf{z}}}\end{bmatrix} = \begin{bmatrix}\mathbf{A}_N & -\mathbf{B}_N * \mathbf{K}_{SL}\\ \mathbf{L} * \mathbf{c} & \mathbf{A}_N - \mathbf{B}_N * \mathbf{K}_{SL} - \mathbf{L} * \mathbf{c}\end{bmatrix}\begin{bmatrix}\mathbf{z}\\ \hat{\mathbf{z}}\end{bmatrix} + \begin{bmatrix}(\mathbf{B}_\alpha)_N\\ 0\end{bmatrix}[\alpha] \tag{5.28}$$

or
$$\dot{\mathbf{X}} = \mathbf{A}_{cl}\mathbf{X} + \left[(\mathbf{B}_\alpha)_N\right]_{cl}\alpha \tag{5.29}$$

which represents the combined controller-observer closed loop system. Briefly, by using feedback of the states of a completely controllable and completely observable estimated realization of the original transfer function, we can obtain a new internally stable realization whose natural frequencies and dynamic modes are completely under our

control. The observer may or may not have as many states as the original system and need not be constructed in the same way as the original system.

5.4 Simulation Study

In order to verify the entire control system design a model is developed using MATLAB and SIMULINK. The structure of the SIMULINK model is kept in compliance with the Figure 5.2 to represent the actual compensator. Figure 5.3 represents the detailed nonlinear engine model. The different subsystems of Figure 5.3 are modeled seperately and shown in successive Figures 5.4 to 5.12. The control algorithm is put to test on this model to provide useful insight regarding the performance of the system. Moreover the system is studied with and without the use of the observer to understand the difference in performance.

5.4.1 Simulation Structure

This distinction is done for the sake of clarity and to simulate the performance of the compensator. One model is known as the *simulation model* and the other one is known as the *embedded model*. The simulation model is the linear or nonlinear model developed in the Chapter 3 and represents the actual engine behavior under varying conditions. The embedded model is the one developed to function as an observer in the control algorithm and discussed in Section 5.3 of this chapter. The embedded model takes the output from the simulation model and then do the control calculations based on the control algorithm and issues control commands to the simulation model, just as if it were controlling a real engine. The simulation model can be of the same form as the embedded

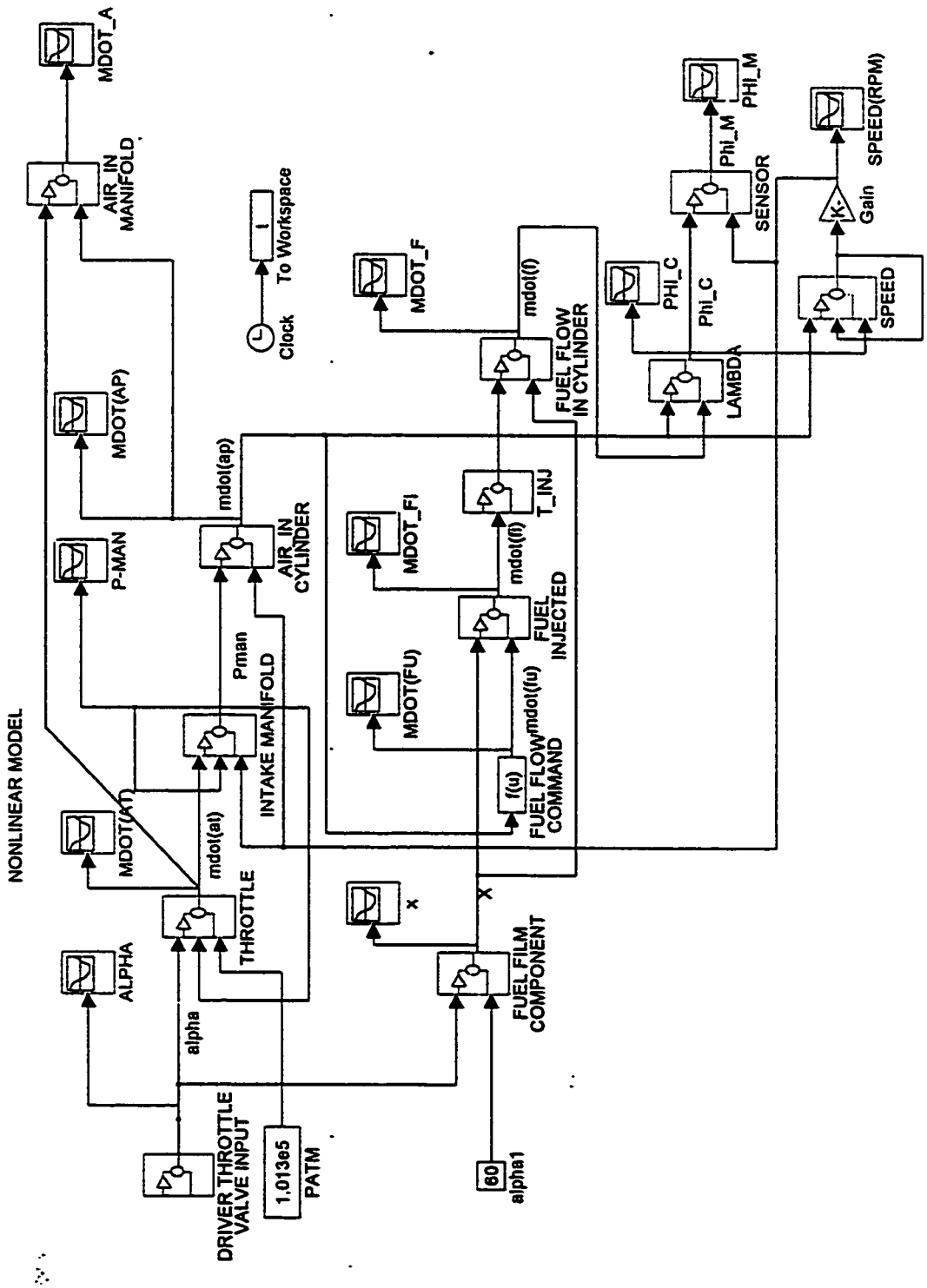

Figure 5.3: Detailed SIMULINK Representation of Nonlinear Engine Model

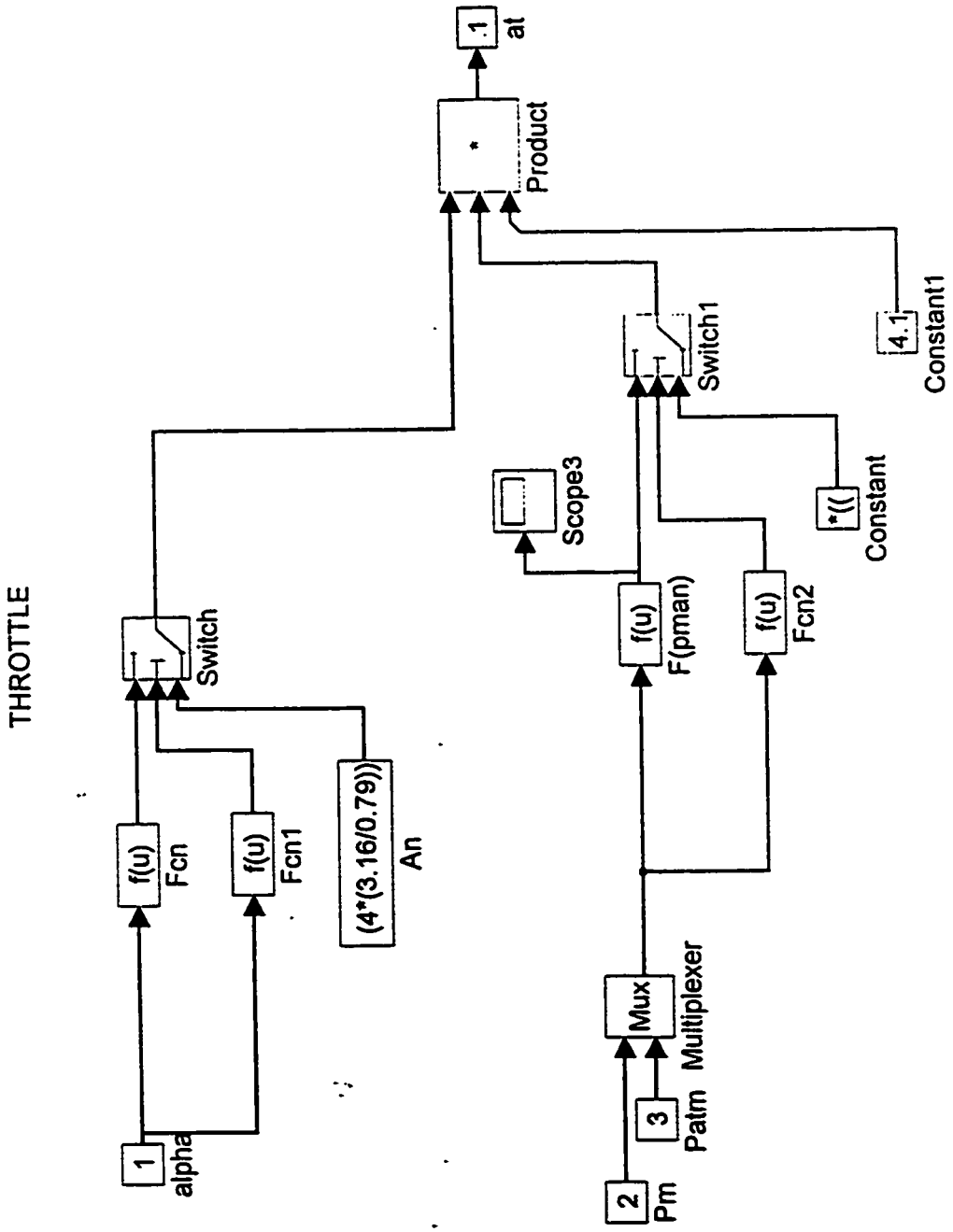

Figure 5.4: SIMULINK Model of Throttle Dynamics (Eq. 3.4)

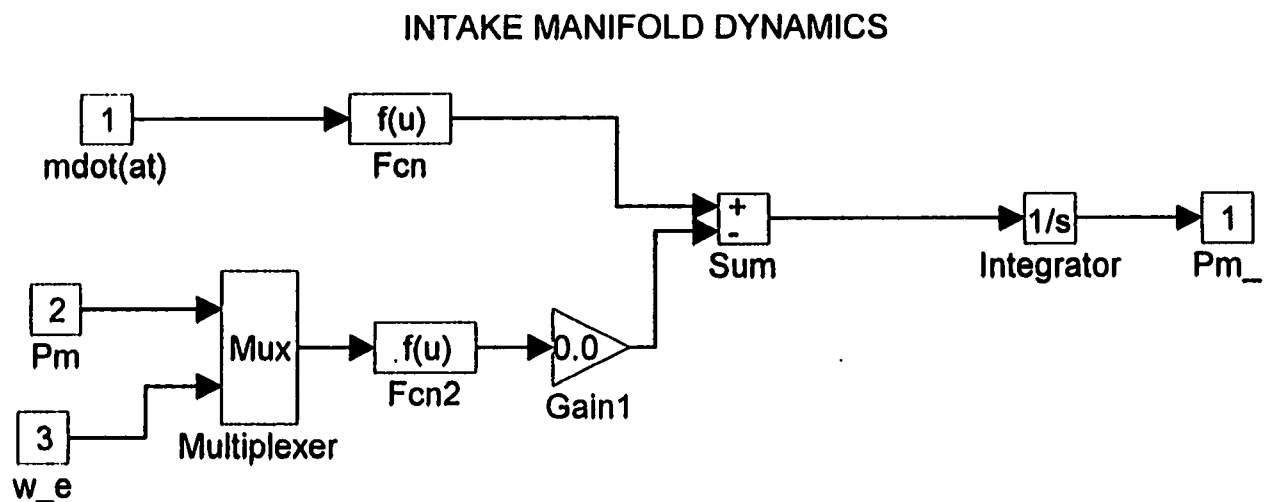

Figure 5.5: SIMULINK Model of Intake Manifold Dynamics (Eq. 3.11)

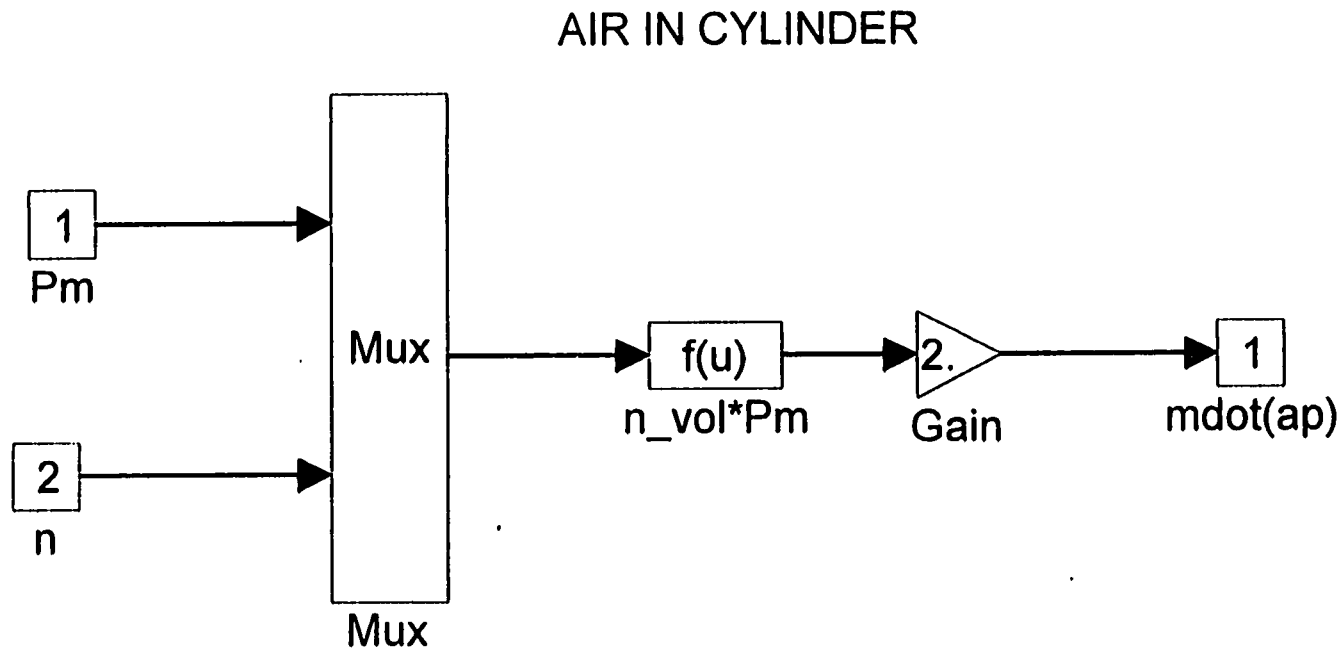

Figure 5.6: SIMULINK Model of Air Flow Entering the Cylinder (Eq. 3.5)

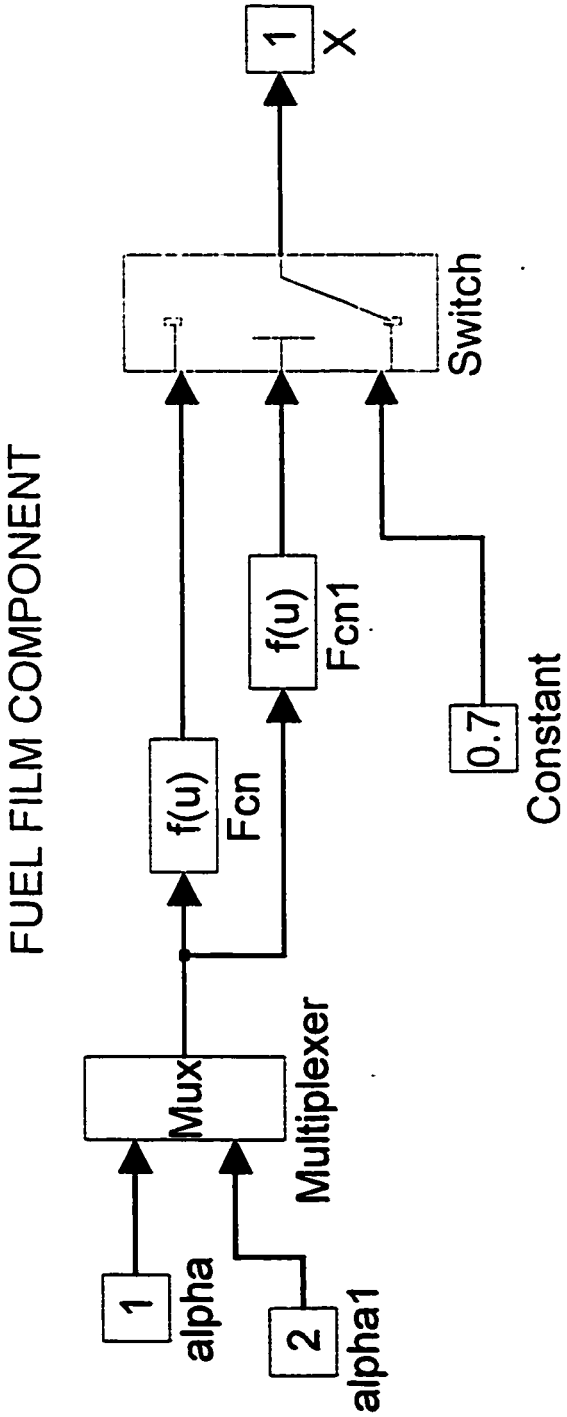

Figure 5.7: SIMULINK Model of Fuel Film on the Intake Manifold Walls (Eq. 3.13)

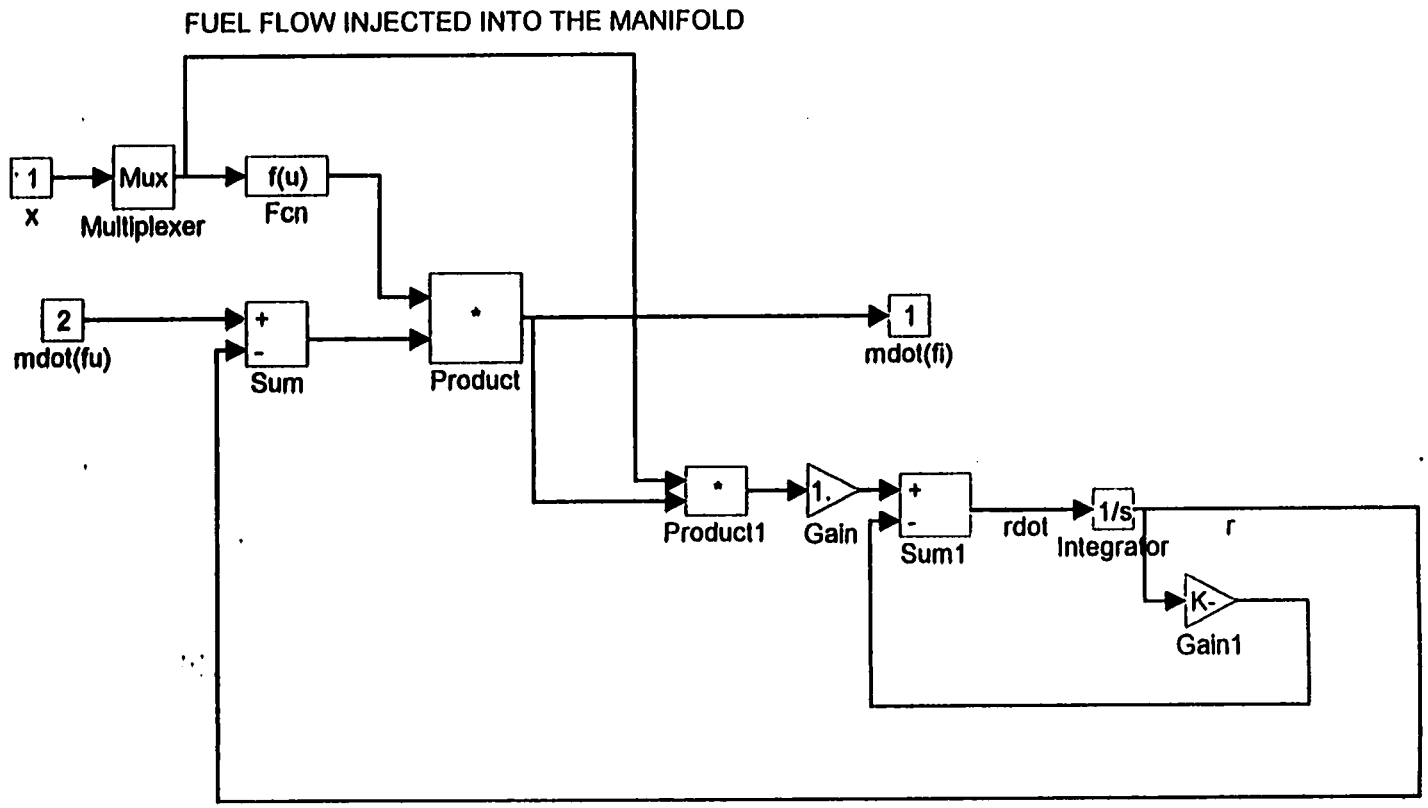

Figure 5.8: SIMULINK Model of the Fuel Flow Injected into the Manifold (Eq. 3.12)

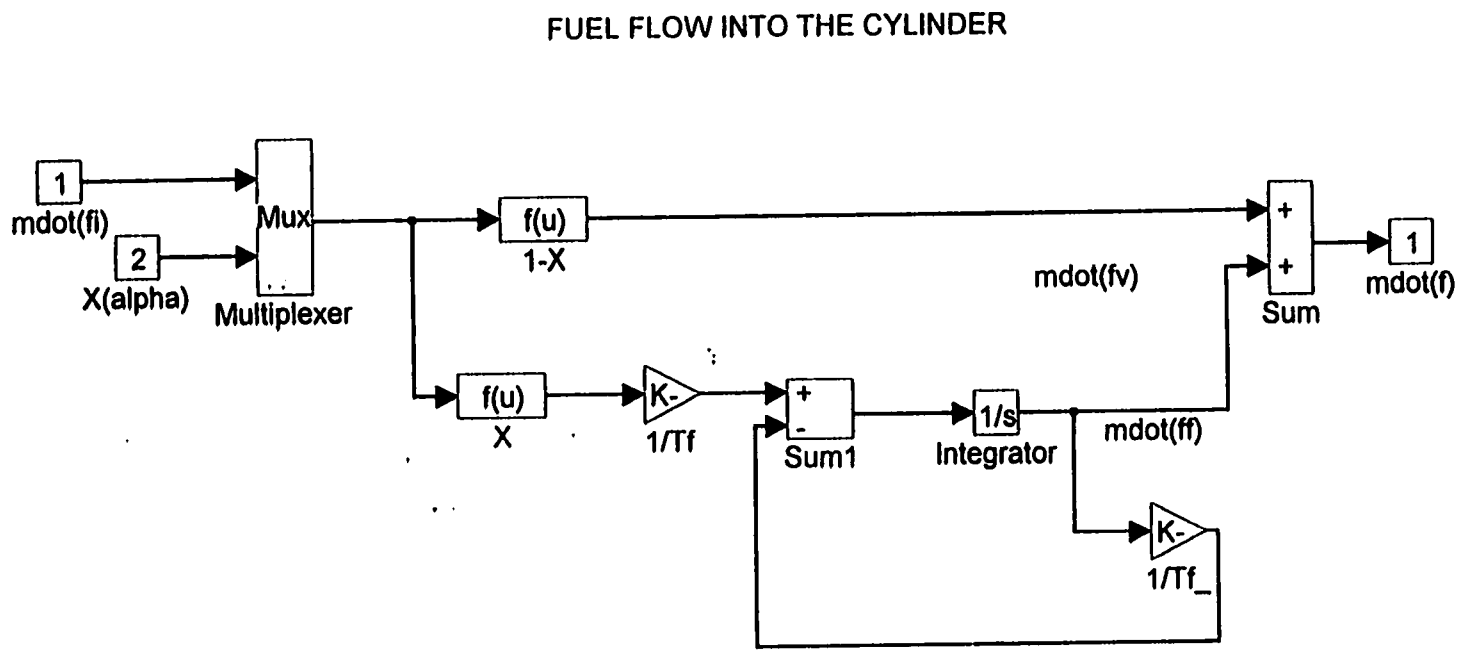

Figure 5.9: SIMULINK Model of the Fuel Flow Entering the Cylinder (Eq 3.12)

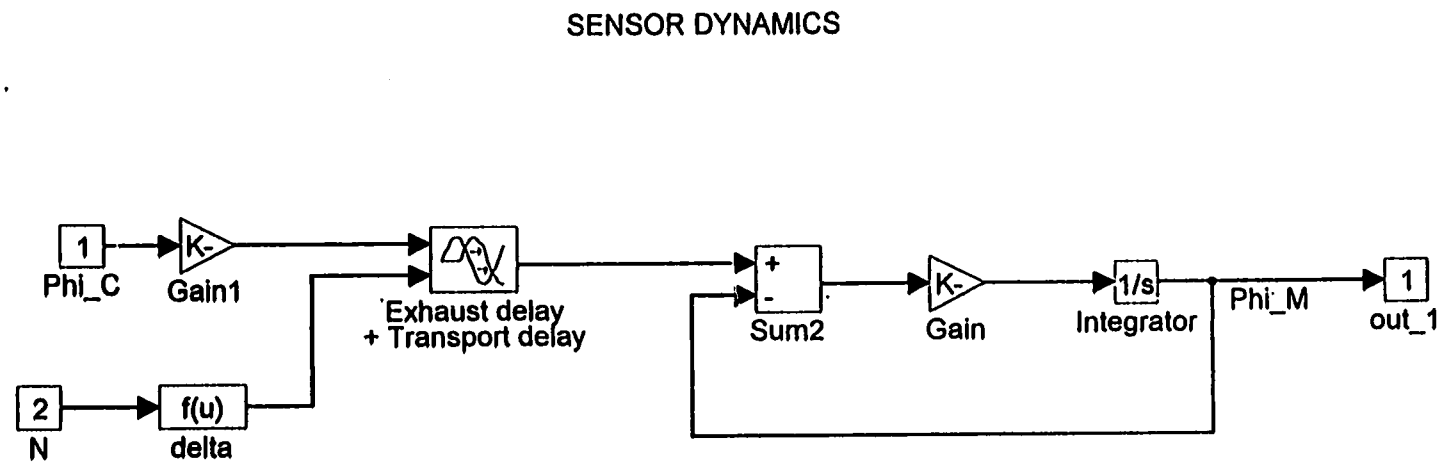

Figure 5.10: SIMULINK Model of UEGO Sensor Dynamics (Eq. 3.20)

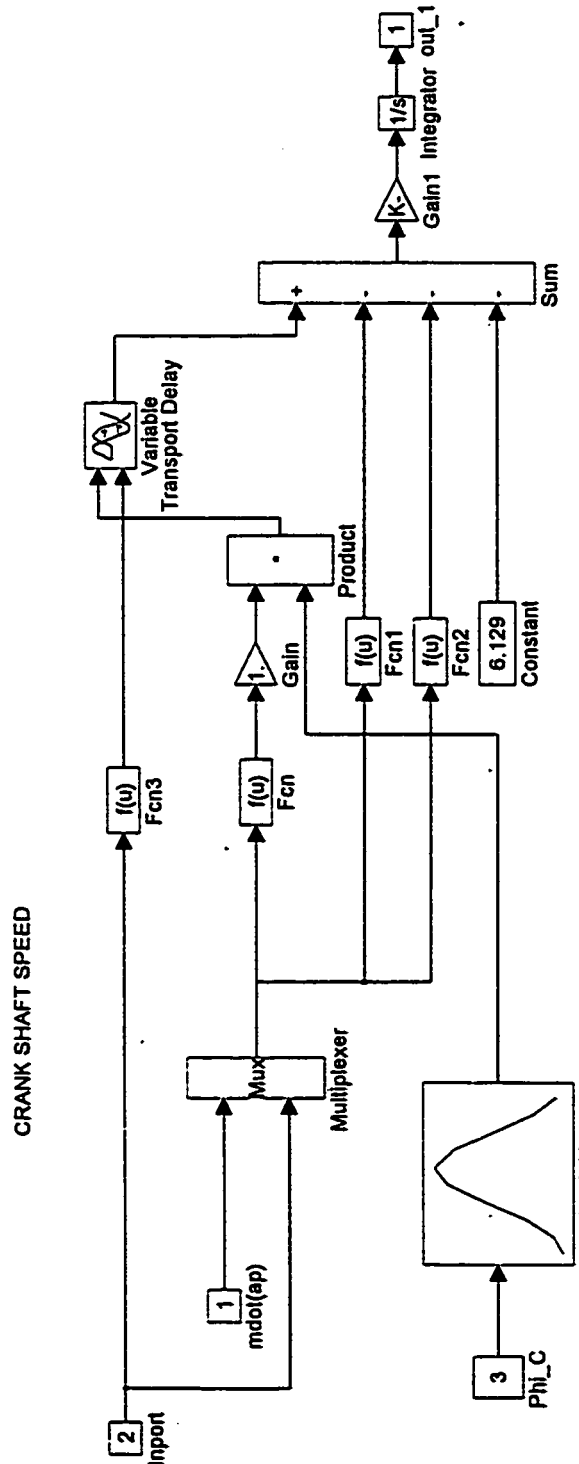

Figure 5.11: SIMULINK Model of the Crank Shaft Speed (Eq. 3.14)

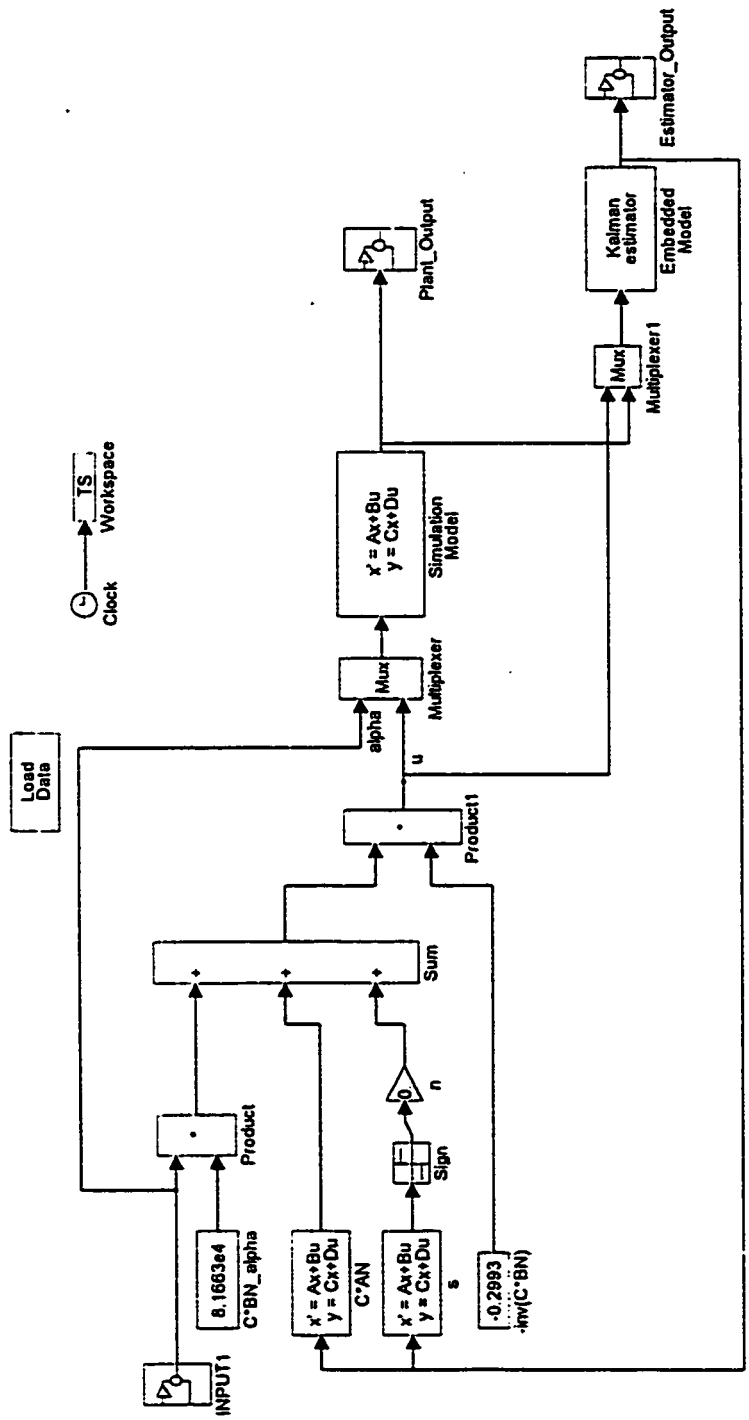

Figure 5.12: SIMULINK representation of Compensator + Linear Model

model. In fact any engine simulation code that includes the key dynamics and specifies the input to output interface can be used for this purpose. In the following simulation, a simulation model of the same form as the embedded model was used. The observer gain L was calculated using the LQG (Anderson and Moore, 1990) method. A complete listing of Q and R weightings used to compute L is given in Sec. 5.4.2.2.2

5.4.2 Simulated System Performance

Automotive engines seldom operate at a steady temperature for prolonged periods during practical driving conditions. So the system is studied for fast throttle tip-in/tip out with varying speeds. The parameters of interest are engine manifold pressure, engine speed and air-fuel equivalence ratio. Throttle is closed at a throttle angle of 14 degrees

5.4.2.1 Open loop - Nonlinear and Linear

Fig. 5.13 and 5.14 shows the open loop engine performance for throttle tip-in. The throttle (α) is given step inputs of 10, 20 and 20 degrees respectively at time equal to 5, 20 and 35 seconds, and the system is studied for varying inertial load. Figs. 5.15 and 5.16 shows the open loop engine performance for combined throttle tip in and tip out. The same set of throttle inputs are applied on the linear engine model and the system performance is studied as shown in Figs. 5.17 to 5.20. In Figs. 5.13, 5.15, 5.17 and 5.19 the throttle angle, intake manifold pressure and speed are shown vs. time whereas in Figs. 5.14, 5.16, 5.18 and 5.20 the throttle angle, air flow rate and fuel flow rate entering the cylinder are shown. The nonlinear nature of intake manifold pressure dynamics given by Eq. 3.11 is shown in Fig. 5.13 and Fig 5.15. As the throttle opens there is sudden inflow

of air into the manifold resulting in pressure rise as shown by the spike in Fig 5.13. The sudden rush of air inflow into the manifold results in a higher fuel flow rate entering the cylinder and this is due to the shear effect discussed in Chapter one, though it is not significant.

For the nonlinear system , the rise in crank shaft speed for the last two throttle step input of 20 degrees is not same as shown in Fig. 5.3 and 5.15 and hence the time constant for the speed responses varies for tip-in and tip-out cases. The non-linearity of crank shaft speed dynamics as expressed by Eq. 3.14 is evident. The air flow rate entering into cylinder given by Eq. 3.5 depends on intake manifold pressure, speed and volumetric efficiency and hence is nonlinear in nature. As shown in Fig. 5.14 and 5.16 the same throttle maneuver of 20 degrees for the last two steps gives the increased rate of airflow into the cylinder for the last step compared to the step before that. This is also due to the input valve closing slightly after the piston reaches the bottom dead center to take advantage of excess air flow into the cylinder to match properly with the excess fuel flow for the acceleration transient.

The increase in manifold pressure is greater for the linear case as compared to the non-linear as shown in Fig. 5.17. The rise in crank shaft speed is less for linear case compared to the non-linear one. The nature of crankshaft speed, air flow and fuel flow is same for both the linear and non linear case. There is a difference in behavior of intake manifold pressure dynamics for the large throttle maneuvers, for linear and nonlinear cases, as shown in Fig 5.13 and 5.17.

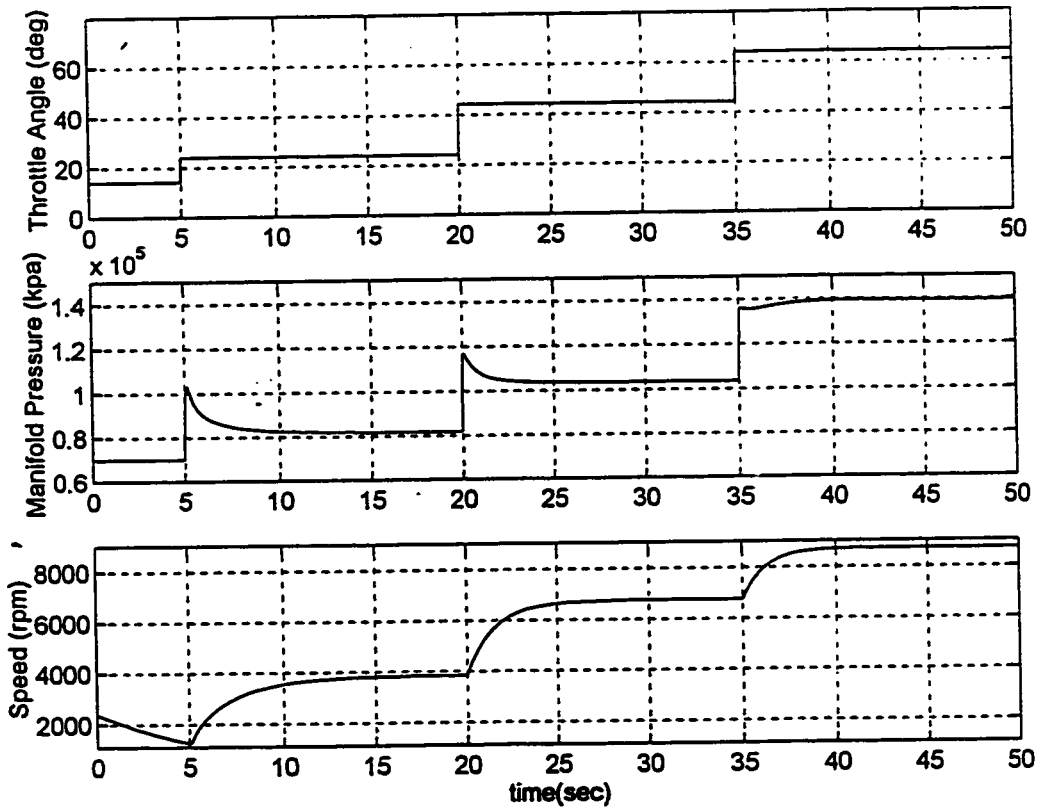

Figure 5.13: Open Loop Nonlinear System Performance for Throttle Tip-in, Intake Manifold Pressure(p_m) and Crankshaft Speed (N).

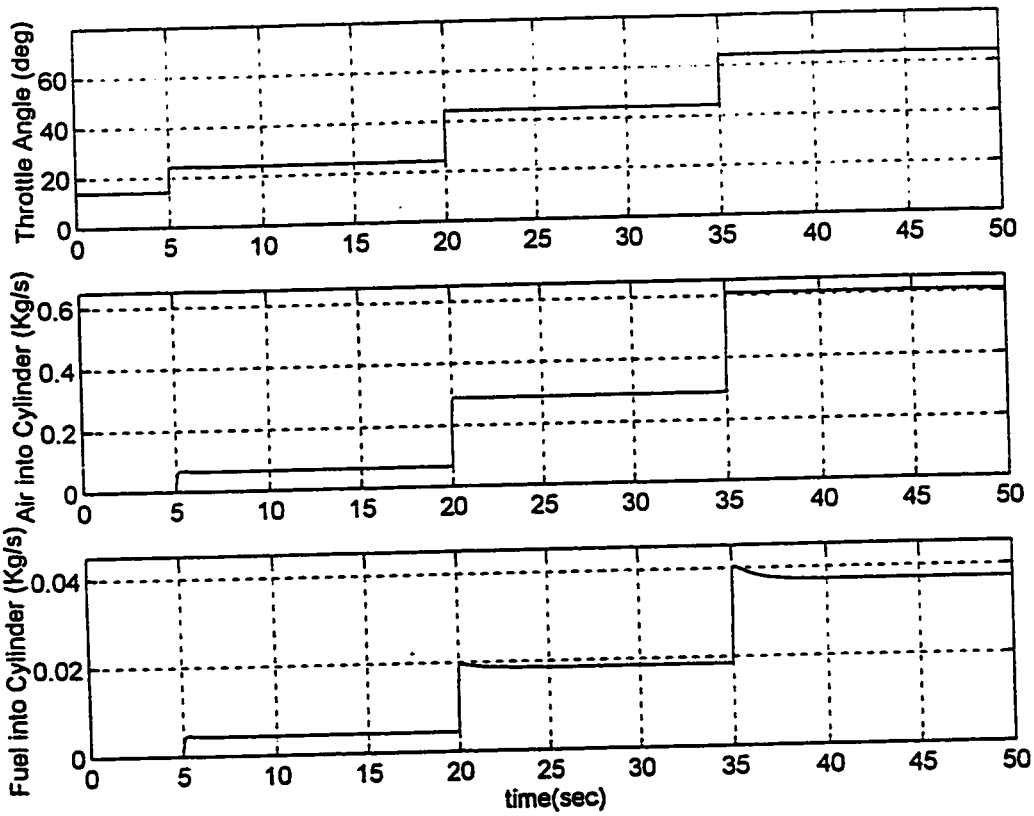

Figure 5.14: Open Loop Nonlinear System Performance for Throttle Tip-in, Air Flow Rate $(\dot{m}_{ap})$ and Fuel Flow Rate $(\dot{m}_f)$ into the cylinder

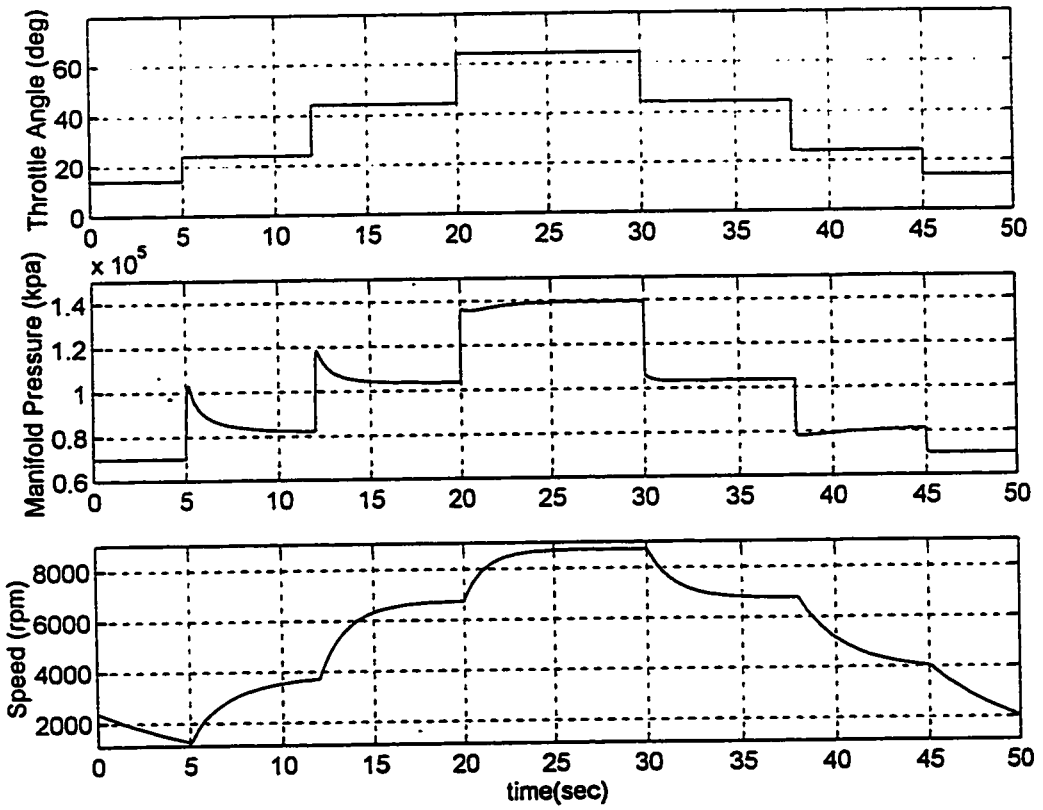

Figure 5.15: Open Loop Nonlinear System Performance for Throttle Tip-in/Tip-out Combined, Intake Manifold Pressure (p_m) and Crankshaft Speed (N).

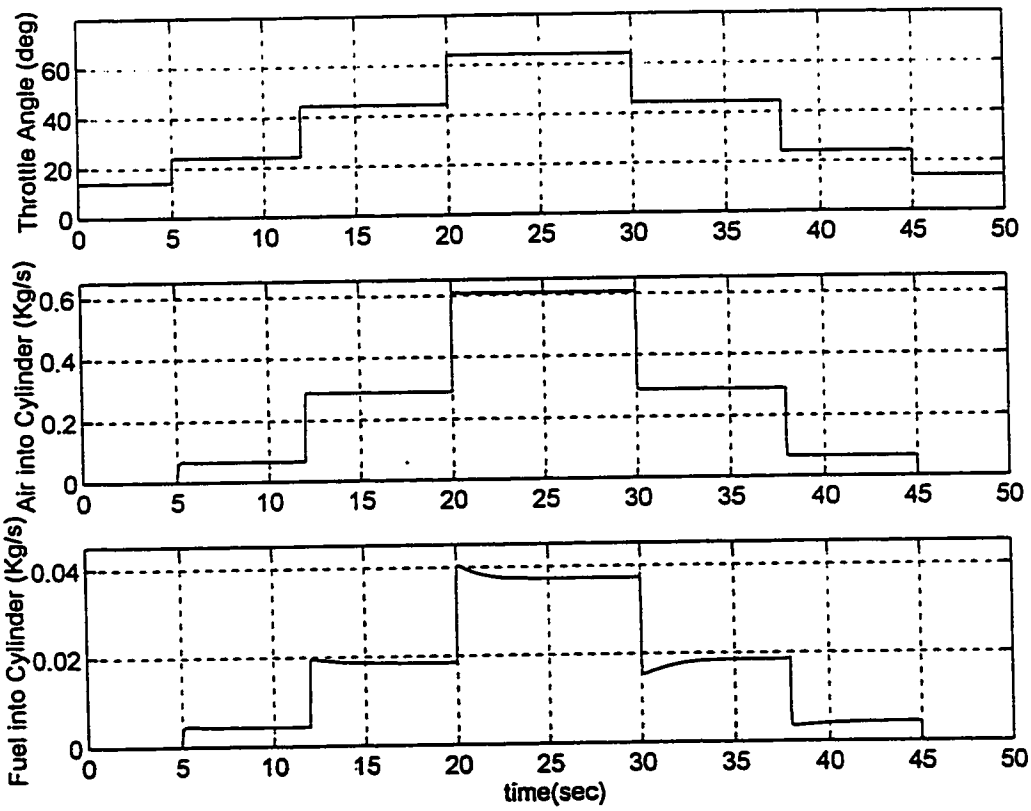

Figure 5.16: Open Loop Nonlinear System Performance for Throttle Tip-in/Tip-out Combined, Air Flow Rate $(\dot{m}_{ap})$ and Fuel Flow Rate $(\dot{m}_f)$ into the cylinder

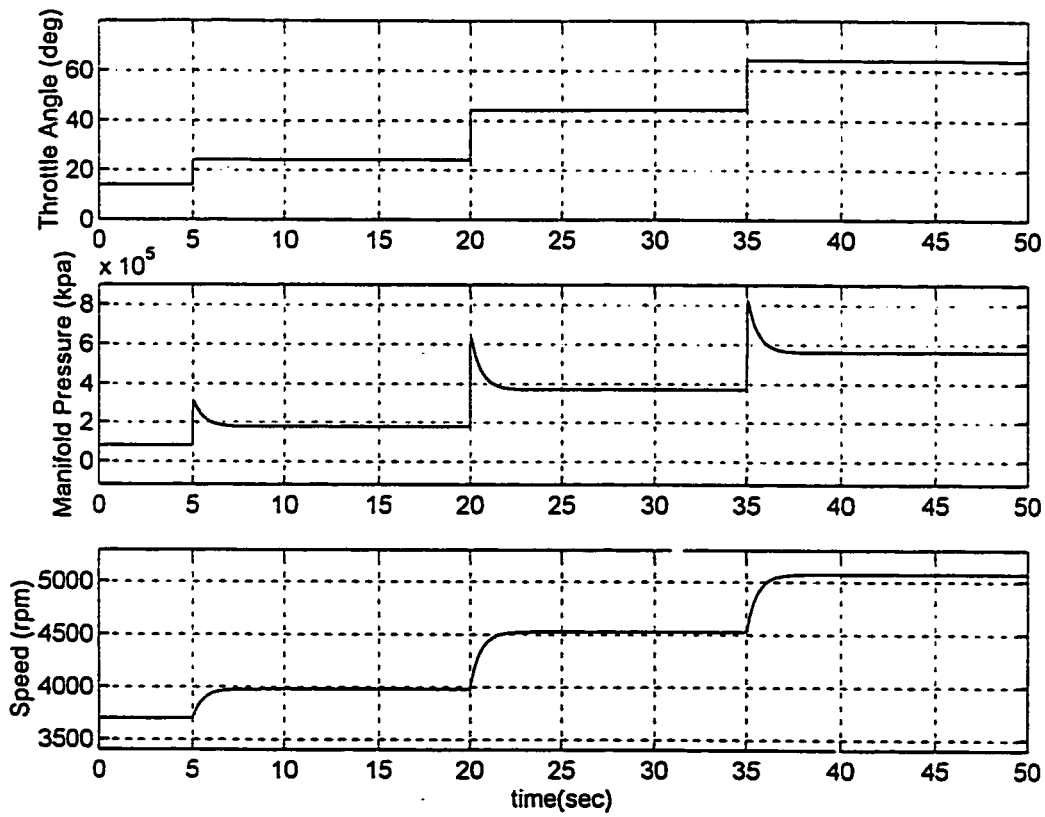

Figure 5.17: Open Loop Linear System Performance for Throttle Tip-in, Intake Manifold Pressure (p_m) and Crankshaft Speed (N)

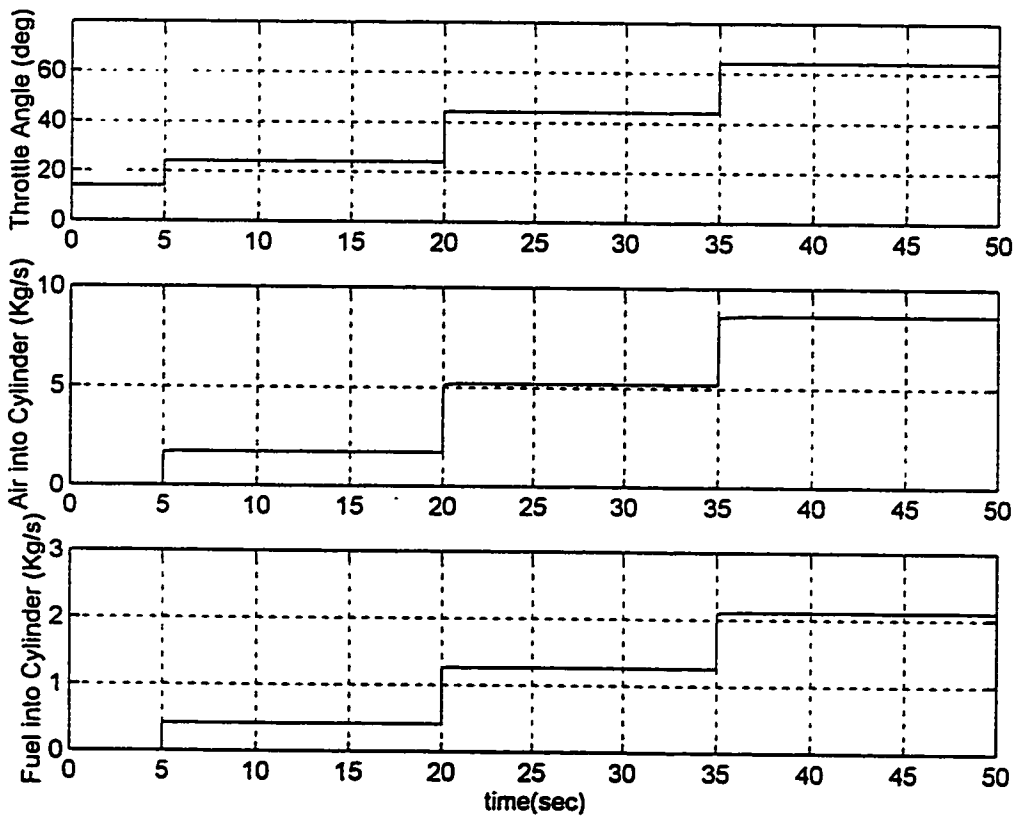

Figure 5.18: Open Loop Linear System Performance for Throttle Tip-in, Air Flow Rate $(\dot{m}_{ap})$ and Fuel Flow Rate $(\dot{m}_f)$ into the Cylinder

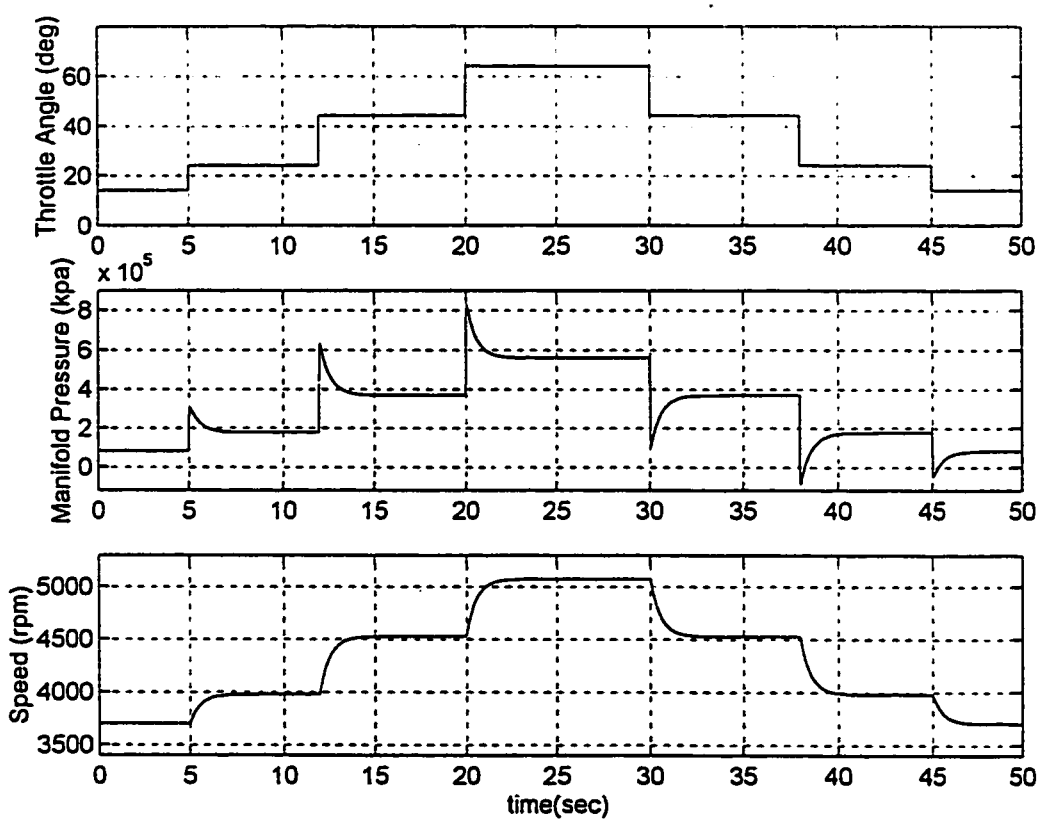

Figure 5.19: Open Loop Linear System Performance for Throttle Tip-in/Tip-out Combined, Intake Manifold Pressure (p_m) and Crankshaft Speed (N)

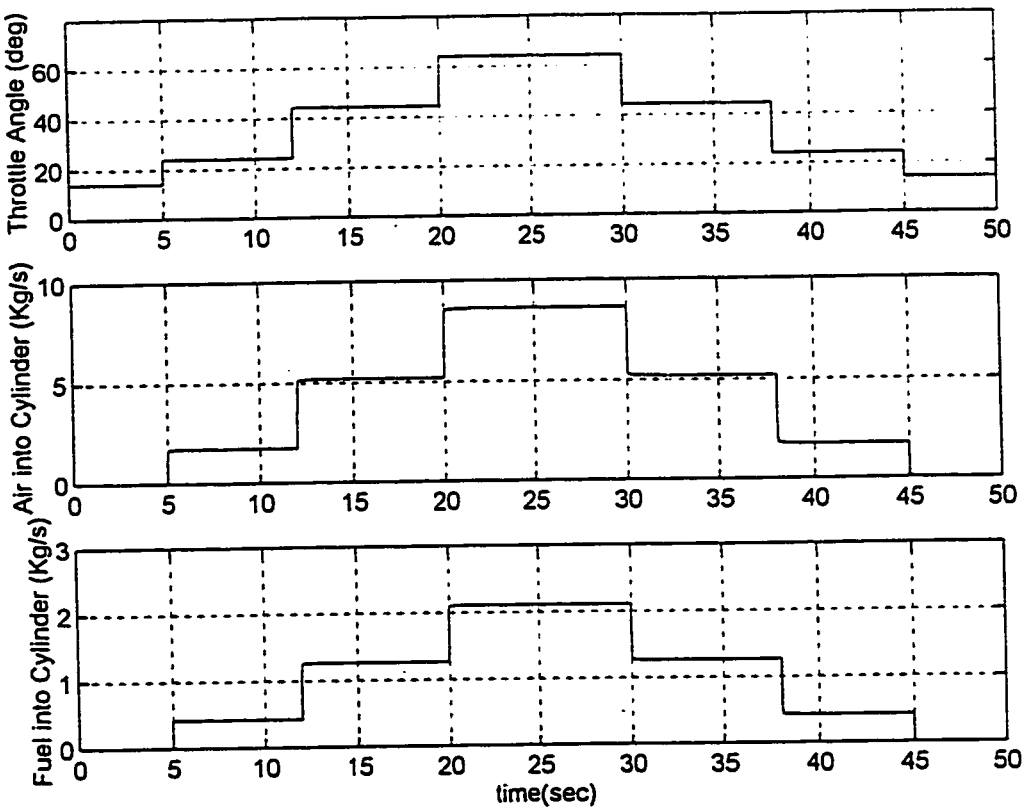

Figure 5.20: Open Loop Linear System Performance for Throttle Tip-in/Tip-out Combined, Air Flow Rate $(\dot{m}_{ap})$ and Fuel Flow Rate $(\dot{m}_f)$ into the Cylinder

5.4.2.2 First Order Filtering

The results are shown first simply using feedback control and then with the observer in the feedback loop

5.4.2.2.1 Closed loop with state feedback

The single loop filtering design of Sec. 4.3.2 is applied by using Eqs. 4.11 to design a hyperplane which is used in the control law of Eq. 4.9, on the linear model using only state feedback. In this work there is only a single input and hence a single hyperplane suitable for the input is designed. The sliding surface matrix definer C is

$$\mathbf{C} = [0.0404 \quad -3.261\mathbf{e}4 \quad -5.79\mathbf{e}-5 \quad 5.19\mathbf{e}-5 \quad 1.48\mathbf{e}-5 \quad 0.0918 \quad 0.6406 \quad 0.0028]$$

The design used a filter time constant of 0.2 for all the simulations. The closed loop system eigen values of the system are all negative representing a stable system.

$$(\mathbf{eigValue})_{\text{state\_feedback}} = \begin{bmatrix} 0 \\ 0 \\ 0 \\ 0 \\ -1..1 \\ -1.9 \\ -6.7 \\ -83.5 \end{bmatrix}$$

The system is studied both for throttle tip-in and tip-in/tip-out combined. Fig. 5.21 gives the system response for tip in case and Fig. 5.22 shows the response for tip-in and tip-out combined. Throttle is at a closed throttle angle of 14 degrees and step inputs of 5, 10 and 15 degrees are given at time equal to 5, 20 and 35 seconds to study the simulated

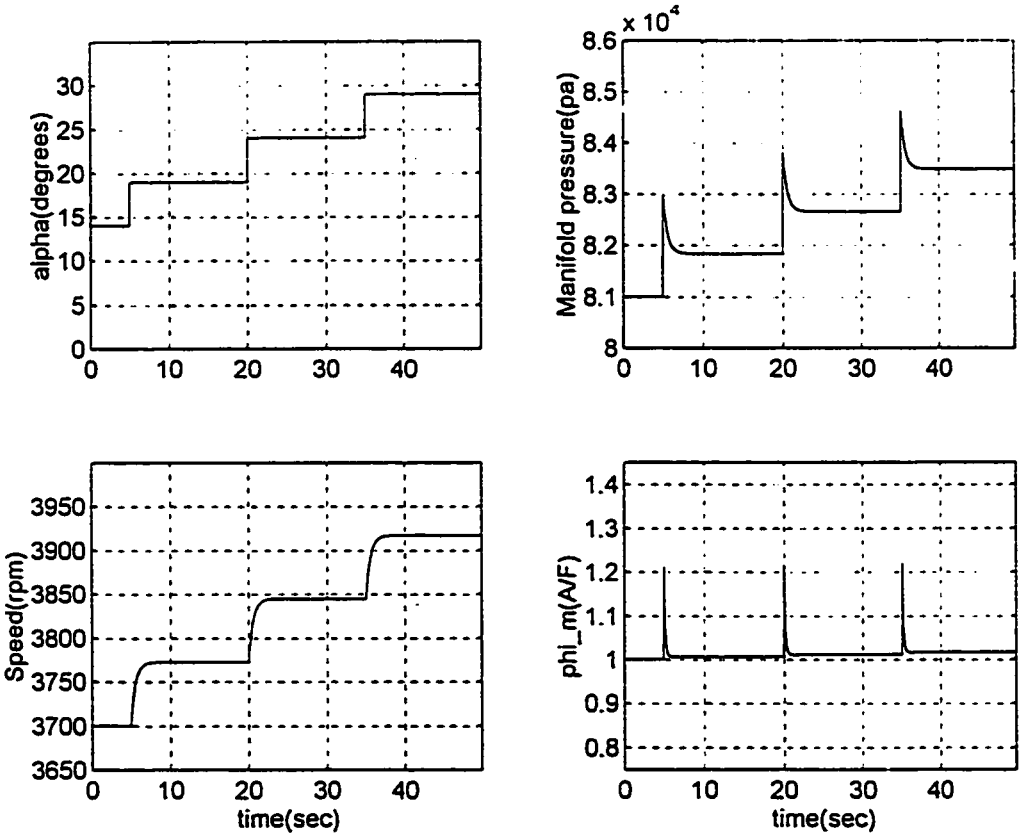

Figure 5.21: Simulated Response of Sliding Mode Controller with State Feedback using Single Loop Filtering Design for Throttle Tip-in

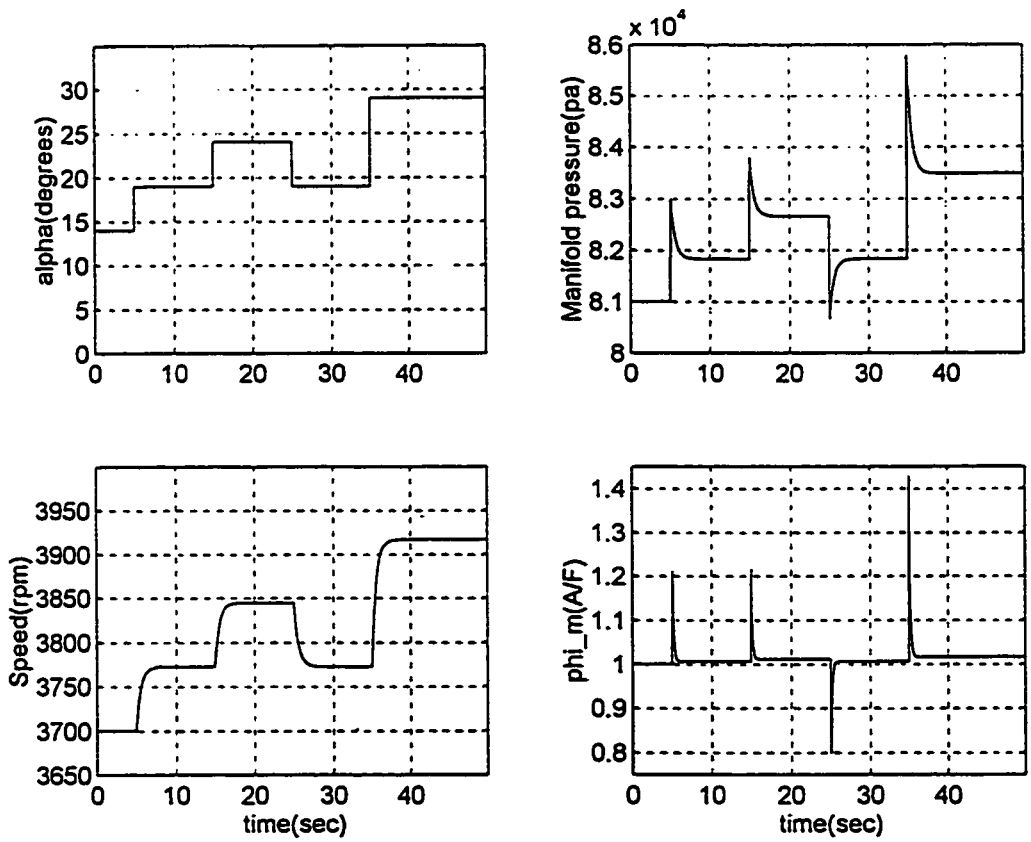

Figure 5.22: Simulated Response of Sliding Mode Controller with State Feedback using Single Loop Filtering Design for Throttle Tip-in/Tip-out Combined

performance as shown in Fig, 5.21. The intake manifold pressure (p_m) is always below the atmospheric pressure which was not the case with the open loop system. It is because of this pressure difference the air enters the intake manifold to match the amount of fuel injected. The indicated torque given by Eq. 3.16 is constantly varying with the throttle maneuvers and hence the step response in the speed of the system is observed. AFR is precisely controlled within the limits of commanded AFR of 1. Spikes are present at the throttle angle steps but after the throttle angle flanks (both rising and falling) there is no tendency in the sliding mode (Fig. 5.21 and 5.22) to over or undershoot the steady state value of 1 (stoichiometry). The AFR equivalence ratio during steady state operation held nearly constant at stoichiometry as desired. The state matrix A_N and the control input matrix B_N are as follows:

$$A_N = 1e3 * \begin{bmatrix} -0.08 & 0 & 0 & 0 & 0 & 0 & -1.5 & 0 \\ 0 & 0 & 0 & 0 & 0 & 0 & 0 & 0 \\ 0 & 0 & 0 & 0.001 & 0 & 0 & 0 & 0 \\ 0 & 0 & 0 & -0.0011 & 0 & 0 & 0 & -0.06 \\ 0 & 0 & 0 & 0 & 0 & 0 & 0 & -0.9 \\ 0 & 0 & 0 & 0 & 0 & -0.0067 & 0 & 0 \\ 0.0001 & 0 & 0 & 0 & 0 & -0.003 & -0.0007 & 0 \\ 0 & 0 & 0 & 0 & 0 & 0 & 0 & -1 \end{bmatrix}$$

$$B_N = 1e3 * \begin{bmatrix} 0 \\ 0 \\ 0. \\ 0.06 \\ 6.94 \\ 0 \\ 0 \\ 1 \end{bmatrix}$$

5.4.2.2.2 Closed Loop with Estimator

An estimator is designed and inserted in the feedback loop as discussed in the Sec. 5.2 of this chapter. The estimated states are used as the input to the sliding mode controller based on single loop filtering. The simulated system performance for the throttle tip in and throttle tip-in/tip-out combined is shown in Figs.. 5.23 and 5.24. The estimator response is shown in Figs. 5.25 and 5.26. The Figs.. 5.23 to 5.26 portrays the same simulated test conditions as in Figs. 5.21 and 5.22 and shows the same plotted variables (intake manifold pressure, crankshaft speed and AFR equivalence ratio). In the design, the state weightings were chosen

$$\mathbf{Q} = \mathbf{diag}(1000 \quad 0.01 \quad 1e-3 \quad 1e-5 \quad 1e-5 \quad 1e4 \quad 10 \quad 1e-7)$$
$$\mathbf{R} = 10$$

to give the estimator gain matrix (L)using the Kalman Filter Method (Anderson and Moore, 1990) which tend to induce the desired behavior in the system. The gain matrix is

$$\mathbf{L} = \begin{bmatrix} 7.73e6 \\ 1.385 \\ 3.19e4 \\ 2.86 \\ -0.058 \\ 100.6 \\ 9.36e3 \\ 0 \end{bmatrix}$$

As shown in Fig. 5.23 the simulated response with estimator in feedback loop matches closely for intake manifold pressure and crankshaft speed in comparison to response with out estimator as shown in Fig. 5.21. The spikes for the AFR equivalence ratio are relatively large with the estimator compared to what has been shown earlier in

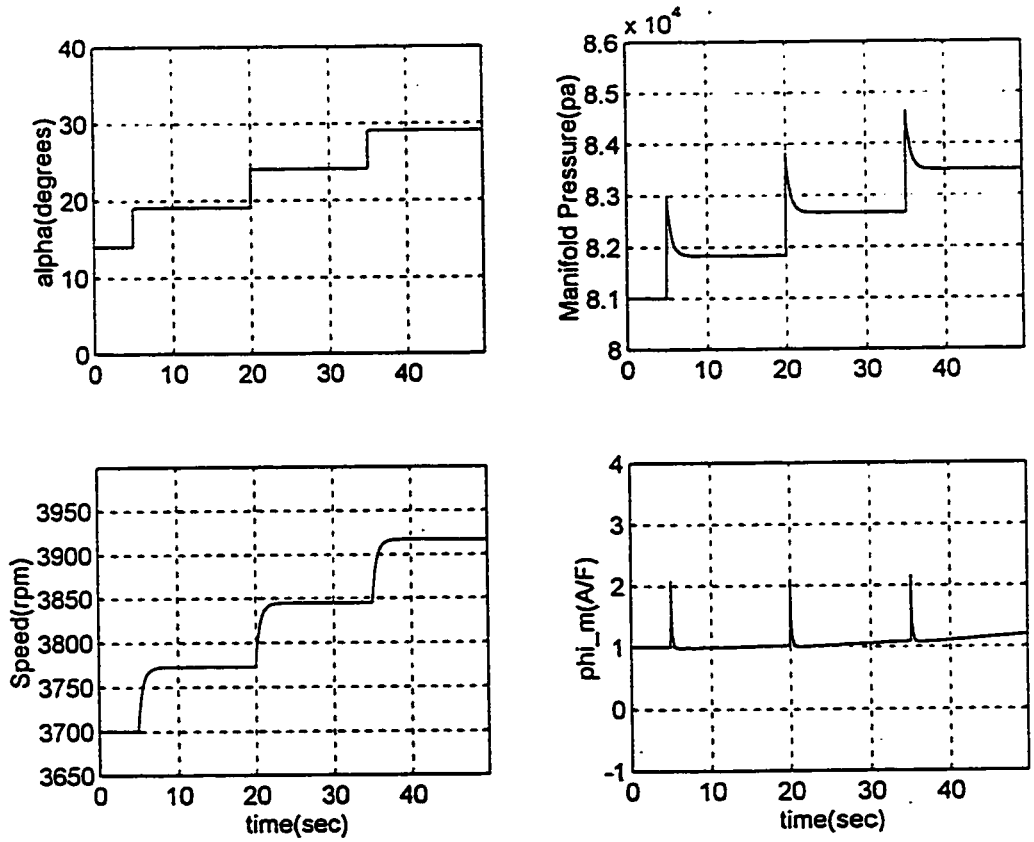

Figure 5.23: Simulated Response of Sliding Mode Controller with State Estimator using Single Loop Filtering Design for Throttle Tip-in

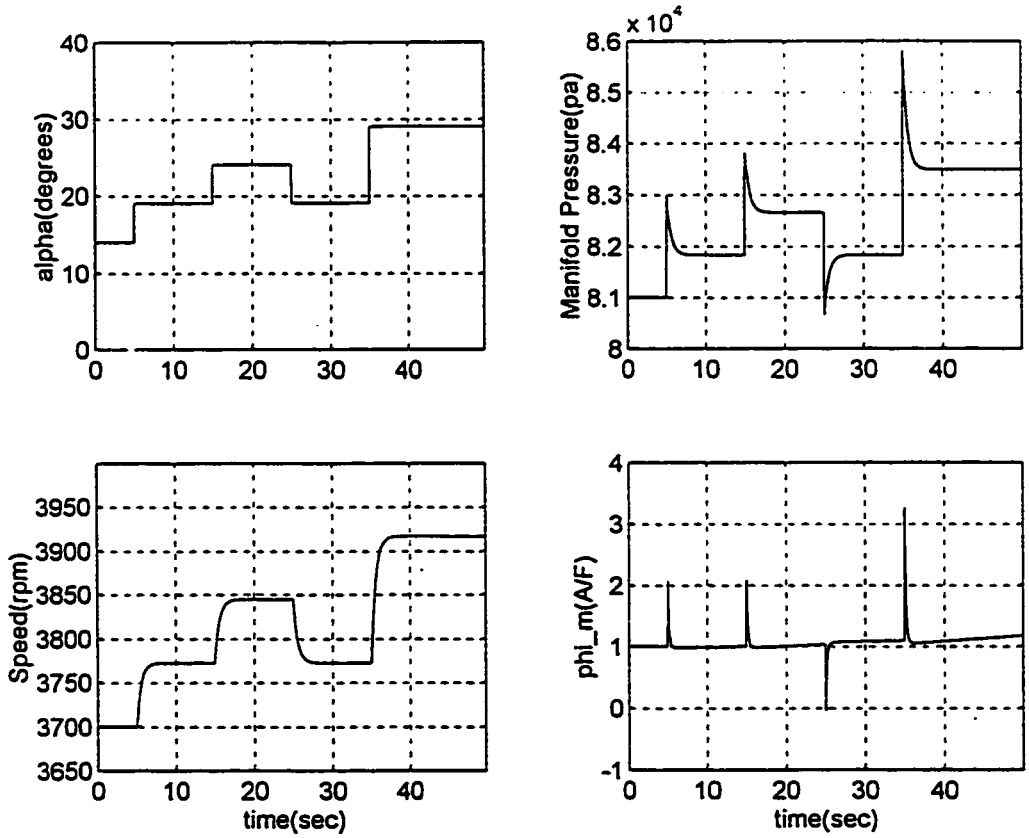

Figure 5.24: Simulated Response of Sliding Mode Controller with State Estimator using Single Loop Filtering Design for Throttle Tip-in/Tip-out Combined

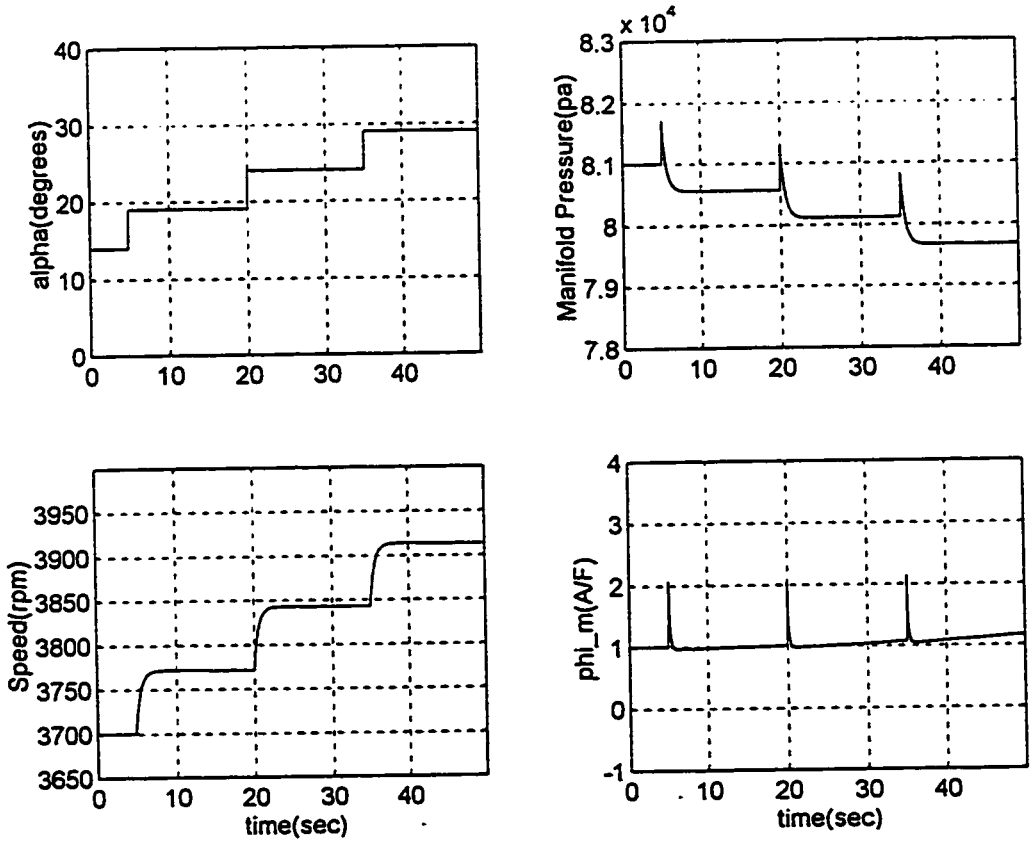

Figure 5.25: Simulated Response of State Estimator using Single Loop Filtering Design for Throttle Tip-in

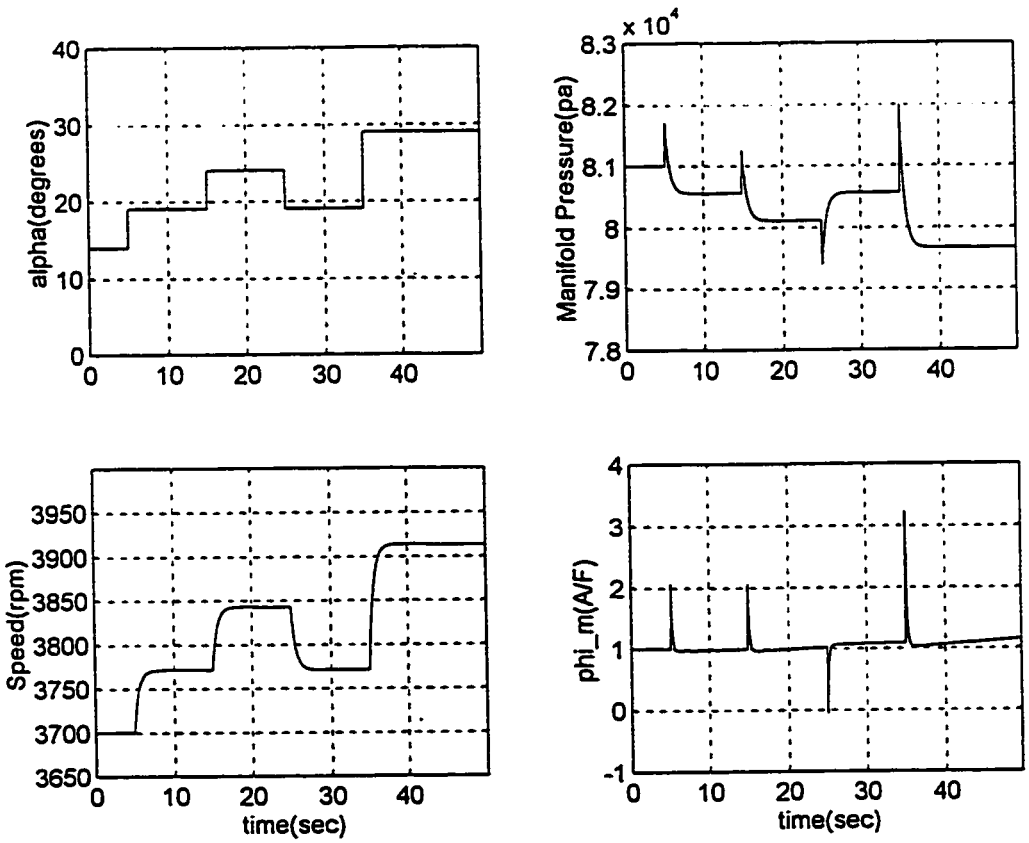

Figure 5.26: Simulated Response of State Estimator using Single Loop Filtering Design for Throttle Tip-in/Tip-out Combined

Fig. 5.21 with state feedback but other than that there is no tendency to over or undershoot the stoichiometric value of 1. The overall performance of the system with estimator in feedback loop is satisfactory and the controller output calculated using estimated states work as desired at all operating conditions. Fig. 5.24 confirms the performance of the compensator for the system operating under tip-in and tip-out conditions combined. The eigen values of the closed loop system with estimator are

$$(\mathbf{eigValue})_{\mathbf{compensator}} = \begin{bmatrix} -95.4+74.8\mathbf{i} \\ -95.4-74.8\mathbf{i} \\ -83.6 \\ -1000 \\ -6.7 \\ -1.9 \\ -1.1 \\ -1.9 \\ -1.1 \\ 2.17\mathbf{e}-4 \\ -8.96\mathbf{e}-5 \\ -4.9\mathbf{e}-6 \\ 1.28\mathbf{e}-9+2.\mathbf{e}-9\mathbf{i} \\ 1.28\mathbf{e}-9-2.\mathbf{e}-9\mathbf{i} \\ -1.84\mathbf{e}-9 \\ -4.83\mathbf{e}-15 \end{bmatrix}$$

The eigen values of the closed loop system are all negative representing a stable system. The non-linear compensator compensates the inherent process delay and the transport delay and regulates the fuel flow to match the air flow commanded by the driver through throttle maneuvers.

Fig 5.25 and 5.26 shows the estimated intake manifold pressure, crankshaft speed and the AFR equivalence ratio for throttle tip-in and tip-in/tip-out combined respectively. Except for the intake manifold pressure, crank shaft speed and the AFR equivalence ratio matches exaxtly compared to the simulated response of the compensator shown in Fig. 5.23 and 5.24.. The good transient performance is due to the observer in the feedback loop, while the good steady state performance and fast recovery is due to the sliding mode AFR controller.

5.4.2.3 Optimal Hyperplane Design

An optimal hyperplane was designed for the linear system developed in Chapter 3. and the results are shown in Fig. 5.27 and Fig 5.28 using state feedback and then in Fig. 5.29 to 5.32 using state estimator.

5.4.2.3.1 Closed loop with state Feedback

The optimal hyperplane design scheme of sec. 4.3.3 is employed by using Eqs. 4.12 to 4.23 to design a hyperplane which is used in the control law of Eq. 4.9, on the linear engine model and system is subjected to same throttle maneuvers as in Fig. 5.21 and 5.22. that is, first throttle tip-in and then throttle tip-in/tip-out combined. In the design, the state weightings were chosen

$$\mathbf{Q} = \mathbf{diag}(1 \quad 1e-6 \quad 1e-6 \quad 0.1 \quad 1e-6 \quad 1 \quad 0.01 \quad 0.001)$$
$$\mathbf{R} = 10$$

to give weights which tend to induce the desired behavior in the system. The slding surface matrix definer C in this case is

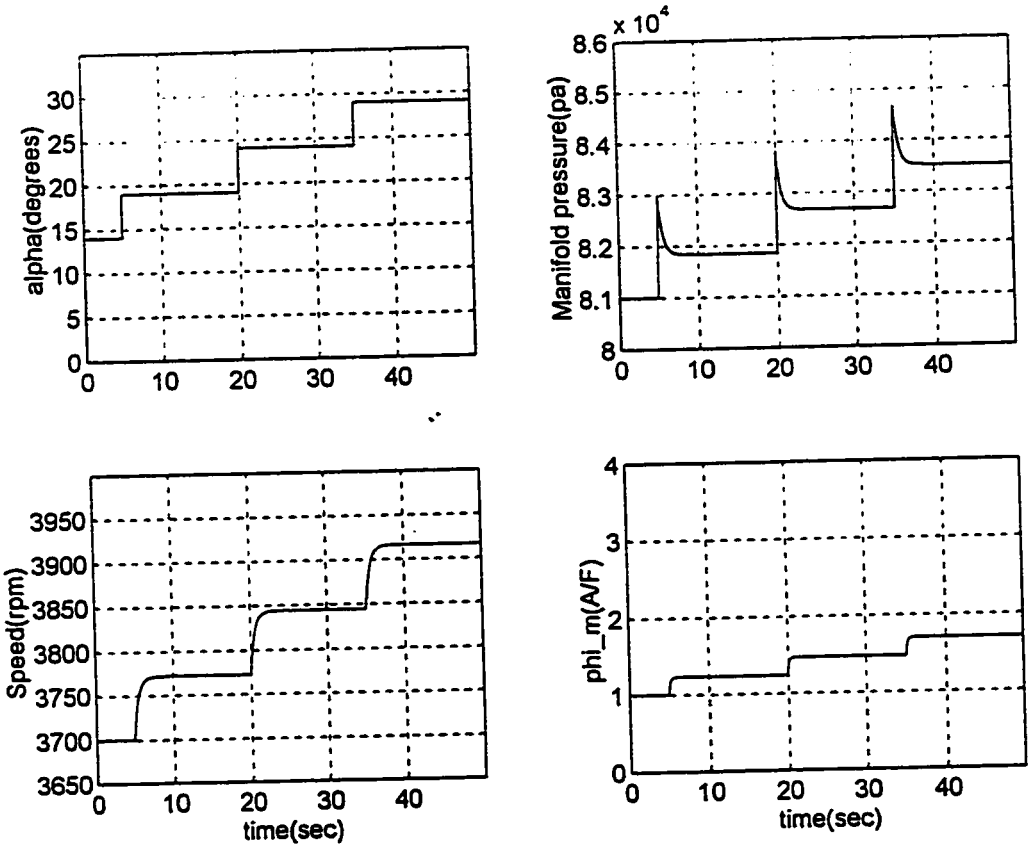

Figure 5.27: Simulated Response of Sliding Mode Controller with State Feedback using Optimal Hyperplane Design for Throttle Tip-in.

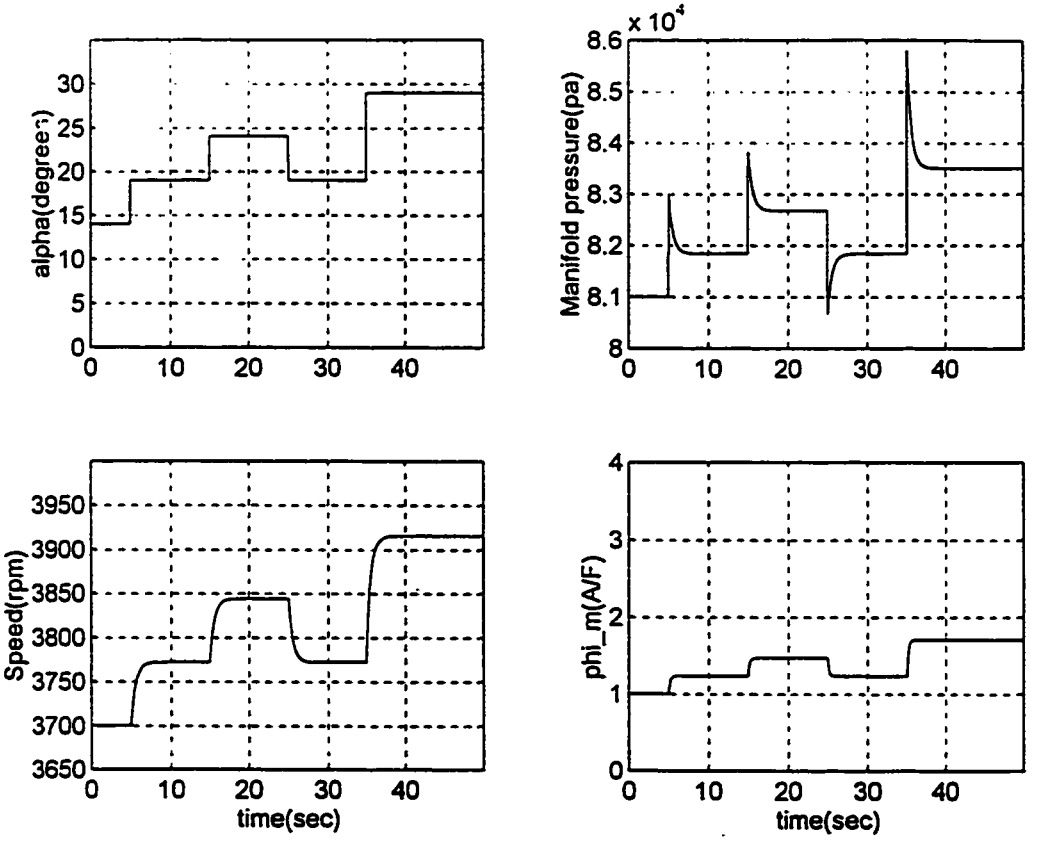

Figure 5.28: Simulated Response of Sliding Mode Controller with State Feedback using Optimal Hyperplane Design for Throttle Tip-in/Tip-out Combined.

$$C = [0 \quad -0.366 \quad -0.022 \quad -0.019 \quad -0.026 \quad 0.001 \quad -0.003 \quad 0.027]$$

The response of intake manifold pressure (p_m) and crankshaft speed (N) is similar to that of single loop filtering using state feedback. The response of equivalence AFR (ϕ_m) is different from that of Fig. 5.21. The response is smooth and fast but precise tracking of commanded AFR of 1 is . not achieved in this case. There is no tendency in the sliding mode to over or undershoot the value of 1 and there is no spiking or ringing behavior exhibited.. The system has good performance for combined tip-in and tip-out of throttle as shown in Fig. 5.28. and response in stable for entire operating range.

5.4.2.3.2 Closed Loop with Estimator

Based on the discussion in sec. 5.3, and using the same estimator as designed for single loop filtering design simulations were carried out with estimator in feedback loop. The system is subjected to throttle transients of the same nature as used for single loop filtering with the estimator in Fig. 5.23 and 5.24. The results are shown in Fig. 5.29 and 5.30 for both throttle tip-in and tip-in/tip-out combined. Fig. 5.31 and 5.32 shows the estimator response for the same throttle transients.

As shown in Fig 5.30 and Fig. 5.31 the responses are very similar to that with the state feedback using the optimal sliding modes and there is no spiking behavior exhibited in the AFR equivalence ratio (ϕ_m). The estimator response shown in Fig. 5.31 and 5.32 is similar to that shown in Fig 5.25 and Fig 5.26 for single loop filtering case except the one for AFR equivalence ratio which has no spikes and the estimated AFR is very close to the

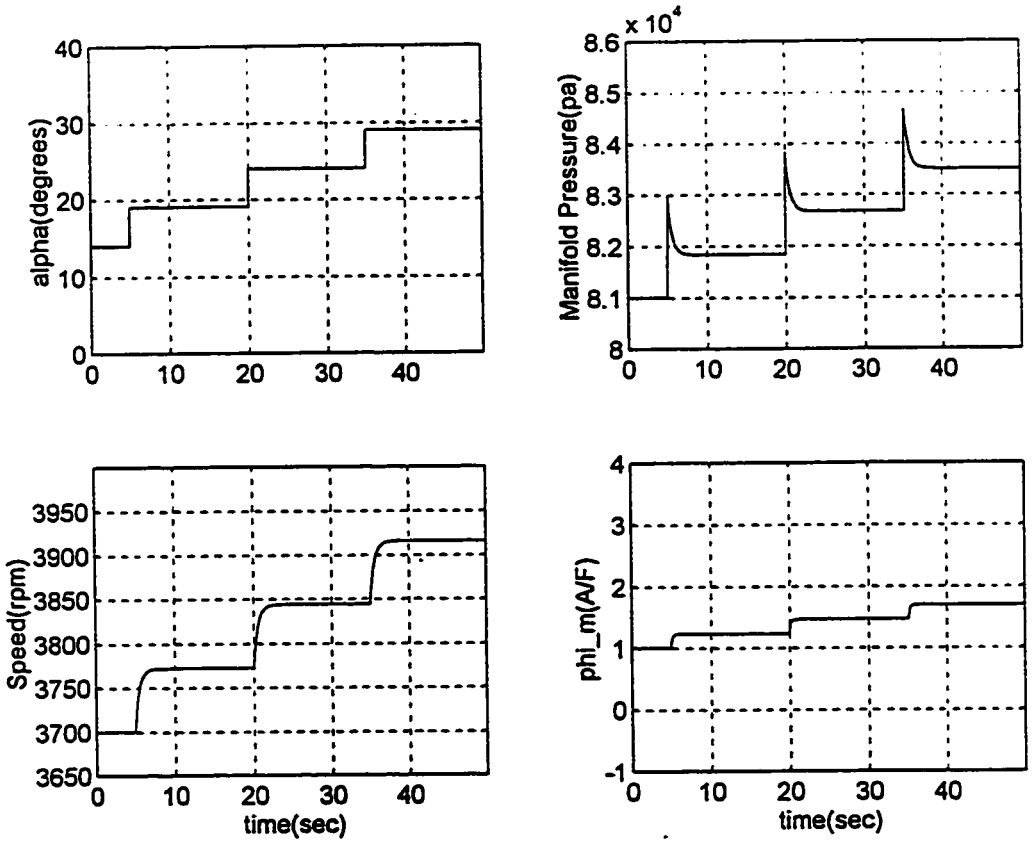

Figure 5.29: Simulated Response of Sliding Mode Controller with State Estimator using Optimal Hyperplane Design for Throttle Tip-in.

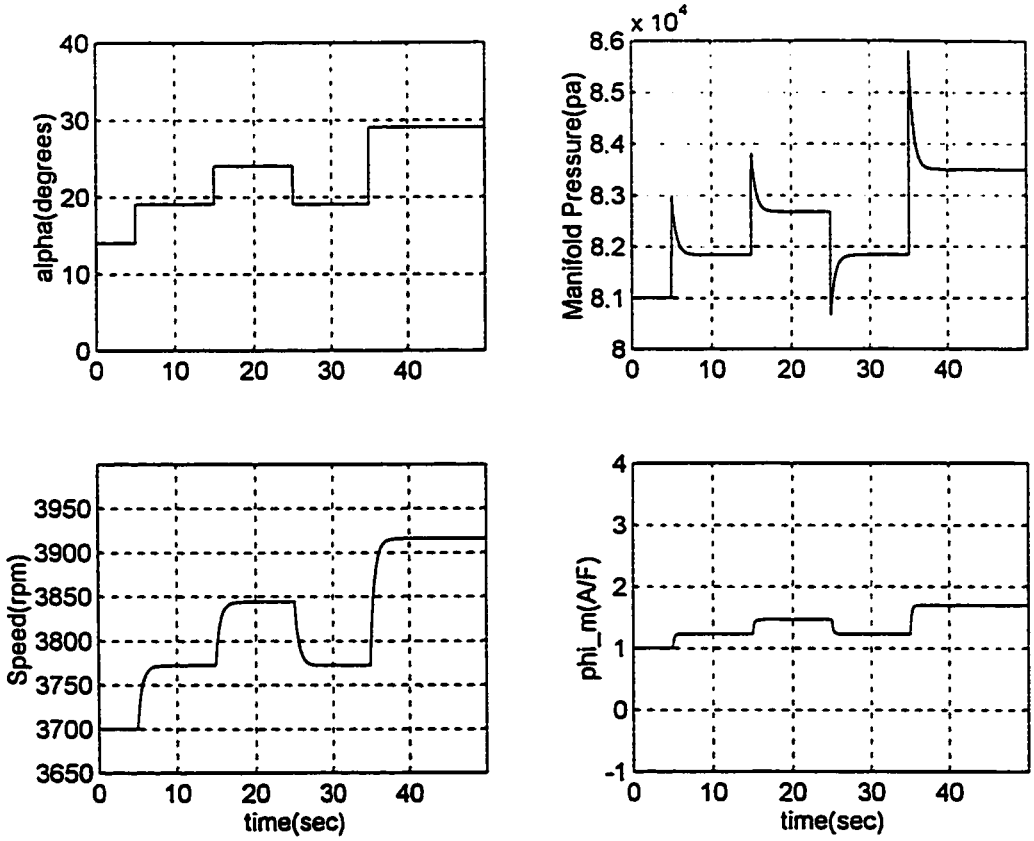

Figure 5.30: Simulated Response of Sliding Mode Controller with State Estimator using Optimal Hyperplane Design for Throttle Tip-in/Tip-out Combined.

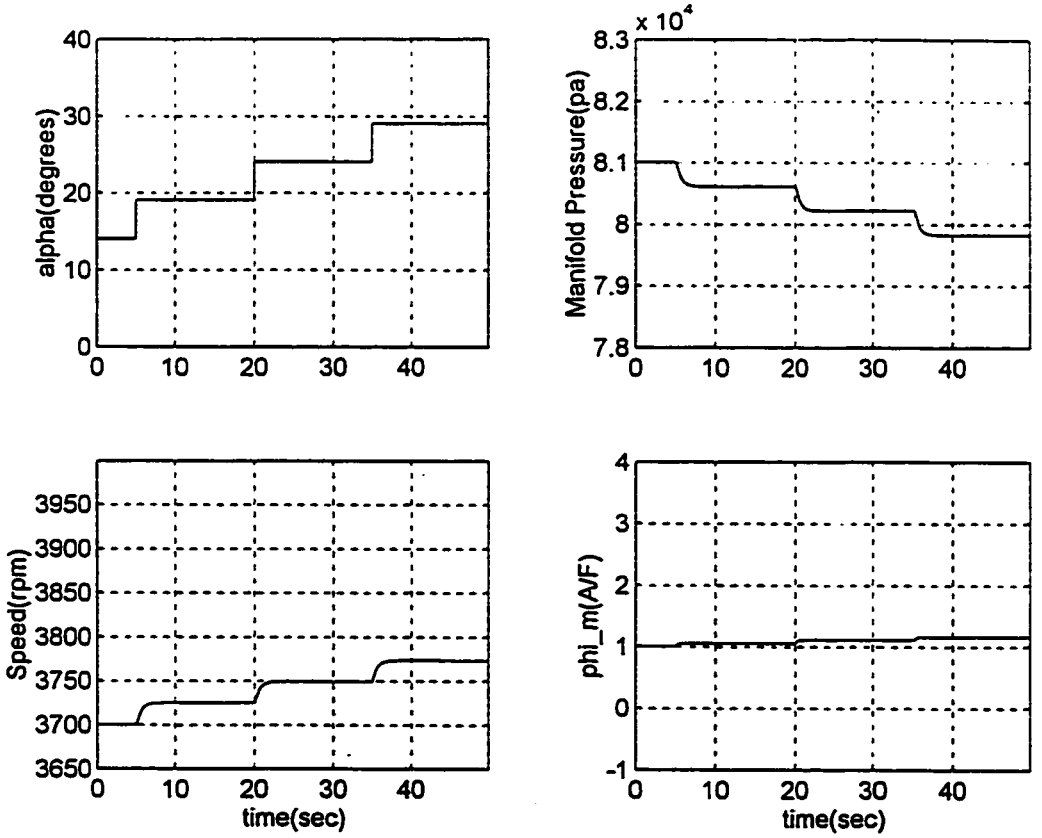

Figure 5.31: Simulated Response of State Estimator using Optimal Hyperplane Design for Throttle Tip-in.

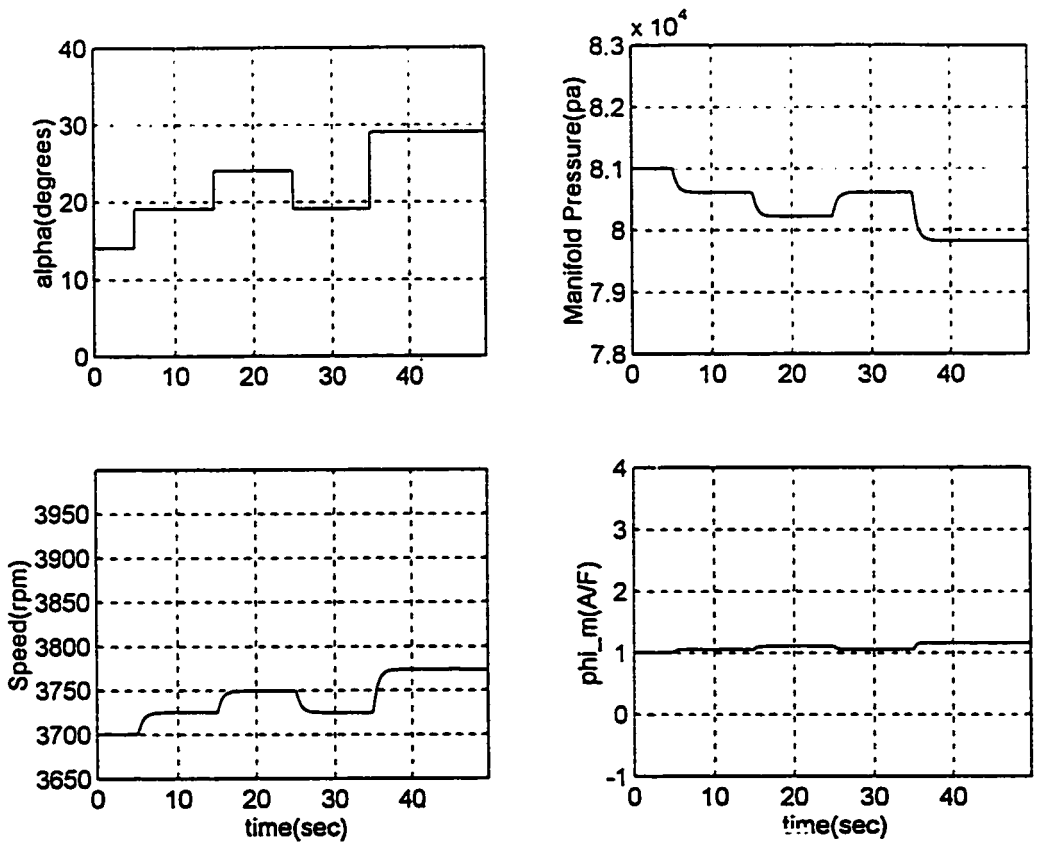

Figure 5.32: Simulated Response of State Estimator using Optimal Hyperplane Design for Throttle Tip-in/Tip-out Combined.

stochiometric AFR value of 1. Given the complicated nature of the engine and the size of the throttle angle steps introduced the overall results are quite convincing in that the control design method appears to be successful

5.5 Conclusion

Simulation results show a good system performance by maintaining near constant air fuel ratio close to stoichiometric despite large throttle command changes and associated speed and pressure changes. The optimal estimator developed was successful in estimating the states correctly except the intake manifold pressure and thereby the overall compensator was successful in tracking the AFR value of 1. The simulations verify that the sliding-mode controller is robust in the sense that the control system had good performance for both transient and steady state, over the entire operating range of the engine.

CHAPTER 6

Conclusions

6.1 Summary

A nonlinear engine model was presented which models port-fuel injected four cycle spark-ignition (SI) engines. It includes separately validated models of the most important engine subsystems: fuel vapor and fuel film, manifold air mass flow, crank shaft and loading and process delays inherent in the four-stroke engine operation. A series of simulations conducted at widely separated points over the entire operating range of the engine confirms the steady state and transient accuracy of the model. The basic model can be seen as an inexpensive engineering tool having wide applications to engine control problems.

Causes of air to fuel ratio(AFR) excursions during engine transients were examined. Air flow and fuel-wall wetting dynamics in the intake manifold has a significant impact on transient AFR excursion and the strategy used to eliminate the problem is to incorporate the important dynamics in the model for controller deign. There are undetected throttle movements during the critical period and the way to overcome this problems is to use a drive-by-wire (DBW) system which will avoid the AFR errors by moving the throttle in a predictable fashion.

The model was used as an observer in a high bandwidth air-fuel ratio (AFR) control structure. Large transient AFR excursions during fast throttle angle inputs requires a very fast system response and less sensitivity to the model errors. If feed forward control is used the system response is fast but then it requires a precise model of the process whereas the feedback control limits the speed of the system though it makes the system less sensitive to the model errors and other disturbances. In the proposed AFR control structure an observer based on the engine model is used which provides the estimated states to be used in the control calculations.

A sliding mode AFR controller taking all the time delay into account was derived. The sliding mode controller was designed in such a way that the amplitude of the oscillations in the normalized AFR under steady state operation could be controlled. The stability properties of this controller were analyzed using the eigen values of the combined controller-observer, and the analysis predicted that the controller should be stable at all accessible operating points. When the sliding mode controller was used with the nonlinear observer and the nonlinear fuel flow compensator, the control system had good

performance, both transient and steady state, over the entire operating range of the engine. The good transient performance was due to the observer and the nonlinear fuel flow compensator, while the good steady state performance and fast recovery was due to the sliding mode AFR controller

6.2 Conclusions

The main results of this research are:

- A physically motivated nonlinear SI engine model was developed which incorporates the important subsystems affecting AFR and predicts the actual engine behavior. A sliding mode controller was then designed based on the linearized version of the mathematical engine model. The linear model was compared favorably with the nonlinear model in open loop simulated throttling tests.
- High bandwidth closed loop AFR control can be achieved inspite of significant system delays by using the embedded engine model as an observer in the modern state space control structure.
- The designed controller can achieve a commanded air-to-fuel ratio with excellent transient properties which offers the potential for improving fuel economy, torque transients, and emission levels.
- The controller is robust to model errors and as well as to rapidly changing movements of the throttle.

- Coordinated control of the air flow and fuel flow provided more precise AFR control.
- The sliding mode control method offers a great potential for future engine control problems, since it results in a relatively simple control structure that requires little on-line computing; it is robust to model errors and disturbances ; and it can be easily adapted to a family of engines.

6.3 Recommendations

Some recommendations for future work are given:

- In this work every design is done for a single cylinder engine. The control structure and the model should be extended for multi-cylinder engines. In the case of multi-cylinder engines, many cylinders interact with the intake manifold at the same time and hence the intake manifold dynamics need to be modeled differently and the control algorithm should be changed accordingly in order to estimate the precise air flow induced.
- Before the introduction of three-way catalyst converters, exhaust gas recirculation(EGR) was primarily used to reduce NO_x emissions. Exhaust gas recircualtion is still used in conjunction with a three-way catalytic converter to improve the fuel economy of engines. The modeling and control of the EGR constitutes an additional area of interest.

- Control of the spark advance also affects the engine torque output under varying load conditions. The next generation vehicles demands the dynamic coordination between the engine and the transmission for smoother operation.
- Experimental implementation of the proposed control scheme using a port fuel injected single cylinder engine and its comparison to simulation results can become additional research work in the future.

Bibliography

Amann, C.A. (1990), "Control of the homogeneous-charge passanger car engine - defining the problem," SAE Paper No. 801440.

Amann, C. A.(1985), "Cylinder-pressure measurement and its use in engine research," SAE Paper No. 852067.

Anderson, R.L.(1986), "In-cylinder- measurement of combustion characteristics using ionazation sensors, "SAE Paper No. 860485.

Anderson, B.D.O. and J.B. Moore (1990), Optimal Control: Linear Quadratic Methods, Prentice Hall, New Jersey.

Aquino, C. F.(1981), "Transient A/F control characteristics of the 5 liter central fuel injection engine ," SAE paper No. 810494.

Athans, M. (1978), "The role of modern control theory for automotive engine control," SAE Paper No. 780852.

Cassidy, J.F., M. Athans and W.-H.Lee (1980), "On the design of electronic automotive engine controls using linear quadratic control theory," *IEEE Trans. Automat.Contr., vol.* AC-25, no. 5, pp.901-912, Oct. 1980.

Chang,C.-F., N.P.Fekete and J.D.Powell (1993), "Engine air-fuel ratio control using an event based observer," SAE Paper No. 930766.

Chin, Y.-K. and F. E. Coats (1986), "Engine dynamics time based versus crank angle based ," SAE Paper No. 860412 .

Chen-Fang Chang , Nicholas P. Fekete, Alios Amstutz and J.David Powell(1995), "Air-Fuel Ratio Control in Spark-Ignition Engines Using Estimation Theory." pp 22 -30 ,*IEEE Transactions on Control Systems Technology*, Vol . 3, No. 1, March 1995

Danno,Y., K. Togai, T.Fukui and M.Shimada (1989), "Powertrain control by DBW system-strategy and modeling," SAE Paper No. 890760.

Dobner , D. J. (1980), " A mathematical engine model for development of dynamic engine control," SAE Paper No. 800054.

Dobner, D.J. (1983), "Dynamic engine models for control development - Part 1: Nonlinear and linear model formulation," in Application of Control Theory in the Automotive Industry, pp. 54-74, Int. J. Vehicle Design, SP4.

Dorling C.M. and A.S.I. Zinober (1986), "Two Approaches to Hyperplane Design in Multivariable Variable Structure Control Systems", International Journal of Control, vol. 44, no. 1, pages 65-82.

Eaton, A. R. and R. S. Patrick (1992), personal communication.

Fekete, N.P (1994), *IC Engine Air Control: Foundation of an Observer-Based Air-Fuel Ratio Control Structure*. PhD thesis, Stanford University, Stanford, CA, to be published, 1994.

Franklin, G. F., J. D. Powell and M.L.workman (1990), *Digital Control of Dynamic Systems*. Addison-Wesley, Reading,MA,2nd ed..

Ganoung, D.(1990), "Fuel economy and drive-by-wire control," SAE Paper No. 900160.

Gassenfeit, E. H. and J. D. Powell (1990), "Algorithms for air-fuel ratio estimation using internal combustion engine cylinder pressure," SAE Paper No. 890300.

Hamann, E. H. Manger and L. Steinke (1977), " Lambda-sensor with Y_2O_3-stabilized ZrO_2-ceramic for application in automotive emission control systems," SAE Paper No. 770401.

Harrington, D. L. and J. A. Bolt (1970), " Analysis and digital simulation of carburetor metering." SAE Paper No. 700082.

Hazell, P.A. and J. O. Flower (1971), "Sampled-data theory applied to the modelling and control analysis of compression ignition engines - Part 1," *Int. J. Contr.*, vol. 13, no. 3, pp.549-562.

Hedrick, J.K., and D.Cho (1988), " A nonlinear controller design method for fuel-injected automotive engines," *ASME Trans. J. of Engineering for Gas Turbines and Power*, July 1988.

Hendricks, E. and S. C. Sorenson (1990), " Mean value modelling of spark ignition engines," SAE Paper No. 900616.

Hendricks, E. T. Vesterholm and S.C.Sorenson (1992), "Nonlinear, closed loop, SI engine control observers," SAE Paper No. 920237.

Heywood, J. B. (1988), Internal Combustion Engine Fundamentals , McGraw Hill, New York

Hires, S. D. and M. T. Overington (1981), " Transient mixture strength excursions - an investigation of their causes and the development of a constant mixture strenth fueling strategy," SAE Paper No. 810495.

Hubbard, M. P. D. Dobson and J. D. Powell (1976), "Closed loop control of spark advance using a cylinder pressure sensor," *ASME J. Dyn. Sys., Meas., and Contr.*, pp. 414-420, Dec. 1976.

Ishii, J., N. Kurihara, M. Shida, H. Miwa and T. Sekido (1992), "An automatic parameter matching for engine fuel injection control," SAE Paper No. 920239.

Iwano, H., M. Saitoh, K. Sawamoto and H. Nagaishi (1991), "An analysis of induction port fuel behavior," SAE Paper No. 912348.

Kay, I. W. (1978), "Manifold fuel film effects in an SI engine," SAE Paper No. 780994.

Kummer, J.T. (1980), "Catalysts for automobile emission control," *Prog. Energy Combust. Sci*, vol. 6, pp. 177-199.

Leonhardt, S., Ch. Schimdt, K. Voigt and R. Isermann (1992), "Real-time simulation of drive chaines for use in dynamical engine test stands," in *Proc. 1992 Amer. Contr. Conf.*, Chicago, IL, pp. 521-525.

Matekuins, F. A. (1986), "Engine combustion control with ignition timing by pressure ratio management," U.S Patent No. 4,622,939, Nov. 18, 1986.

Matsumura, T. and Y. Nanyoshi (1991), "New fuel metering technique for compensation wall flow in a transient condition using the model matching method," Int. J. Veh. Design, vol. 12, no.3, pp. 315-323.

Mondt, J. R. (1982), "An historical overview of emission-control techniques for spark-ignition engines," Tech. Rep. GMR-4228, General Motors Research Laboratories, Dec. 1982.

Moskwa, J. J and J. K. Hedrick (1989), "Modeling and validation of automotive engines for control algorithm development," in *Advanced Automotive Technologies - 1989, pp. 237-247*, ASME DSC-Vol. 13.

Nakaniwa, S., J. Furuya and N. Tomisawa (1991), "Development of nest-structured learning control system," SAE Paper No. 910084.

Nishiyama, R., S. Ohkubo and S. Washino (1989), "An analysis of controlled factors improving transient A/F control characterstics ," SAE Paper No. 890761.

Patrick, R. S., A. R. Eaton and J. D. Powell (1991), " A study of electronic engine control system structures for lean-burn, natural gas operation and in a spark ignition engine," in *Fuels, Controls, and Aftertreatment for Low Emissions Engines*, pp. 39-50, ASME ICE-Vol. 15.

Pieper, J.K (1992), *Discrete Time Sliding Mode Control*, Phd Thesis, Queen's University.

Pieper, J.K (1994), " Application of Sliding Mode Control to a Particular Helicopter Flight Control Problem.", *Proc. CSME Forum*, pp. 756-776.

Powell, B. K. (1978), "A simulation model of an internal combustion engine - dynamometer system," in *Proc. 1978 Summer Computer Simulation Conf.* , Newport Beach, CA, pp. 464-473.

Powell, B. K. (1979), " A dynamic model for automotive engine control analysis," in *Proc. 18th IEEE Conf. Decision Contr.*, Boston, MA, pp. 120-16.

Powell, B. K. and J.A. Cook (1987), "Nonlinear low frequency phenomenological engine modelling and analysis," in *Proc. 1987 Amer. Contr. Conf.*, Minneapolis, MN, pp. 332-340.

Powell, B.K., G. P. Lawson and G. Hogh (1987), " Advanced real time powertrain system analysis," ASME Paper No. 87-ICE-46.

Powell, J. D. (1987), " A review of IC engine models for control systems design," in *Proc. IFAC 10th Terminal World Congress*, vol. 3, Munich, FRG, pp. 235-240.

Powell, J. D (1993), " The use of cylinder pressure for engine monitoring and control," *ASME J. Dyn. Sys. Meas., and Contr.*

Powers, W. F., B. K. Powell and G. P. Lawson (1983), "Appliction of optimal control and Kalman filtering to automotive systems," in *Application of Control Theory in the Automotive Industry*, pp. 39-53, *Int. J. Vehicle Design*, SP4.

Safonov, M. G. and M. Athans (1978), "Robustness and computational aspects of nonlinear stochastic estimators and regulators," IEEE Trans. Automat. Contr., vol. AC-23, no. 4, pp. 717-725, Aug. 1978.

Slotine, J.J. and S.S. Sastry (1983), "Tracking Control of Nonlinear Systems Using Sliding Surfaces with Application to Robotic Manipulators", International Journal of Control, vol. 38, no. 2, pp. 465-492.

Sohma, K., T. Yukitake, S. Azuhata and Y. Takaku (1991), " Application of rapid optical measurement to detect the fluctuations of the air-fuel ratio and temperature of a spark ignition engine," SAE Paper No. 910499.

Stivender, D. L. (1978), "Engine air control - basis of a vehicular systems control hierarchy," SAE Paper No. 780346.

Tanaka, M. and E. J. Durbin (1977), "Transient response of a carburetor and engine," SAE Paper No. 770046.

Taylor, C. F. (1985), *The Internal Combustion Engine in Theory and Practice*, vol. I. MIT Press, Cambridge, MA, 2nd ed., revised.

Utkin, V.I. (1997), "Variable Structure Systems with Sliding Modes," IEEE Transactions on Automatic Control, vol. AC-22, no. 2, pp. 212-222.

Vesterholm, T., E. Hendricks and N. Houbak (1992), " Higher order continous SI engine observers," in *Proc. 1992 Amer. Contr. Conf.*, Chicago, IL, pp. 510-515.

V.K. Jones, Brian A. Ault, Gene F. Franklinand J. David Powell(1995), " Identification and Air-Fuel ratio control of a Spark Ignition Engine."pp 14- 21, *IEEE Transactions on Control Systems Technology*, Vol . 3, No. 1, March 1995

Wibberely, P. and C. A. Clark (1989), "An investigation of cylinder pressure as feed-back for control of internal combustion engines," SAE Paper No. 890396.

Woods, R.L (1979), "An air-modulated fluidic fuel-injection system ," *ASME J. Dyn. Sys. Meas., and Contr.* ,vol. 101, pp. 71-76, Mar. 1979.

Wu, H. (1980), " A computer model for a centrally-located, closed loop automotive fuel metering system," in *Advanced in computer Technology- 1980*, pp. 98-104, ASME.

Wu, H. and P. N. Blumberg(1979), "An attenuation and transport delay model for single point closed loop fuel metering systems," SAE Paper No. 790172.

Yoerger, D.R. and J.-J.E. Slotine (1986), " Task-resolved motion control of vehicle manipulator systems, Int. J. Robotics and Automation.

Yamada, T., N. Hayakawa, Y. Kami and T. Kawai (1992), " Universal air-fuel ratio heated exhaust gas oxygen sensor and further applications," SAE Paper No. 920234.

TEST TARGET (QA-3)

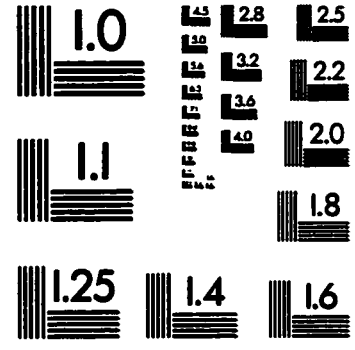

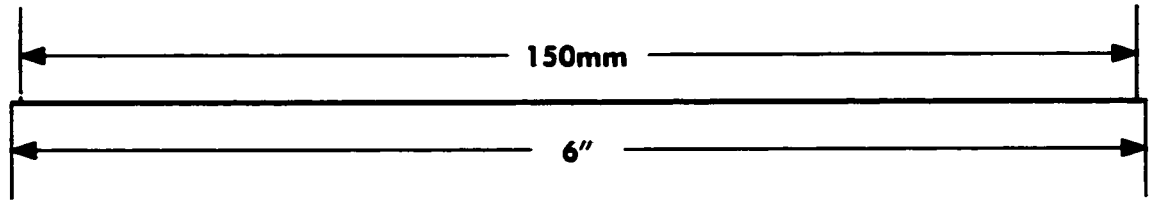

APPLIED IMAGE, Inc
1653 East Main Street
Rochester, NY 14609 USA
Phone: 716/482-0300
Fax: 716/288-5989